Chromatic Properties of Bipolar Cells in the Mouse Retina

Tobias Breuninger

Heidelberg, 2010

Dissertation

submitted to the
Combined Faculties for the Natural Sciences and for Mathematics
of the Ruperto-Carola University of Heidelberg, Germany

for the degree of

DOCTOR OF NATURAL SCIENCES

presented by

TOBIAS BREUNINGER

Dipl. Ing. (FH) Optoelektronik
M.Sc. Biomedical Engineering
born in Stuttgart, Germany

Oral-examination: 23. Nov. 2010

Nature is relentless and unchangeable, and it is indifferent as to whether its hidden reasons and actions are understandable to man or not.

Galileo Galilei (1564 – 1642)

Work for this thesis was done to three-fourths at the Max Planck Institute for Medical Research, Heidelberg in the period from the 15th of October 2006 to the 31st of December 2009 and one fourth at the Centre for Integrative Neuroscience, Tübingen from the 1st January 2010 to the 15th of October 2010. During the whole period I was registered as a PhD student at the University of Heidelberg.

1st adviser:	Institute:
Prof. Dr. Stephan Frings	Institute of Zoology, Department of Molecular Physiology, University of Heidelberg
2nd adviser:	Institute:
Prof. Dr. Thomas Euler	Max Planck Institute for Medical Research, Department of Biomedical Optics, Heidelberg
	Ophthalmic Research, Centre for Integrative Neuroscience (CIN), University of Tübingen
3rd evaluator:	Institute:
Prof. Dr. Thomas Holstein	Institute of Zoology, Department of Molecular Evolution, University of Heidelberg
4th evaluator:	Institute:
PD Dr. Georg Köhr	Max Planck Institute for Medical Research, Department of Molecular Neurobiology, Heidelberg

I herewith declare that I wrote this Doctoral Thesis independently under the supervision of Prof. Dr. Stephan Frings and Prof. Dr. Thomas Euler and used no other sources and aids than those indicated.

Date: Signature:

ACKNOWLEDGEMENTS

I would especially like to thank my supervisor und tutor Prof. Dr. Thomas Euler for his constant and strong support throughout my PhD.

I would like to thank my first PhD thesis advisor Prof. Dr. Stephan Frings for joining my thesis advisory committee, his helpful feedback and evaluation of my doctoral thesis.

I would like to thank Prof. Dr. Winfried Denk for frequent support and professional feedback.

I would like to thank Prof. Dr. Thomas Holstein and PD. Dr. Georg Köhr for being members of my examination board and the evaluation of my Disputation.

I would especially like to thank PD. Dr. Silke Haverkamp and Dr. Christian Puller (MPI for Brain Research, Frankfurt/M., Germany) for close collaboration.

I would like to thank Prof. Dr. Ilme Schlichting for joining my thesis advisory committee and her helpful feedback.

My thanks also go to all the present and past lab members in Tübingen and Heidelberg for strong support and the excellent work environment.

In particular I want to thank Siddharth Nanguneri and Le Chang for help with modeling and calculations, Timm Schubert and Kevin Briggman for helpful discussions, as well as Tom Baden and Daniel Rathbun for proofreading.

I would like to thank my family, my friends, and especially my wife Sonja Breuninger for being always by my side.

I would like to thank Prof. Dr. Thomas Kuner for providing the CLM1 and -12 mouse line (Berglund et al., 2004). Also I would like to thank for the permission to use the GUS8.4GFP mouse (Wong et al., 1999) line and the mitoP mouse line (Misgeld et al., 2007).

The study was supported by the Max-Planck Society (MPG), the Deutsche Forschungsgemeinschaft (DFG, FOR 701 and EXC 307), and the Centre for Integrative Neuroscience (CIN).

TABLE OF CONTENTS

LIST OF PUBLICATIONS

Breuninger, T., Puller, C., Haverkamp, S., Euler, T. (2010). Chromatic Bipolar Cell Pathways in the Mouse Retina. JNeurosci. Submitted in November 2010.

Euler, T., Hausselt, S.E., Margolis, D.J., Breuninger, T., Castell, X., Detwiler, P.B., and Denk, W. (2009). Eyecup scope--optical recordings of light stimulus-evoked fluorescence signals in the retina. Pflugers Arch 457, 1393-1414.

Dedek, K., Breuninger, T., de Sevilla Muller, L.P., Maxeiner, S., Schultz, K., Janssen-Bienhold, U., Willecke, K., Euler, T., and Weiler, R. (2009). A novel type of interplexiform amacrine cell in the mouse retina. Eur J Neurosci 30, 217-228.

For detailed information about the authors contributions to each of these publications, see section 3.6.

ABBREVIATIONS

2P	|	two-photon
AMPA	|	α-amino-3-hydroxyl-5-methyl-4-isoxazole-propionate; a specific agonist for AMPA-type glutamate receptors
Ca^{2+}	|	calcium (cation)
Cl^-	|	chloride (anion)
CLM	|	Clomeleon; the CLM mouse lines express a fluorescent chloride indicator protein under the control of the thy1-promotor (Berglund et al., 2004)
Cre	|	Cre recombinase; a Type I topoisomerase from P1 bacteriophage that catalyzes site-specific recombination of DNA
cx36	|	Connexin 36, a trans-membrane protein expressed in cone photoreceptors that forms hemichannels and gap junction (Goodenough, 1974; Bennett and Goodenough, 1978)
GABA	|	gamma-aminobutyric acid (neurotransmitter)
GCL	|	ganglion cell layer
GFP, CFP, YFP	|	green, cyan, and yellow fluorescent protein, GFP was originally isolated from *Aequorea victoria* (Chalfie et al., 1994; Shimomura, 2005), in this work no differentiation between GFP and EGFP (enhanced GFP) was made
Glu	|	glutamate (neurotransmitter)
GluR	|	glutamate receptor
Gus	|	α-Gusducin; the GUS8.4GFP mouse line expresses green fluorescent protein in a α-gustducin-positive subset of cells (Wong et al., 1999; Huang et al., 2003)
iGluR	|	ionotropic glutamate receptor
INL	|	inner nuclear layer
IPA	|	Interplexiform amacrine cell
IPL	|	inner plexiform layer
K^+	|	potassium (cation)
L (-cone)	|	long wavelength sensitive (cone)
M (-cone)	|	medium wavelength sensitive (cone)
mGluR	|	metabotropic glutamate receptor
mitoP	|	mitochondrially targeted fluorescent protein; the Thy1-mitoCFP mouse line expresses the cyan fluorescent protein under the control of thy1-promoter (Misgeld et al., 2007)

Na^+	|	sodium (cation)
OFF (-response)	|	decrease in light level (causes the depolarization of a retinal neuron)
ON (-response)	|	increase in light level (causes the depolarization of a retinal neuron)
OPL	|	outer plexiform layer
Parv	|	parvalbumin; a calcium binding albumin protein mainly present in GABAergic interneurons
Parv-Cre (mouse line)	|	parvalbumin-Cre; transgenic mouse line in which the green fluorescent protein (GFP) is specifically expressed in parvalbumin-positive neurons (Maxeiner et al., 2005; Fuchs et al., 2007)
PMT	|	photo multiplier
S (-cone)	|	short wavelength sensitive (cone)
thy1	|	thymocyte protein 1, protein of the immunoglobulin super-family that is expressed in many neuronal and several no-neuronal cells, including thymocytes (Giguere et al., 1985)

1 ABSTRACT (ENGLISH)

The retina performs a wide range of computations to process visual signals. Feature extraction, such as the detection of edges, motion, and color originate in specialized retinal circuits. In this study we investigated the circuits underlying chromatic processing in the mouse retina.

Although color vision is wide spread among mammals, its research tends to focus on primates. Studying non-primate mammals can be advantageous in understanding the general principles of retinal chromatic processing. Like most mammals, mice feature dichromatic color vision based on short (S) and medium (M) wavelength-sensitive cone types. It is thought that mammals share a common retinal circuit that compares S- and M-cone output (in trichromats S- and M+L-cone) to generate blue/green (blue/yellow) opponent signals, with distinct bipolar cells providing separate chromatic channels. While S-cone selective ON-bipolar cells (in mouse "type 9") have been anatomically identified, little is known about other cone selective channels, such as, for instance, M-cone selective OFF-bipolar cells. Here, we characterized cone connectivity and light responses of selected mouse bipolar cell types using immunohistochemical and electrophysiological methods.

Our anatomical data indicate that four of the five mouse OFF-bipolar cell types (types 2, 3a/b and 4) as well as type 7 (as an example for ON-bipolar cells) indiscriminately contact both S- and M-cones. Using a marker that labels dendrites of both type-1 and -2 OFF-bipolar cells we found reduced immunofluorescence at S-cone, suggesting that type 1 avoids S-cones. Recordings of light responses showed that the chromatic tuning of bipolar cells strongly depended on their position along the dorso-ventral axis – due to the dorso-ventral gradient in S-opsin co-expression in mouse M-cones. In dorsal retina, where co-expression is low, most type-2 (and type-7) cells were green-biased, with a fraction of cells (≈ 14 %) displaying strongly blue-biased responses, likely reflecting S-cone input. Type-1 cells were also green-biased but did not include blue-biased "outliers", consistent with type-1 cells avoiding S-cones. We therefore suggest that type 1 represents the green^{OFF} pathway in mouse. In addition, we confirmed that type-9 bipolar cells display blue^{ON} responses. In ventral retina, all bipolar cell types studied here displayed similar blue-biased responses, suggesting that color vision may be only supported in the dorsal mouse retina.

In conclusion, our data supports an antagonistically organized blue/green circuit with bipolar cells functioning as chromatically defined channels, which form the common basis for mammalian dichromatic color vision.

2 ABSTRACT (GERMAN)

In der Netzhaut findet auf vielfältige Weise eine Verarbeitung von visuellen Signalen statt. In spezialisierten Schaltkreisen werden charakteristische Bildinformationen extrahiert; beispielsweise werden Kanten, Bewegung und Farbe detektiert. In dieser Arbeit werden die Schaltkreise untersucht, die chromatische Signale in der Mausretina verarbeiten.

Obwohl die meisten Säugetiere über die Fähigkeit des Farbsehens verfügen, konzentriert sich die Forschung meist auf das Farbsehen von Primaten. Doch kann auch die Erforschung anderer Säuger dem Verständnis genereller Verarbeitungsmechanismen helfen. Wie die meisten anderen Säuger verfügen auch Mäuse über dichromatisches Farbsehen basierend auf zwei Zapfentypen, den S- und M-Zapfen, die spektrale Sensitivitäten im kurzen (engl. „short wavelength" – S) und mittleren („medium wavelength" – M) Wellenlängenbereich besitzen. Es wird vermutet, dass alle Säuger homologe retinale Schaltkreise besitzen, die für die differenzielle Verrechnung der Ausgangssignalen von S- gegenüber M-Zapfen (bei Trichromaten: S- gegen M- und L-Zapfen) verantwortlich sind, woraus sich schließlich farbantagonistische blau/grüne (bei Trichromaten: blau/gelbe) Signale ergeben. Bipolarzellen dienen dabei als separate Kanäle für die Weiterleitung der chromatischen Signale. ON-Bipolarzellen, die selektiv S-Zapfen kontaktieren, wurden anatomisch bereits identifiziert (in der Maus: Typ 9). Hingegen ist wenig bekannt über andere selektive Kanäle, beispielsweise M-Zapfen-selektive OFF-Bipolarzellen. In der vorliegenden Arbeit werden Bipolarzellen mit immunohistochemischen und elektrophysiologischen Methoden bezüglich ihrer Zapfenkontakte sowie ihrer Lichtantworten charakterisiert.

Wie unsere anatomischen Ergebnisse zeigen, kontaktieren vier der fünf OFF-Bipolar-Zelltypen (die Typen 2, 3a/b und 4) und mindestens ein ON-Bipolar-Zelltyp (Typ 7) beide Zapfentypen unselektiv. Bei der Verwendung eines Markers für die Dendriten von Typ 1 und Typ 2 Zellen fanden wir Belege dafür, dass Typ 1 Bipolarzellen Kontakte mit S-Zapfen vermeiden. Unsere elektrischen Ableitungen von Bipolarzellen zeigen ein starkes Abhängigkeits-Verhältnis der chromatischen Lichtantworten von der dorso-ventralen Position der Zelle, welches durch den dorso-ventralen Gradienten der Koexpression von S-Opsin in M-Zapfen erklärt werden kann. In der dorsalen Retina, in der Koexpression nur im geringen Maße vorkommt, ist das chromatische Antwortverhalten der meisten Typ 2 (und Typ 7) Zellen in Richtung grün verschoben. Allerdings zeigt ein kleiner Anteil (≈ 14 %) der Zellen ein stark blau verschobenes Antwortverhalten. Diese „Ausreißer" konnten wir im Fall der Typ 1 Zellen nicht finden. Dies deuten wir als Übereinstimmung mit unseren anatomischen Daten (Typ 1 Zellen meiden S-Zapfen) und schließen daraus, dass der grüne OFF-Signalweg durch Typ 1 repräsentiert wird. Zusätzlich konnten wir bestätigen, dass Typ 9 Zellen blaue ON-Lichtantworten zeigen. Alle ventral abgeleiteten Zellen zeigten ebenfalls ein deutlich blau verschobenes Antwortverhalten. Eine chromatische Verarbeitung in der ventralen Netzhaut ist somit wahrscheinlich kaum oder gar nicht möglich.

Unsere Daten unterstützten die Hypothese eines homologen, farbantagonistischen blau/grün Schaltkreises als Grundlage für das Farbsehen in Säugetieren, wobei Bipolarzellen chromatisch definierte Kanäle durch die Netzhaut darstellen.

3 INTRODUCTION

3.1 Visual perception

For humans vision is one of the most important senses to perceive the environment. Through the optical components of the eye, the visual scene is projected onto the retina at the back of the eye. The retina is, at the same time, an image detector and a processing unit. It extracts features, including motion (see, e.g., Olveczky et al., 2003), edges (see, e.g., Cleland and Levick, 1974) and color (for review, see Dacey and Packer, 2003) and it codes luminosity changes over a tremendous range (for review, see Stockman and Sharpe, 2006). It also codes with high spatial resolution (see, e.g., Kolb and Marshak, 2003) but compresses the overall information to a minimal amount of data (see, e.g., Zhaoping, 2006). Signal processing occurs already at the first synaptic level in the outer plexiform layer (OPL; Figure 1) where the photoreceptor terminals are in contact with each other and the postsynaptic processes. Horizontal cells stratify in the OPL and facilitate lateral processing and adaptation. Vertical interneurons (bipolar cells) function as discrete channels that transmit the signal to the inner retina. Amacrine cells, the second class of lateral interneurons are involved in complex computational steps. Ganglion cells, the output neurons of the retina, send the signals in parallel to higher centers of the central nervous system (for review, see Wassle, 2004), where the various distinct features are combined to form an overall perception.

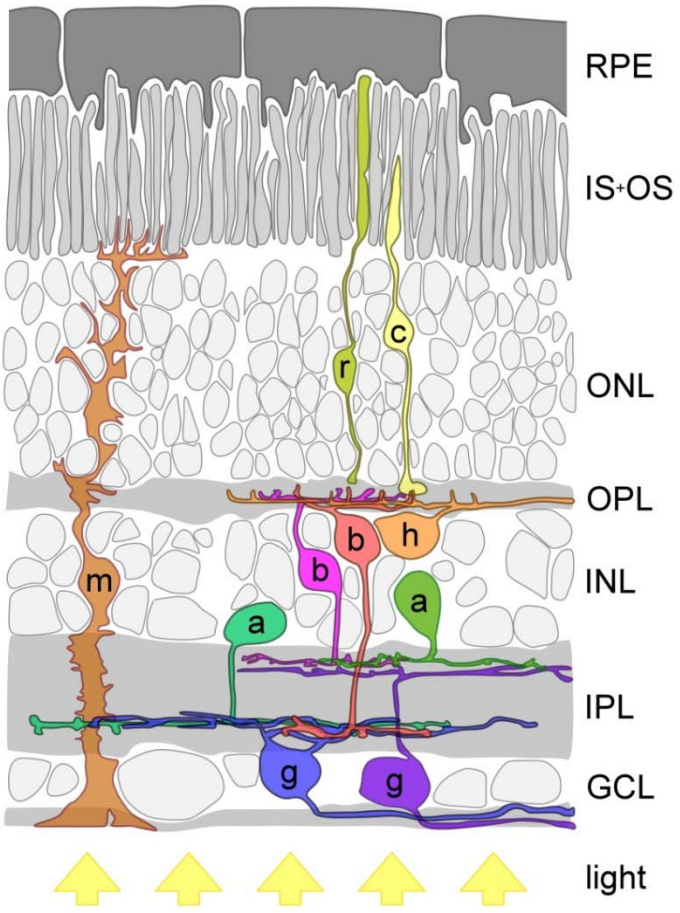

Figure 1: Schematic structural organization of the mammalian retina with the rod (r) and cone (c) photoreceptors, horizontal (h), bipolar (b), amacrine (a), ganglion (g) cells, and the non-neuronal Müller (m) cells. The light enters the tissue from the ganglion cell layer (GCL) side, passing through the almost transparent layers of the retina to reach the photoreceptors. The outer and inner plexiform layer (OPL and IPL) contain synaptically connected dendritic and axonal processes. The outer and inner nuclear layers (ONL and INL) contain the cell bodies of photoreceptors and bipolar, amacrine and horizontal cells, respectively. Photoreceptors consist of outer and inner segments (OS and IS), cell bodies, and terminals. The outer segments are in contact with the retinal pigment epithelium (RPE). Figure modified from Euler et al., 2008.

3.2 Color perception

The nature of color has puzzled scientists throughout the centuries. It turned out that is not trivial to infer from the subjective human color perception to physical properties of light. Newton (1643 - 1727) demonstrated that using a dispersive prism “white” sunlight can be decomposed into a spectrum of colors. Today we know that the electromagnetic emission of the sun, which represents an approximately continuous spectrum, has its maximum in the visible range at ~ 500 nm. The solar spectrum measured on the earth surface is not constant over time. At lower solar altitude, in the morning and evening hours, blue light is removed from the incident spectrum due to stronger dispersion of short wavelength light in the earth's atmosphere.

Our visual world appears in different colors. Opaque objects, when illuminated, absorb and reflect fractions of the incident light; the resultant spectral fingerprint of the object depends on the reflectance properties of the object's surface and the spectrum of the incident light. The robustness of our color vision in different light conditions, for example in morning vs. evening light, may easily lead to the false assumption that color is a true physical object property and independent of observer and ambient conditions. This reliability (often referred to as “color constancy”; for review, see Conway, 2009) is an integral part of polychromatic vision and the result of complex neuronal computation. Indeed, the ability to discriminate different wavelengths is not only crucial for color vision itself, but also a requirement for constancy mechanisms, such as the impression of same lightness of an object under variable spectral illuminations.

Color perception emerges from neuronal computations performed in concert by a number of brain areas (for review, see Leamey et al., 2009). However, its basis - the detection of chromatic information and the creation of initial color opponent signals (section 3.4) – already takes place in the retina. Although the reliability of color constancy is surprisingly high human subjects are susceptible to optical illusions and it becomes obvious that ambient light and assumptions made by the visual system of the observer dramatically influence color sensation.

Differences between individuals in photoreceptor spectral sensitivity can also lead to variations in individual color vision. Indeed, mutations in one of the opsin genes occur relatively frequent within the human population (8 % of men, < 1 % of women; for review, see Conway, 2009). Red-green color vision deficits/anomalies (Protanopia/Protanomaly or Deuteranopia/Deuteranomaly) because of absent or non-functional L- or M-opsins, respectively, occur more frequent in the male population due to the location of L- and M-opsin genes on the X chromosome (Piantanida, 1988), while blue-yellow deficits/anomalies (Tritanopia/Tritanomaly) are more rare for both genders. In contrast, it was found that big variations in the relative number of M- and L-cones between individuals lead to nearly identical color sensation in human subjects (Hofer et al., 2005).

While humans and old world monkeys feature trichromatic vision, most other mammals are dichromats; other vertebrates (fish, amphibians, reptiles, and birds) studied so far often are tetrachromats or even pentachromats. In general, different species exhibit different sets of photoreceptors with unique spectral sensitivities adapted to lifestyle and environment. Therefore

human color definitions cannot be applied to chromatic perception across species. Nevertheless, terms like “green stimulation light” or “blue-cone bipolar cell” are used liberally in this work for the reader’s convenience.

This work focuses on the mechanisms of chromatic processing that take place in retinal neuronal circuits. Therefore, the following sections describe the different retinal neurons and their interactions with respect to chromatic processing.

3.3 Structure of the mammalian retina

Many animals posses organs to detect electromagnetic waves – namely eyes. Evolution produced a number of different designs, for instance the compound eyes of the fruit fly, the pinhole eye of the nautilus, the single-lens eye with everse retina of the squid, or the vertebrate single-lens eye with reverse retina present in humans and mice. This work focuses on the mammalian retina and, although several differences between species are known, it is possible to develop a general blueprint of the mammalian retina. In the highly organized structure of the retina, five neuronal cell classes can be distinguished: photoreceptors, horizontal cells, bipolar cells, amacrine cells, and ganglion cells (Figure 1). Additionally, glia cells, i.e. Müller cells, support the physiological function of the retinal neurons (Newman and Reichenbach, 1996) and even seem to further increase the optical image quality of the retinal tissue by guiding light to the photoreceptors (Franze et al., 2007).

3.3.1 Photoreceptors

Photosensitive visual pigments (rhodopsins and cone opsins) are located in the densely stacked membranes of rod and cone photoreceptor outer segments. Opsins belong to the super-family of G protein-coupled membrane-bound receptors and consist of a protein moiety as well as a reversibly, covalently bound cofactor (11-*cis*-retinal) that undergoes a light induced isomerization to all-*trans*-retinal. In the case of rhodopsin, this photo-isomerization and the complex downstream cascade, together referred to as visual phototransduction, have been intensely studied and will not be described in detail here (for review, see Burns and Baylor, 2001). At low light levels, photoreceptors continuously release glutamate that acts as a neurotransmitter on the postsynaptic neurons. An increase in light level leads to a closure of cGMP-regulated cation channels, which hyperpolarizes the photoreceptor cell and in turn leads to a decrease in glutamate release at the synaptic cleft.

Two sub-classes of photoreceptors subserve different functions; cone photoreceptors show functional activation at photopic light levels when rod photoreceptors are saturated. Rods show functional activity at scotopic light levels; they respond slower but with a higher sensitivity. Under mesopic light conditions both sub-classes of photoreceptors contribute to vision.

The outer segments of photoreceptors are in contact with the light absorbing retinal pigment epithelium (Figure 1). The electrical signal, generated in the outer segment, is relayed inwards to the pre-synaptic output structure of the photoreceptors, the terminals (rod spherules

and cone pedicles). The photoreceptor terminals are located in the outer plexiform layer (OPL) and form highly specialized synapses with bipolar cells and horizontal cells – the triad synapses (described in detail in section 3.3.6). Besides this glutamatergic synapse, cones and rods exhibit homo- and heterotypical electrical coupling via gap junctions, formed by connexins (cx), which allow ions and small molecules up to a mass of ~ 1 kilodalton to pass into neighboring cells (see also section 3.3.6). Therefore changes in the membrane potential of one photoreceptor cell directly affect coupled photoreceptors. The level of electrical conductance between photoreceptors is strictly regulated and highly dependent on the circadian rhythm and possibly on light adaptation (reviewed: Bloomfield and Volgyi, 2009).

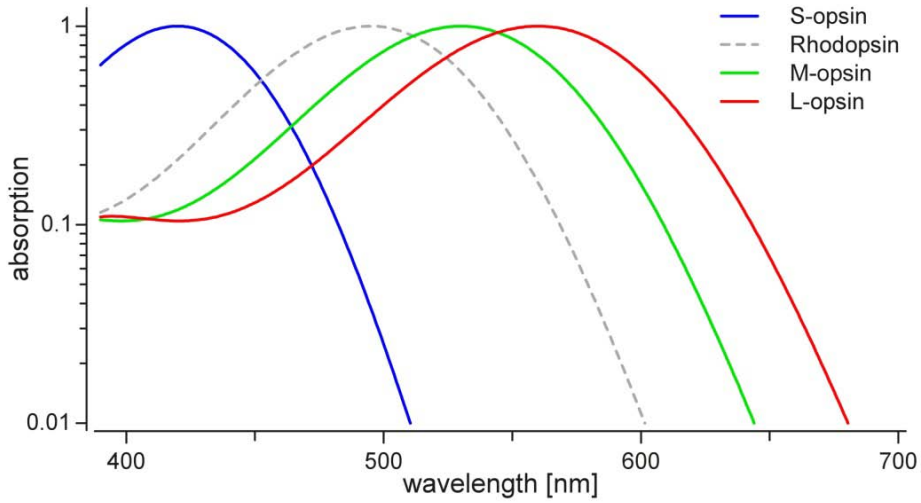

Figure 2: Theoretical spectral absorption curves of the human opsin types; logarithmic scale; peak absorption is normalized to 1; curves are not corrected for absorption that takes place in the lens or other optical components of the eye. Peak values from: Dartnall et al., 1983; used template: Stockman and Sharpe, 2000.

The basis for color vision in humans and old world primates is the presence of three cone types expressing specific opsins with sensitivities in the short (S, “blue”), medium (M, “green”), and long (L, “red”) wavelength range with maximal absorptions at approximately 425 nm, 530 nm, and 560 nm, respectively (Riggs, 1967; Figure 2). Note that heterotypic cone-cone coupling via gap junctions can influence the resulting spectral sensitivity and blur chromatic discrimination. In the primate retina M- and L-cones form such coupling. In ground squirrel it has been shown that S- and M-cones are not coupled (Hornstein et al., 2004; Li and DeVries, 2004). For the case of human M- and L-cone coupling it has been calculated that the spectral blurring is modest and reduces color discrimination by only ~ 20% (Li and DeVries, 2004). In non-primate mammals, maximally two cone types are present: S- and M-cones. Mice express S- and M-opsins with maximal absorption at approximately 360 nm and 510 nm, respectively. In some non-primate mammals, including mice, there is co-expression in the same cone (i.e. S-opsin in mouse M-cones); in case of the mouse, the level of co-expression changes along a dorso-ventral gradient (section 3.5).

Not long ago, another protein from the opsin family, melanopsin, was identified in the vertebrate retina (Provencio et al., 1998; Soni and Foster, 1997; Provencio et al., 2000). It is expressed in intrinsically photosensitive retinal ganglion cells and plays a functional role in the synchronization of circadian rhythms, the modulation of melatonin release, and the regulation of pupil size. Since it does not play a role in classical visual perception, it will not be discussed further (but see Ecker et al., 2010).

3.3.2 Horizontal cells

Horizontal cells are the lateral interneurons of the outer retina (Figure 1). Most mammals have two types of horizontal cells (A- and B-type, in primate H1 and H2), which can be distinguished morphologically (Figure 3); some species, including mice and rats, possess only one type (Suzuki and Pinto, 1986; Peichl and González-Soriano, 1994).

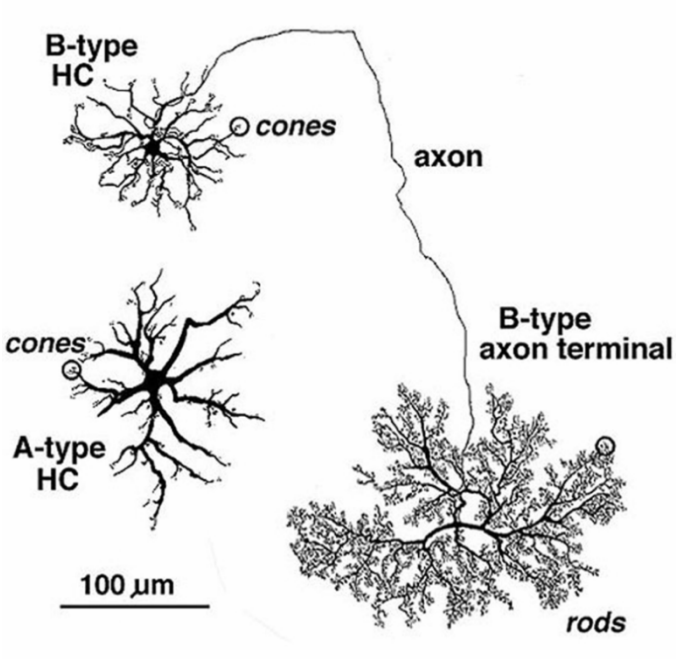

Figure 3: Horizontal cells (HCs) of the cat retina; Golgi stained whole-mount preparation; horizontal view. Two morphological types can be distinguished, A- and B-type horizontal cells. The A-type only contacts cones, the B-type contacts cones with its dendritic tree and rods with its axon terminal. Figure: Kolb et al., 1974.

Injections of small tracer dyes show that horizontal cells are coupled via electrical synapses and form large homotypic networks (Yamada and Ishikawa, 1965; Winslow and Knapp, 1991; Dacheux and Raviola, 1982; Vaney, 1991; Dacey et al., 1996; Trumpler et al., 2008). It is thought that the horizontal cell network carries information about the average ambient illumination, which is crucial for light adaptation (Bloomfield and Volgyi, 2009; but see Dedek et al., 2008).

Horizontal cells adjust the gain of the photoreceptor synapse depending on the light conditions; their lateral inhibition contributes to the generation of receptive field surrounds in bipolar cells (Yang and Wu, 1991; Wu, 1992; Piccolino et al., 1984; Burkhardt, 1993; Kamermans and Spekreijse, 1999; Schwartz, 2002). Horizontal cells receive excitatory glutamatergic input from rod and cone photoreceptors via ionotropic glutamate receptors (GluR2 - 4) of the AMPA-type

(mouse/rat: Brandstatter and Hack, 2001; rabbit: Deng et al., 2006; Pan and Massey, 2007; primate: Haverkamp et al., 2000; Haverkamp et al., 2001a; Haverkamp et al., 2001b), provide inhibitory feedback to photoreceptors (for review, see Fahrenfort et al., 2005), and directly feed forward to bipolar cell dendrites (section 3.3.6; Schwartz, 2002). It is still not completely clear whether the surround response of bipolar cells is the result of direct feedforward input from horizontal cells to bipolar cells or of feedback from horizontal cells to cone photoreceptors, or a combination of both.

Selective synaptic connections between cone types and horizontal cells can support the first step of chromatic signal separation/discrimination, while unselective feedback to different cone types will hamper this. Chromatically opponent signals have been described for horizontal cells in vertebrate species including fish and turtle (Svaetichin and Macnichol, 1959; Burkhardt, 1993; Wietsma et al., 1995). Selective cone-horizontal cell connectivity has been found, in cat and primate (Nelson, 1985; Dacey et al., 1996) but not in rabbit (Hack and Peichl, 1999). Since there is only one horizontal cell type in mouse, selective cone-horizontal cell connectivity is not expected (for review, see Peichl and Gonzalez-Soriano, 1994).

The primate H1 cell morphologically corresponds to B-type in other mammals; the H2 cell corresponds to A-type, but also has a short axon with a terminal contacting cones (Kolb et al., 1980; for review, see Boycott, 1988). H1 cells mainly receive input from M- and L-cones, and only weak input from S-cones (Dacey et al., 1996). H2 cells mainly receive input from S-cones onto the dendritic tree as well as onto the axon terminals (Ahnelt and Kolb, 1994; Dacey et al., 1996; Goodchild et al., 1996a; Chan and Grunert, 1998). As recently shown, blue/yellow opponency is to some extend already generated at the level of the S-cone through (L+M)-cone biased inhibitory feedback from H1 cells (Field et al., 2007; Packer et al., 2010).

3.3.3 Bipolar cells

Bipolar cells are the only interneurons that connect the outer with the inner retina and transmit signals from photoreceptor cells to ganglion cells. Mammals have about ten to twelve types of bipolar cells, based on morphological studies (gray squirrel: West, 1978; primate: Boycott and Wassle, 1991; rat: Euler and Wässle, 1995; mouse: Ghosh et al., 2004). In recent years, an increasing number of specific antibodies that label subpopulations of bipolar cells have been identified. With these immunohistochemical markers it became possible, for instance, to divide the morphological type-3 and -5 mouse bipolar cells each into subtypes (Wassle et al., 2009; Figure 4). In the present work, different immunohistochemical markers were used to study the connectivity between bipolar cell dendrites and S- and M-cones (for type 9, see Haverkamp et al., 2005). In addition, different mouse lines expressing fluorescent proteins in subsets of neurons were used to specifically target types of bipolar cells for electrophysiological experiments (see Material and Methods).

One bipolar cell type selectively receives rod input (Figure 4; the contribution of the rod pathway to chromatic processing is discussed in section 6.6) – all others types mainly receive cone input and therefore are termed cone bipolar cells. Bipolar cells can be divided by their

physiology and the stratification level of their axon terminal system into two major sub-classes: ON- and OFF-bipolar cells. ON-bipolar cells depolarize in response to increases in light level and stratify in the inner part of the IPL; OFF-bipolar cells depolarize in response to decreases in light level and stratify in the outer part of the IPL (Nelson et al., 1978; for review, see Wassle, 2004).

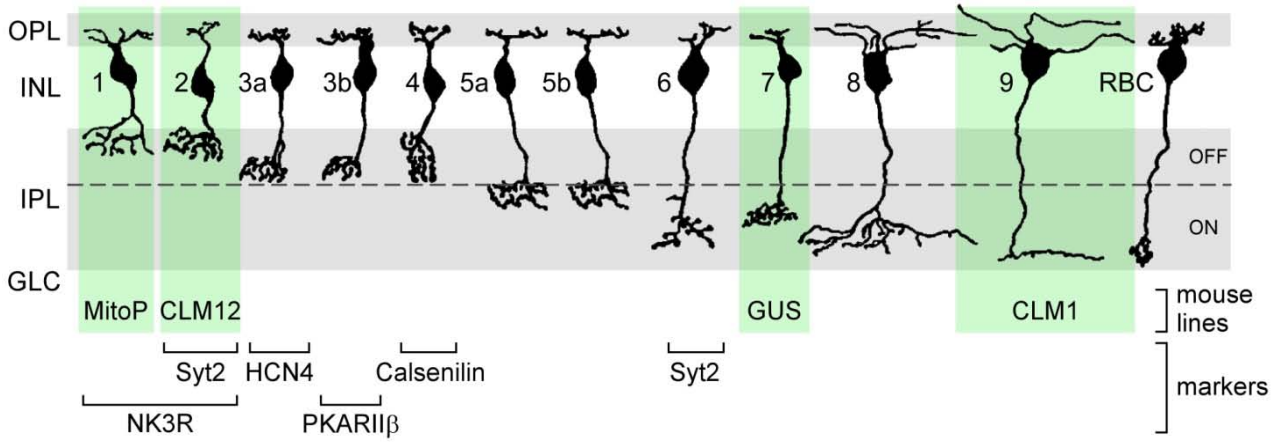

Figure 4: Bipolar cells of the mouse retina. There are five OFF-cone bipolar cell types, six ON-cone bipolar cell types, and one ON-rod bipolar cell (RBC) type. In this work the mouse-lines mitoP, CLM12, Gus-GFP, and CLM12 were used to specifically target type-1, type-2, type-7, and type-9 cone bipolar cells, respectively. The immunohistochemical markers NK3R, Syt2, HCN4, PKARIIβ, and calsenilin were used to specifically label type-1 and -2, type-2, type-3a, type-3b, and type-4 respectively (for details, see Methods). Figure modified from Wassle et al., 2009.

Since photoreceptors increase their release of glutamate when light levels decrease – they are basically OFF-cells – a signal inversion is necessary to achieve the response observed in ON-bipolar cells. This inversion takes place postsynaptically and involves the metabotropic glutamate receptor mGluR6 that is present in all ON-bipolar cells including the rod bipolar cell (Nakajima et al., 1993; Kikkawa et al., 1993; Nakanishi et al., 1994). OFF-bipolar cells express ionotropic glutamate receptors of AMPA (GluR1) and kainate subunits (GluR5 - 7 and KA2) that preserve the polarity of the signal (mouse/rat: Brandstatter and Hack, 2001; primate: Haverkamp et al., 2001a/b; Puller et al., 2007; ground squirrel: DeVries, 2000). Different types of OFF-bipolar cells can achieve different temporal response kinetics by predominant expression of either AMPA or kainate receptors (DeVries, 2000). ON- and OFF-bipolar cells also differ in their morphological fine structure; ON-bipolar cells invaginate the photoreceptor terminals with their dendritic tips; OFF-bipolar cells make basal contacts. (For details on the functional concept of the specialized complex synapse between photoreceptors, bipolar cells, and horizontal cells, see section 3.3.6.) Note that mammalian bipolar cells – like photoreceptor cells, horizontal cells, and many types of amacrine cells – do not generate “classical” action potentials and therefore are often referred to as non-spiking neurons: in these graded neurons, membrane potentials modulate transmitter release.

In addition to coding signal properties, such as polarity (ON vs. OFF) and different temporal frequency bands, some bipolar cells also represent separate channels to transmit cone-selective

signals through the retina. In primate retina (Mariani, 1984; Kouyama and Marshak, 1992) as well as in several other species – including rabbit (MacNeil and Gaul, 2008), rat (Euler and Wässle, 1995) ground squirrel (Linberg et al., 1996; Li and DeVries, 2006) and mouse (Haverkamp et al., 2005) – one type of S-cone selective ON-bipolar cell (also referred to as “blue-cone bipolar cell”) has been morphologically identified. However, M-cone selective OFF-bipolar cells that could act as counterparts to generate chromatic antagonism have not yet been unambiguously identified in most of these species (described in more detail, see sections 3.4 and 3.5).

3.3.4 Amacrine cells

With about 20 to 30 different types, amacrine cells are the most diverse class of mammalian retinal neurons (Figure 5). Aside from horizontal cells, amacrine cells are the second class of lateral retinal neurons and presumably are involved in a great variety of signal processing steps. The term “amacrine” (from Greek: a- "no", makrós "big", and inós "fiber") was coined by Ramón y Cajal (1852–1906) and means “axon-less”. Today we know that some types, in fact, feature axons, such as the poly-axonal amacrine cells (Famiglietti, 1992; Volgyi et al., 2001; Olveczky et al., 2003). In contrast to ganglion cells, however, amacrine cells do not send axons out of the retina via the optic nerve. The dendritic arbors of amacrine cells stratify in the IPL; their cell bodies are located in the INL, or in case of the “displaced” amacrine cells in the GCL. Amacrine cells receive input from bipolar cells as well as from other amacrine cells and provide input to bipolar cells, other amacrine cells and ganglion cells. Interplexiform amacrine cells are a mentionable exception as they also stratify in the IPL, but send sparse processes into the OPL. One type of interplexiform amacrine, the IPA-S4/5 (= interplexiform amacrine cell, stratifying in stratum 4 and 5 of the IPL) was examined in more detail in the present work. Since it co-stratifies with the S-cone selective typ-9 bipolar cell, it had been considered to play a role in chromatic processing (see section 5.4 and Dedek et al., 2009 for details).

Amacrine cells use a great variety of neurotransmitters (including GABA, glycine, dopamine, acetylcholine, and others). In most cases, a single type of amacrine cell releases either GABA or glycine plus additional co-transmitters or -modulators. Furthermore, amacrine cells can form electrical synapses with bipolar cells, ganglion cells, and/or other amacrine cells.

Because of their soma’s location in INL and the great functional diversity of amacrine cells, single-cell electrophysiology (e.g. patch-clamp recordings) is often not easily reproducible, with the exception of amacrine cell types that occur very frequently in the studied animals. For sparser amacrine cell types single-cell recordings with sufficient yield only becomes more feasible when using genetically-modified animals that express cell markers, for instance GFP, in specific subsets of cells.

So far, only a few amacrine cell types are functionally well understood. These intensely studied types include AII (for review, see Bloomfield and Dacheux, 2001), A17 (for review, see Schubert and Euler, 2010), polyaxonal (Famiglietti, 1992; Volgyi et al., 2001; Olveczky et al., 2003), and starburst amacrine cells (reviewed in Masland, 2005; Zhou and Lee, 2008). While AII and A17 cells play important roles in the classical rod pathway (discussed in section 6.6), polyax-

onal amacrine cells and starburst cells are involved in processing motion- and motion direction-dependent information, respectively.

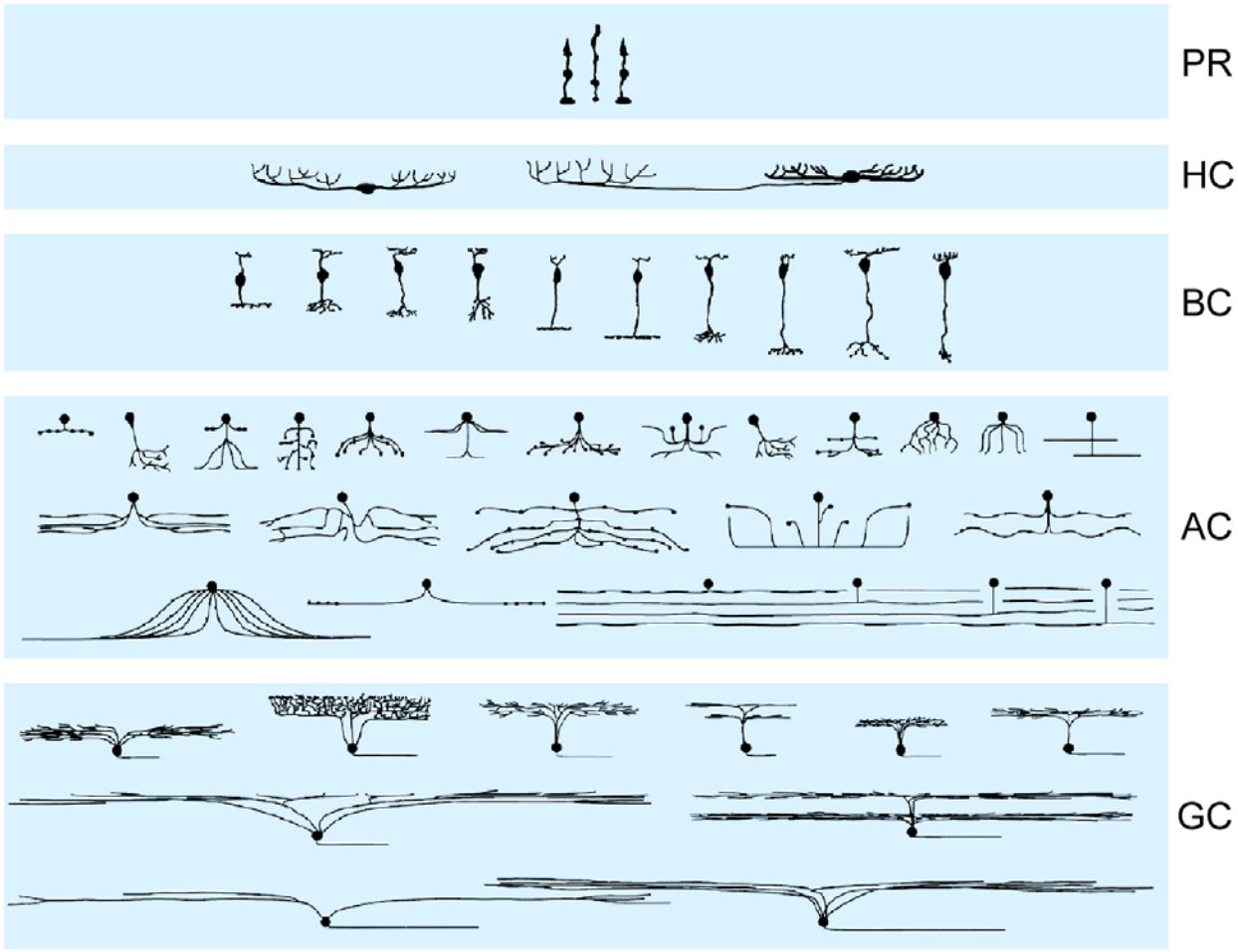

Figure 5: The neuronal cell classes of the mammalian retina. Photoreceptors (PR), horizontal cells (HC), bipolar cells (BC), amacrine cells (AC), and ganglion cells (GC). Amacrine cells are the most diverse class (MacNeil and Masland, 1998). Due to space restrictions, only a subset of the wide-field amacrine cells is shown. Figure modified from Masland, 2001.

The functional relevance of amacrine cells for chromatic processing is largely unknown. It is thought that amacrine cells play a role in the red/green midget pathway of primates to create the antagonistic surround that has been observed in midget ganglion cells (for review, see Dacey, 1996). As more and more mouse lines expressing fluorescent proteins in specific subsets of retinal neurons will be available, the prospects for revealing the functional role of further amacrine cell types are improving.

3.3.5 Ganglion cells

Ganglion cells are the output neurons of the retina (Figure 5); their axons form the optic nerve. They are spiking neurons since their signals have to travel the long distance from the retina to their various destinations in the brain. The optic nerve is often referred to as the bottleneck for the flow of visual information, because the output signals from ~ 130 million photoreceptors need to converge to ~ 1 million ganglion cells (in human retina). The limited bandwidth of the optic nerve is considered to be one important reason for the extended signal processing within the retina. Ganglion cells receive input from bipolar and amacrine cells via chemical synapses. In addition, they form electrical synapses with amacrine and other ganglion cells (Schubert et al., 2005; Bloomfield and Volgyi, 2009). Some types of ganglion cells are functionally well understood, for instance parasol cells (also "P alpha cells", primate: Rodieck et al., 1985; Dacey and Petersen, 1992; Grunert et al., 1993), midget ganglion cells (primate: Polyak, 1941; Rodieck et al., 1985; Dacey, 1993; Dacey, 1996; Calkins and Sterling, 1999; Kolb and Marshak, 2003), small bistratified cells (primate: Dacey and Lee, 1994; Dacey, 1996; Calkins et al., 1998; Dacey and Packer, 2003), and ON-OFF-direction-selective ganglion cells (rabbit: Barlow et al., 1964; Oyster, 1968; Amthor et al., 1989; He and Masland, 1997; mouse: Weng et al., 2005). In the mouse, ~ 22 types of ganglion cells have been morphologically identified (Sun et al., 2002; Badea and Nathans, 2004; Kong et al., 2005; Coombs et al., 2006; Volgyi et al., 2009); most of them are reminiscent of the times described in other mammals (e.g. cat or human retina).

Small bistratified ganglion cells (Figure 8; see also section 3.4) play an important role in primate color vision (Dacey, 1993; Dacey and Lee, 1994; Dacey, 1996; Dacey and Packer, 2003; Crook et al., 2009), since they have been shown to respond to light in a color-opponent (blue^{ON}/yellow^{OFF}) manner. Midget ganglion cells have been reported to display red/green (center/surround) responses with both polarities in central primate retina (reviewed in Dacey, 1996; Calkins and Sterling, 1999). Ganglion cells processing chromatic signals are described in more detail in section 3.4.

3.3.6 Input to bipolar cells

In this work, we examined the connectivity and the chromatic properties of mouse cone bipolar cells. They receive input from cone photoreceptors via a complex synapse in the OPL. The input is modulated by horizontal cells, which provide feedback to cones and possibly also feedforward to bipolar cell dendrites. The mechanisms of signal transmission and shaping are described in detail below.

Triad synapse at the cone pedicle

Although the retina has often been described as a simple model for neuronal networks, a large number of specialized and highly complex synaptic structures and electric coupling mechanism have been found in the mammalian retina that appear to be even more complex than what yet was found in the rest of the nervous system (Haverkamp et al., 2000). This is particularly true for the synapse between photoreceptors and their postsynaptic neurons.

The cone pedicle is invaginated by the dendritic tips of ON-bipolar cells and horizontal cells; OFF-bipolar cells make flat and basal contacts (Figure 6). The structures of invaginating processes of ON-bipolar cells and horizontal cells are remarkably well-arranged on nanometer scale (Figure 6 B); these structures are collectively termed “triad synapses”. Dependent on the light level, cones continuously release varying amounts of glutamate into the synaptic cleft. To allow for continuous glutamate release, the vesicles are transported to the release-site along a complex intracellular protein structure, the ribbon. Ribbon synapses are also known to exist in other sensory cells and specialized neurons (retinal bipolar cells, cochlear hair cells, vestibular organ receptors, and sensory cells of the lateral line organs in amphibians and fish). The protein composition of the ribbon has been intensely studied and will not be described here (reviewed in Vollrath and Spiwoksbecker, 1996; Zanazzi and Matthews, 2009).

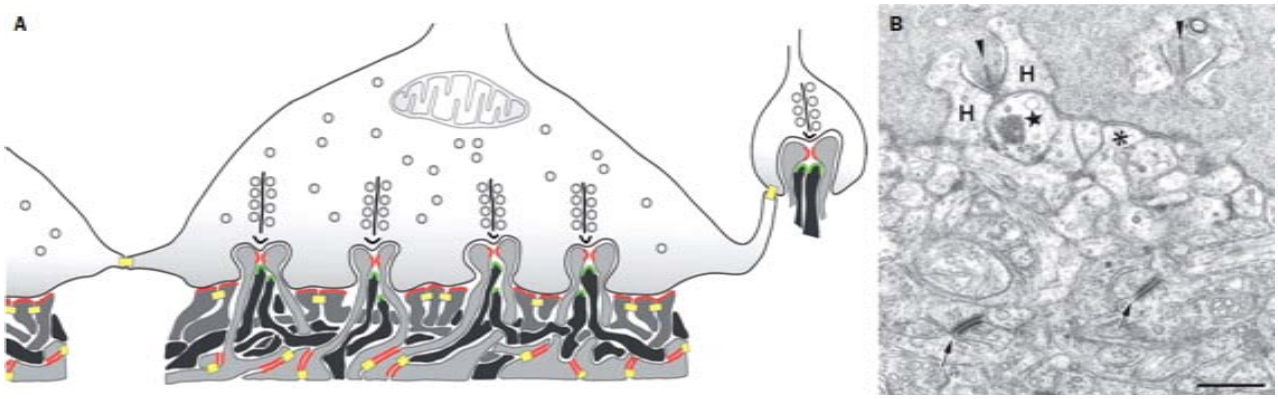

Figure 6: Synaptic structure at the cone pedicle. A: Schematic drawing of a cone pedicle contacted by the dendritic tips of postsynaptic neurons. Glutamate vesicles are tethered to the ribbon (above the invaginating triads). Dark gray: Processes of ON-bipolar with metabotropic glutamate receptors (GluRs, green). Light gray: Horizontal cells with ionotropic GluRs (iGluRs; red). Medium-gray: OFF-bipolar cells make basal contacts with iGluRs. Yellow: gap junctions between photoreceptor terminals, horizontal cell dendrites, and OFF-bipolar cell dendrites. B: Electron micrograph of the synaptic area of a cone pedicle. Arrowheads point to postsynaptic ribbons, horizontal cell (H) and ON-bipolar cell (star) dendrites are the post-synaptic partners. The asterisk marks a basal OFF-bipolar cell contact. Two arrows point to desmosome like junctions. Scale bar: 0.5 µm. Figure 6 A: from Puller et al., 2009; B: from Haverkamp et al., 2000.

While glutamate is released only into the triad-structure, the dendritic tips of OFF-bipolar cells are located at the basal side of the cone pedicle (Figure 6). GluRs of the AMPA-type were shown to operate more transient than of kainate-type. Also AMPA-type receptors were shown to be located closer to the triad, whereas kainate-type are not directly triad-associated (Haverkamp et al., 2001b; Puller et al., 2007). Therefore, the path of glutamate diffusion to the triad-associated processes is shorter than to the non-associated dendritic tips consistent with the functional finding that OFF-bipolar cells expressing mainly the AMPA-type of receptors exhibit faster and more transient responses compared with the kainate type (DeVries, 2000). The dendritic tips of horizontal cells in the triad are both, input and output structures; they receive excitatory glutamatergic input, feed back onto cones, and feed forward onto bipolar cells (see next section).

Cone photoreceptors pedicles are electrically coupled gap junctions to each other and to rods. These gap junctions are located at the tips of fine processes, called telodendria, that merge from the base of the cell and contact adjacent photoreceptors (Figure 6). Changes in membrane potential of one photoreceptor cell will affect the membrane potential of electrically coupled cells. In the case of cone-cone coupling the responsible protein is cx36 (in primate and mouse retina), but for rod-cone coupling the opposed protein partner is still unknown.

The primary advantage of electrical cone-cone coupling is noise reduction. Photoreceptor activation is strongly influenced by stochastic processes like the probability of photon absorption, fluctuations in local concentration of the signal cascade molecules, and ion channel opening probabilities. It has been calculated that homotypic cone coupling in the human fovea improves the signal-to-noise ratio in each cone by nearly 80% while the expected loss in visual resolution due to blurring is comparably small (DeVries et al., 2002).

Feedback and feedforward

Photoreceptors transmit their information to bipolar cells, but already at this first synaptic level horizontal cells serve as lateral interneurons to facilitate adaptation and the formation of receptive field surrounds in bipolar cells (Yang and Wu, 1991; Wu, 1992; Piccolino et al., 1984; Burkhardt, 1993; Kamermans and Spekreijse, 1999; Schwartz, 2002).

In the retina of several vertebrates, it has been shown that the horizontal cell feedback to cones is GABAergic (turtle: Kaneko and Tachibana, 1986; Tatsukawa et al., 2005; goldfish: Studholme and Yazulla, 1988; Verweij et al., 1998; salamander: Skrzypek and Werblin, 1983; Wu, 1991; Yang and Wu, 1993). In mammals, horizontal cells release GABA, at least during development; cones and horizontal cells express ionotropic GABA-receptors (Schubert et al., 2010). However, the functional relevance of GABAergic feedback mechanism in adult animals is still discussed controversially (reviewed by Kamermans and Fahrenfort, 2004; but see Guo et al., 2010).

In the last ~ 20 years two additional, ephaptic feedback mechanisms – involving “hemi-channels” and/or changes in pH – have been identified (Byzov and Shura-Bura, 1986; Kamermans et al., 2001; Kamermans and Fahrenfort, 2004; Barnes and Bui, 1991; Barnes et al., 1993; Davenport et al., 2008). Both mechanisms presumably directly influence the activation of voltage-gated Ca^{2+} channels in the cone terminals (Verweij et al., 1996; Hirasawa and Kaneko, 2003; Cadetti and Thoreson, 2006). Ephaptic interactions (current modulation through the extracellular space between neighboring neurons) have been shown to play a role in other parts of the brain (goldfish mesencephalon: Furukawa and Furshpan, 1963; rat cerebellum: Korn and Axelrad, 1980; rat olfactory system: Bokil et al., 2001). In the case of horizontal cell feedback it has been proposed that the extracellular concentration of cations in the synaptic cleft of the triad synapse is modulated via hemi channels (for review, see Kamermans and Fahrenfort, 2004). These are “half gap junctions” with connexins located at the invaginating tips of the horizontal cell dendrites but not in the membrane of the opposed cone pedicles. This directly affects the activation-probability of voltage-gated Ca^{2+} channels located in the cone membrane. A second me-

chanism was demonstrated in pharmacological experiments in which pH-buffering had a strong effect on horizontal feedback and surround formation (tiger salamander: Barnes and Bui, 1991; Barnes et al., 1993; primate: Davenport et al., 2008). This sensitivity to pH buffers, such as HEPES, supports a proton-dependent mechanism, according to which light-driven hyperpolarization of the horizontal cell alkalinizes the cone synaptic cleft. The decrease in proton concentration shifts the activation curve of voltage gated Ca^{2+} channels toward lower voltages.

In addition to the feedback to cones, at least in some vertebrate species horizontal cells directly feed-forward to bipolar cells (salamander: Hare and Owen, 1996; Yang and Wu, 1991; carp: Toyoda and Kujiraoka, 1982) and both sub-classes, ON- and OFF-bipolar cells possess dendritic ionotropic GABA receptors (Enz et al., 1996; Greferath et al., 1994; Vardi and Sterling, 1994). It has been shown that GABA has a depolarizing effect on mammalian ON-bipolar cells while it hyperpolarizes OFF-bipolar cells due to a higher Cl^- concentration in the dendrites of ON-bipolar cells (rat: Euler and Wässle, 1998; mouse: Satoh et al., 2001; Varela et al., 2005; Duebel et al., 2006).

Other potential sources for GABA in the OPL, besides the release from horizontal cells, are interplexiform amacrine cells (Dedek et al., 2009). In any case, it remains unclear whether GABAergic feed-forward, as well as GABAergic feedback are common mechanisms for lateral inhibition in all adult mammals.

3.4 Chromatic processing in the primate retina

Already in the early 19th century two modern and complementary theories of color vision were proposed. The trichromatic theory, proposed by Thomas Young and Hermann von Helmholtz around 1850, stated that there are three types of receptors in the human eye that are primarily sensitive to violet-blue, green-yellow, and orange-red.

The opponent process theory proposed in 1872 by Ewald Hering was based on psychophysical experiments and suggested that color vision is organized in opponent channels (blue vs. yellow, red vs. green, and white vs. black). The underlying observation was that objects appear to an observer, for instance, as either yellow or blue but never show a mixture of yellowish-blue (see also Hurvich and Jameson, 1957). In 1960, Hubel and Wiesel directly demonstrated with extracellular recordings from the optic nerve of spider monkeys that color opponent signals are present in the visual stream as early as at the level of the retinal output.

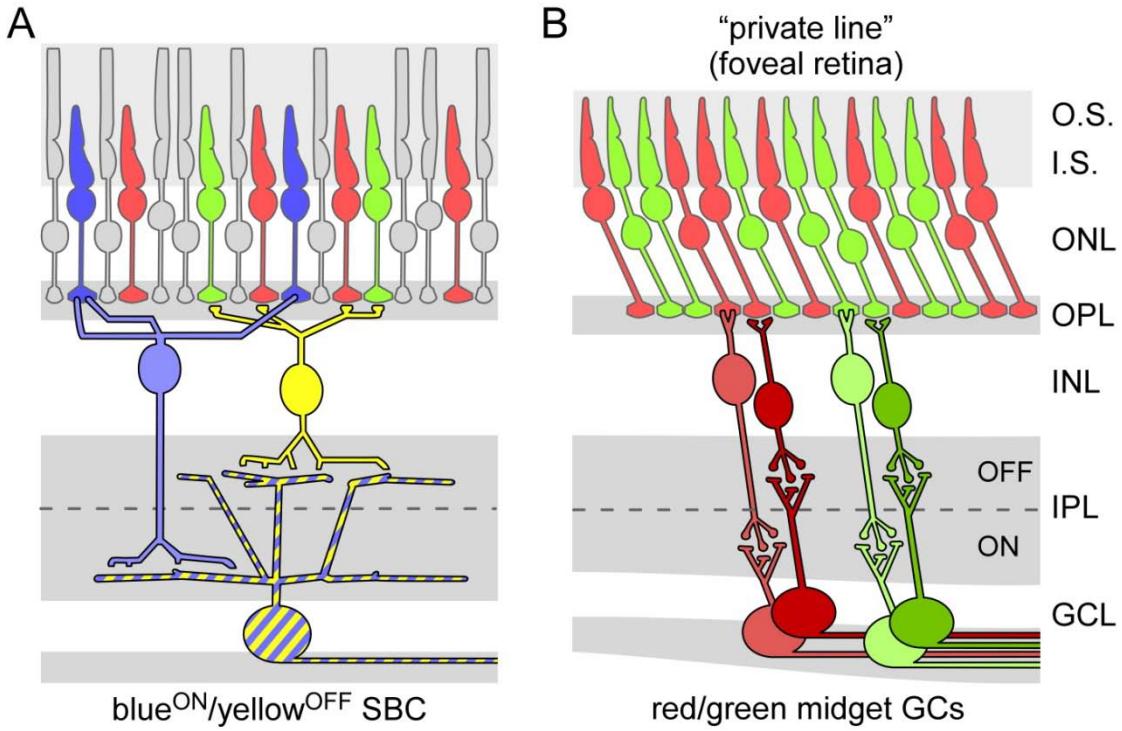

Figure 7 A: The blue^{ON}/yellow^{OFF} small bistratified (SBC) pathway in primate retina. S-cone selective ON-bipolar cells receive input from S-cones and transmit the signal to the outer dendritic tree of the SBC. Diffuse OFF-bipolar cells contact M- and L-cones and transmit the signal to the inner dendritic tree of the SBC. B: In the fovea (specialized center of primate retina) ON- and OFF-midget bipolar cells contact a single cone. In a "private line" connection they transmit the signal to ON- and OFF-midget ganglion cells. Therefore these cells are by definition chromatically selective.

3.4.1 Blue/yellow-antagonistic pathways

Because the sensitivity spectra of the cone types overlap extensively (Figure 2; section 3.3.1) comparative computation in postsynaptic neurons is a necessary step to allow for reasonable chromatic discrimination. Bipolar cells act as parallel channels to transmit cone specific signals through the retina and provide selective input to ganglion cells. In primate retina the small bistratified ganglion cell responds to light in a color-opponent (blue^{ON}/yellow^{OFF}) manner (Figure 7 A; Figure 8; for review, see Dacey and Packer, 2003). Small bistratified ganglion cells receive direct input from S-cone selective ON-bipolar cells (Mariani, 1984; Kouyama and Marshak, 1992) and diffuse OFF-bipolar cells (Calkins et al., 1998; Crook et al., 2009). The latter have been shown to show some bias for M- and L-cones (Lee and Grunert, 2007).

Aside from the small bistratified cell, two other blue/yellow opponent ganglion cells have been reported in primates (Dacey and Packer, 2003). One of these ganglion cells is a large sparse monostratified cell that exhibits yellow^{ON}/blue^{OFF} responses, possibly involving amacrine cells to create the chromatic antagonism. The other is a large sparse bistratified cell exhibiting blue^{ON}/yellow^{OFF} responses.

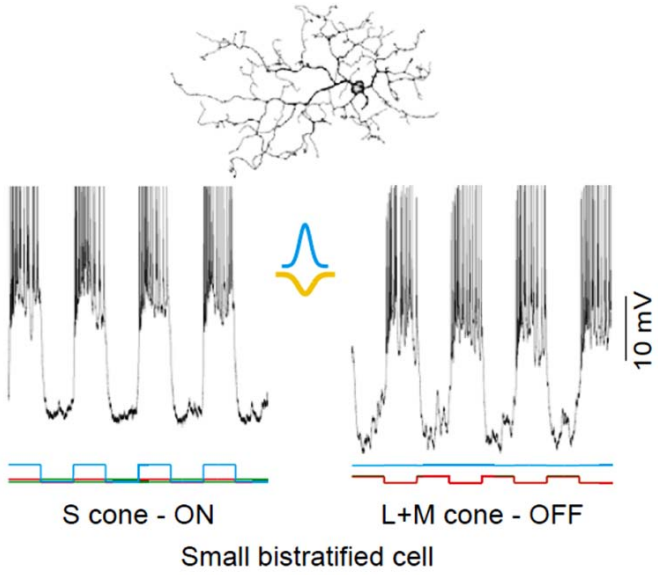

Figure 8: Small bistratified ganglion cell; electrophysiology (intracellularly recorded light responses). Top: dendritic morphology. Center: a schematic of the receptive field structure is shown (blue^{ON}/yellow^{OFF}); it was estimated using the intracellular responses to drifting gratings that modulated either the S-cones or the L- and M-cones in isolation. The stimulus was a 2 Hz square wave modulation. Figure: from Dacey and Packer, 2003.

3.4.2 Red/green-antagonistic pathways

In primates, color is processed along two primary axes: blue/yellow and red/green. The origin of red/green opponency has turned out to be more difficult to study than the origin of blue/yellow opponency. Midget ganglion cells, which had been suggested candidate cells carrying the red/green signal, rarely show clear red/green-opponency when recorded in peripheral primate retina. However, in the central retina a high number of color-opponent midget ganglion cells have been found with either red or green center responses and opposite or mixed (L + M) surround (reviewed in Dacey et al., 1996; Calkins and Sterling, 1999).

These findings can be explained by the concept of “private line” connections (Kolb and Dekorver, 1991; Boycott and Wässle, 1991; Calkins et al., 1994; Kolb and Marshak, 2003). In the fovea, the highly specialized central area of the primate retina, a single midget ganglion cell receives input from a single midget bipolar cell, which in turn receives input from a single cone (Figure 7 B). Therefore, central midget ganglion cells fulfill two functions at the same time: they serve as a channel for high visual acuity and as a dedicated red- or green-center channel. With increasing distance from the center, midget bipolar cell dendritic fields grow in size and in the number of contacted cones. This results in chromatically “impure” center responses. Thus, the persistence of strong red/green antagonistic signals also in the retinal periphery is still not completely understood. It was suggested that the inhomogeneous shape of dendritic trees of midget ganglion cells could enhance chromatic bias of midget cells in the periphery (Wässle and Boycott, 1991). Also the “clumpy” arrangement of the L- and M- cone mosaic leads to an enhanced chromatic bias in some midget ganglion cells and increase red/green discrimination (Goodchild et al., 1996b).

Recent findings based on quantitative analysis of peripheral midget bipolar cells (Diller et al., 2004; Jusuf et al., 2006; Telkes et al., 2008) are more consisted with a “random connection

model" (Lennie, 1980; Paulus and Kroger-Paulus, 1983) than with a "selective connection model" (Reid and Shapley, 1992; Dacey, 1993; Lee et al., 1998; Martin et al., 2001); therefore higher visual centers may use the partially red/green opponent signals produced by the midget pathway to create robust red/green color vision The finding, that no other ganglion cell type besides is known to carry antagonistic red/green-signals supports the idea that the midget pathway provides the basis for red/green vision in primate retina.

3.5 Chromatic processing in the mouse retina

Color vision tends to focus on primates which are color specialists. In contrast, most non-primate mammals are dichromats. Nonetheless blue/green (primate: blue/yellow) chromatic processing is thought to be organized in homologues pathways. The demonstration of the presence of a blue/green circuitry in animals specialized in vision at low light intensities would lend strong support to the idea of a common blueprint for chromatic processing in the mammalian retina. The retinas of rats and mice as important model animals in neuroscience, are strongly dominated by rods and contain only low percentages of cones (mice ≈ 3 %, Jacobs et al., 2004; rats ≈ 1 %, Szél and Roehlich, 1992). Note, however, that the peripheral human retina is also strongly rod dominated (~ 90 % rods of total photoreceptor density; Curcio et al., 1987; Jonas et al., 1992).

Figure 9: Distribution of blue cones across the mouse retina. A: Horizontal view of S-opsin-expressing cone outer segments in a whole-mounted mouse retina. In the dorsal retina (left), only a few cones express S-opsin; in the ventral retina, the vast majority of cones express S-opsin (right). B: Cell density (logarithmic scale) over retinal distance (for details, see (Haverkamp et al., 2005)). Open circles represent cone pedicles contacted by blue-cone bipolar cells, asterisks represent blue-bipolar cells, and filled circles represent S-opsin-expressing cones. Scale bar in A: 50 µm. Figure modified from Haverkamp et al., 2005.

Despite the numerical dominance of rods, mice feature – like most non-primate mammals – two types of cones: M-cones with their absorption peak at ≈ 510 nm, and S-cones with their absorption peak in the near UV spectral range at ≈ 360 nm (Jacobs et al., 1991). Mice possess a dorso-ventral gradient of opsin expression. At first, it was thought that the two cone types topographically are separated, with S-cones only present in the ventral half and M-cones only present in the dorsal half (Szel et al., 1992). However, closer examinations have shown that both cones types are present throughout the whole retina, with the great majority of mid and ventral M-cones expressing both S- and M-opsin. The level of S-opsin co-expression has been shown to strongly depend on the location of the M-cone along the dorso-ventral axis (Roehlich et al., 1994;

Applebury et al., 2000; Haverkamp et al., 2005; Figure 9). It is important to note that "true" S-cones, such as those in primates and other species, exist in ventral and dorsal retina at similar densities and are selectively contacted by S-cone selective bipolar cells (Haverkamp et al., 2005). Nonetheless, the opsin expression gradient affects retinal blue/green opponency, as shown in guinea pig (Yin et al., 2009). Thus, the mouse also offers the possibility of studying circuit performance as a function of opsin co-expression ratio. Note that similar dorso-ventral gradients have been described for other mammalian species, including guinea pig (Roehlich et al., 1994) and rabbit (Juliusson et al., 1994; Famiglietti and Sharpe, 1995).

Cone-type selective bipolar cells, such as the blue-cone bipolar cell in primate (section 3.3.3; Mariani, 1984; Kouyama and Marshak, 1992), have been also identified in other species – including rabbit (MacNeil and Gaul, 2008), rat (Euler and Wässle, 1995), ground squirrel (Linberg et al., 1996; Li and DeVries, 2006), and mouse (Haverkamp et al., 2005). However, M-cone selective OFF-bipolar cells that could act as counterparts to generate chromatic opponent signals in ganglion cells, have not yet been unambiguously identified in most of these species. With respect to chromatic bipolar cell pathways, the ground squirrel – which possesses a cone-dominated retina (Kryger et al., 1998) – is among the best studied non-primate mammals. Immunohistochemistry and dual patch-clamp recordings with electrical cone stimulation have confirmed the presence of S-cone selective bipolar cells (presumably blue^{ON}) and revealed that at least two types of OFF-bipolar cells avoid contacts with S-cones and are therefore expected to relay green OFF-signals (Li and DeVries, 2006). Studying the respective OFF-bipolar cell pathways in the mouse, as performed in the present work, became feasible because in the last years several mouse lines expressing fluorescent proteins in subsets of neurons have been described, including type-1, type-2, type-3a and b, and type-4 OFF-bipolar cells (Berglund et al., 2004); (Misgeld et al., 2007).

As described before (section 0) three different types of primate ganglion display blue/yellow opponent responses (for review, see Dacey and Packer, 2003). Furthermore, large monostratified blue/green opponent ganglion cells of both polarities have been recently described in guinea pig, both with dendrites stratifying in the ON-sublamina of the IPL (Yin et al., 2009). Like in rabbit (Caldwell and Daw, 1978; De Monasterio, 1978) color-opponent ganglion cells have also been reported in mouse retina (Ekesten et al., 2000; Ekesten and Gouras, 2005), but not yet morphologically identified. Morphologically suitable bistratified ganglion cells with dendrites stratifying in the appropriate strata of the IPL have been described in mouse (type-1: Schubert et al., 2005; type G12: Volgyi et al., 2009). Extracellular recordings from mouse striate cortex (Ekesten and Gouras, 2008) provided evidence for the preservation of blue/green opponent signals at higher processing levels in the brain – suggesting that mice possess color perception. Indeed, although color cues appear to play a minor role for mice, they are able to perform color discrimination in carefully designed behavioral tests (Jacobs et al., 2004; Jacobs et al., 2007).

3.6 Purpose and Contributions

3.6.1 Purpose of this Study

The aim of this work was to investigate the chromatic pathways in the retina of the mouse, an animal specialized in vision at low light intensities. Demonstrating the presences a circuit homologues to what has been described in primates would further strengthen the idea of a common blueprint of the mammalian retina. Furthermore, the mouse, featuring the advantage of easy genetic modification, could then be used as a mammalian model for retinal color processing. To investigate cone-connectivity and chromatic tuning of cone bipolar cells we used anatomical methods as well as electrophysiological recordings with dichromatic light stimulation.

In close collaboration with S. Haverkamp and C. Puller (MPI for Brain Research, Frankfurt/M.), immunohistochemical methods and light microscopy were used to study the anatomical connectivity between cones, the different types of OFF-bipolar cells (type 1, 2, 3a, 3b, and 4) and one type of ON-bipolar cell (type 7). To target the cells we made use of transgenic mouse lines and specific antibodies. All immunohistochemical experiments and the analysis of morphological data were performed by S. Haverkamp and C. Puller (see Contributions).

The S-cone selective ON-bipolar cell (type 9) was previously identified morphologically (Haverkamp et al., 2005), but their electrophysiological responses to chromatic light stimulation remained untested. Using the CLM1 mouse line that expresses the fluorescent protein clomeleon in a specific subset of neurons including type-9 cells, it was possible to identify and intracellularly record this cell type while stimulating with dichromatic light.

We also searched for M-cone selective OFF-bipolar cells that could serve as counterparts to S-cone selective ON-bipolar cells in creating S-/M-antagonism in specific ganglion cells. From the anatomical experiments two types of OFF-bipolar cells emerged as candidates for M-cone selective cells. We studied the electrophysiology of these candidate cells to identify differences in chromatic tuning.

We also investigated the impact of the strong cone-opsin expression gradient along dorso-ventral axis in mice using intracellular recordings of bipolar cells at different positions along this gradient. We addressed the questions of whether this gradient is reflected in our electrophysiological recordings and whether chromatic processing is supported in the ventral retina, were co-expression is high.

In addition to the analysis of bipolar cells, we examined chromatic properties of the IPA-S4/5-type interplexiform amacrine cell. We used the $Cx45^{+}$ / fl:Parv-Cre mouse line that expresses GFP in IPA-S4/5 cells (Dedek et al., 2009) to target these amacrine cells. Since IPA-S4/5 cells co-stratify with axon terminals of S-cone selective type 9 bipolar cells in stratum S5 of the IPL (Figure 4; Haverkamp et al., 2005), we wanted to test with electrophysiological methods if these amacrine cells receive input from the S-cone selective type-9 bipolar cells.

3.6.2 Contributions

During my PhD thesis I contributed to three studies, two of which are published, while the third is about to be submitted. All three studies are covered by the present work, with a focus on the third, which represents the main part of my PhD work. Tthe contributions to each publication are listed in detail below.

Contributions to study 1 (Euler et al., 2009)

My main contribution to Euler et al., 2009 was the modification calibration and testing of the visual stimulator (see section 4.3.3), a prerequisite for studies 2 and 3. This amounts to ~ 10% of my PhD thesis.

Contributions to study 2 (Dedek et al., 2009)

My contributions to Dedek et al., 2009 were the electrical recordings with chromatic light stimulation of mouse interplexiform amacrine cells (see section 5.4). This amounts to ~ 10% of my PhD thesis.

Contributions to study 3 (Breuninger et al., to be submitted in Nov. 2010)

This study represents the main part of my PhD thesis (80%). For this purpose I performed following experimental procedures and methods:

- tissue preparation for electrophysiology (section 4.1)
- modification and calibration of the LCoS light stimulator (section 4.3.3)
- design of appropriate stimulation protocols (section 4.3.3 and Figure 18)
- design and construction of a second type of LED-based light stimulator (section 4.3.3)
- electrical recordings and light stimulation of cone bipolar cells (sections 4.3.2 and 4.3.3)
- analysis of electrophysiological data (section 4.3.4)
- development of the statistical model, together with T. Euler (section 4.3.5)

The following experimental procedures and methods were carried out by S. Haverkamp and C. Puller at the MPI for Brain Research (Frankfurt a.M., Germany):

- tissue preparation for immunocytochemistry (section 4.1)
- antibody stainings (section 4.2.1)
- light microscopy (section 4.2.2)
- image analysis (section 4.2.3).

4 MATERIAL AND METHODS

4.1 Animals and tissue preparation

Animals usage

Four mouse lines expressing fluorescent proteins in different subpopulations of bipolar cells were used: mitoP-CFP (Misgeld et al., 2007; Schubert et al., 2008) for type-1 OF-bipolar cells, CLM1 and CLM12 (Berglund et al., 2004) for type-9 ON bipolar cells and type-2 OFF-bipolar cells, respectively, as well as Gus-GFP (GUS8.4GFP: Wong et al., 1999; Huang et al., 2003) for type-7 ON bipolar cells. In addition, one mouse line expressing GFP in IPA-S4/5 cells, the $Cx45^{+}$ / fl:Parv-Cre mouse line (Dedek et al., 2009) was used to target interplexiform amacrine cells. For the physiological measurements, mice (>8 weeks) were dark adapted for at least two hours before the experiment and all subsequent procedures were carried out under dim red illumination. The animals were anesthetized with Isoflurane (Baxter, Unterschleißheim, Germany) inhalation and killed by cervical dislocation. All procedures were approved by the local animal care committee and were in accordance with the law of animal experimentation issued by the German Federal Government (Tierschutzgesetz).

Tissue preparation, immunocytochemistry

For immunecytochemistry, the eyes were removed and dissected, and the posterior eye cup containing the retina was immediately immersed in 4 % (w/v) paraformaldehyde in 0.1 M phosphate buffer (PB), pH 7.4, for 20 minutes. After fixation, the retina was dissected from the eyecup. For cryostat sections it was cryoprotected in graded sucrose solutions (10, 20 and 30 % w/v, respectively) and cut at 25 µm, mounted and stored at -20 °C. For retinal whole-mounts, the tissue was cryoprotected and frozen and thawed several times. Whole-mounts were processed free-floating.

Tissue preparation, electrophysiology

For electrophysiology, the eyes were marked dorsally with a permanent Edding 400 marker (edding GmbH, Ahrensburg, Germany), enucleated and transferred to a Petridish containing carboxygenated (95 % O_2 / 5 % CO_2) Ringer's solution (Biometra, Göttingen, Germany) at room temperature. Then the retina was dissected out from the posterior eyecup – while keeping track of the retinal orientation. Vertical slices (≈ 200 µm thick) were cut manually (Edwards et al., 1989; Euler et al., 1996) with the scalpel blade oriented perpendicular to the retina's dorso-ventral axis. The slices were arranged in the microscope recording chamber, where they were held in place by a platinum "harp" with nylon strings (Edwards et al., 1989) and superfused (at ≈ 3 ml/min) with warmed (≈ 34°C) carboxygenated Ringer's solution.

4.2 Immunohistochemical methods

All immunohistochemical experiments were carried out by S. Haverkamp and C. Puller at the MPI for brain research (Frankfurt a.M., Germany). Since our close collaboration has been addressing the same scientific question with complementary methods the results are presented in this work (for contributions, see also section 3.6.2).

4.2.1 Antibodies

Rabbit anti-GFP (1:2000, Molecular Probes) and goat anti-GFP (1:1000, Rockland) were used to amplify the signal of the different fluorescent proteins (clomeleon, CFP, and GFP) expressed in the transgenic mouse lines. Cone pedicles were labeled with a guinea pig antiserum against glycogen phosphorylase (1:1000; Pfeiffer-Guglielmi et al., 2003), kind gift of B. Hamprecht and B. Pfeiffer-Guglielmi (University of Tübingen, Germany) or goat anti-GluR5 (1:100; Santa Cruz Biotechnology). Goat anti-S-opsin (Santa Cruz Biotechnology) was used at a concentration of 1:1000. To label specific types of bipolar cells we used the following antibodies:

- anti-neurokinin-3 receptor (NK3R; rabbit, 1:500; kind gift of A. Hirano, Geffen School of Medicine at UCLA, Los Angeles, CA) for type-1/2 bipolar cells (Haverkamp et al., 2003; Ghosh et al., 2004; Pignatelli and Strettoi, 2004)
- anti-synaptotagmin II (Syt2/Znp-1; mouse, 1:300; Zebrafish International Resource Center University of Oregon, Eugene, OR) for type-2 bipolar cells (Fox and Sanes, 2007; Wassle et al., 2009)
- anti-hyperpolarization-activated cyclic-nucleotide gated channel 4 (HCN4; rabbit, 1:500; Alamone, Jerusalem, Israel) for type-3a bipolar cells (Mataruga et al., 2007)
- anti-protein kinase A, regulatory subunit IIβ (PKARIIβ; mouse, 1:2000; BD Biosciences, Germany) for type-3b bipolar cells (Mataruga et al., 2007)
- anti-calsenilin (Csen; mouse, 1:2000; kind gift of W. Wasco, Harvard Medical School, Charlestown, MA) for type-4 bipolar cells (Haverkamp et al., 2008).

Antibodies were diluted in PB, containing 0.5 – 1 % Triton X-100, 0.02 % sodium azide, 3 % normal donkey serum, and 1 % bovine serum albumin. In the case of NK3R-staining, antibodies were diluted in 0.01 M phosphate buffered saline, pH 7.4, containing 0.5 – 1 % Triton X-100 and 0.02 % sodium azide but without a blocking substance. Cryostat sections were incubated overnight in a mixture of primary antibodies, followed by incubation (2 hrs) in a mixture of secondary antibodies, which were conjugated to either Alexa Fluor 488 (Molecular Probes), Cy3 or Cy5 (Dianova, Hamburg, Germany). Whole-mounts were incubated for 2 days in the primary and for 3 hrs in the secondary antibody solution. The Alexa Fluor 594 or 647 conjugated lectin peanut agglutinin (PNA, Molecular Probes) was added to the secondary antibody solution and used at a 1:200 concentration.

4.2.2 Light microscopy

Fluorescent specimens were viewed with a Zeiss Axioplan 2 microscope (Zeiss, Jena, Germany). Images were taken using a CCD-camera (Zeiss, AxioCam Mrm) and the Zeiss AxioVision 4.2 software. The microscope was equipped with a Plan-Neofluar 63x/1.4 oil immersion objective and with the Zeiss ApoTome oscillating grating to reduce of out of focus straylight. Confocal micrographs were taken using LSM 5 Pascal (Zeiss) or FluoView 1000 (Olympus) fluorescence microscopes equipped with argon and a HeNe lasers. Scanning was performed with Plan-Apochromate 63x1.4 or UPlanSapo 60x/1.35 oil immersion objectives at 1024 x 1024 pixels and a z-axis increment of 0.32 µm. When projections of image stacks are shown, 3 - 5 serial optical sections were collapsed into a single plane. Brightness and contrast of the final images were adjusted using Adobe Photoshop CS v8.0.1 (San Jose, CA).

4.2.3 Image analysis

ImageJ (v1.38, http://rsbweb.nih.gov/ij/) was used to measure areas of immunoreactivity in micrographs. For this, unmodified grey scale images of single channels were loaded and color-inverted. Scale and threshold of each image was set before the regions of interest were outlined. The pixel size of immunoreactivity within each region was then calculated and summed by the software. If not indicated otherwise, the Student´s *t*-test was used to determine statistical significance between corresponding samples.

4.3 Two-photon microscopy and patch-clamp recordings

4.3.1 Eyecup scope

The eyecup scope is a custom-built two-photon (2P) microscope (Figure 10; Denk et al., 1990) developed at the MPImF Heidelberg and described in detail earlier (Euler et al., 2009). The upright laser scanning microscope was designed to allow 2P epi-fluorescent imaging, electrical recordings, and high-resolution visual stimulation on superfused retinal tissue. Dichromatic high-resolution visual stimuli, spatially and temporally modulated by a LCoS display (section 4.3.3), were delivered through the imaging objective; an additional simple LED-stimulator was installed under the microscope condenser (Figure 10). Two detection channels for fluorescence imaging were used (red, HQ 622 BP 36, and green, D 535 BP 50 or 520 BP 30; AHF/Chroma, Tübingen, Germany). The 2P excitation source was a mode-locked Ti/sapphire laser (Mira-900, Coherent, Dieburg, Germany) tuned to ≈ 925 nm. The 2P microscope was used to visualize retinal slices by adding low concentrations of a non-toxic fluorescent SR101 dye (~ 3 µM, sulforhodamine 101, Sigma) to the perfusion medium (Euler et al., 2009) as well as to identify and target fluorescent protein-expressing bipolar cells for electrical recordings. In addition, the microscope was equipped with simple infrared trans-illumination and a CCD camera.

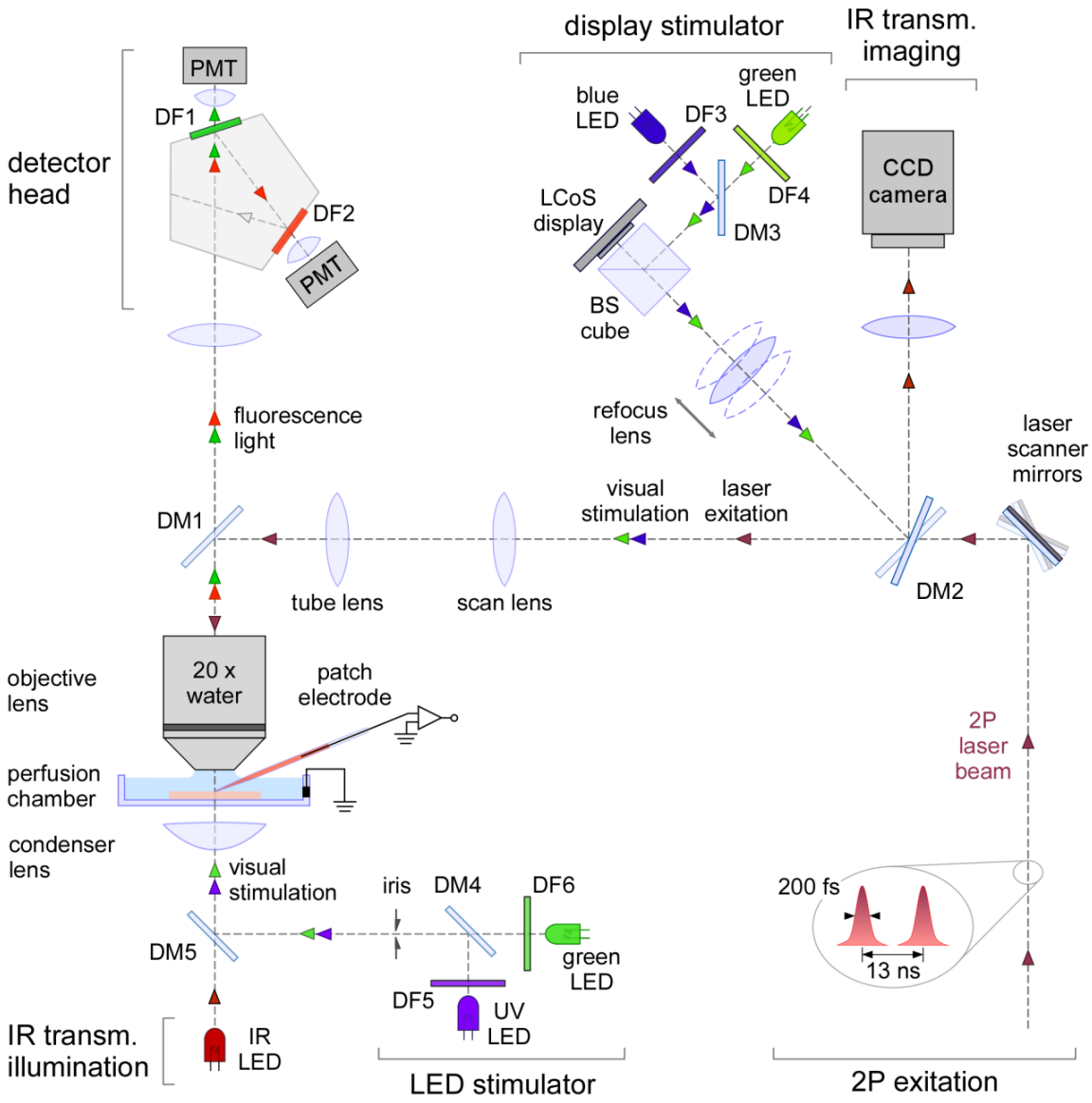

Figure 10: Schematic drawing of the eyecup scope. Fluorescence in the specimen (located in the perfusion chamber) is excited by the 2P laser beam (mode-locked Ti/sapphire laser), which is rastered by two laser scanner mirrors; the dichroic mirror (DM) 1 reflects IR and stimulation light while it transmits fluorescent light; the 20 x water objective lens focuses the beam on the specimen. The detector head holds two band-pass filtered (DF1: 535 BP 50; DF2: 633 BP 36) photo-multipliers (PMTs) and allows two channel recordings. Neurons in the specimen can be patched either under infrared (IR) transmission imaging or 2P fluorescence imaging (components for IR imaging: IR LED and CCD camera). High resolution visual stimulation is applied through the objective; the LCoS (liquid crystal on silicon) display stimulator is illuminated via the polarizing beam splitter (BS) cube by two band-pass filtered (DF3 and 4) commercial light emitting diodes (LEDs, blue: 400 BP 20; green: 578 BP 10) combined by DM3; the refocus lens allows adjusts of the stimulus focal plane; the DM2 reflects visual stimulation light while it transmits the infrared 2P laser beam. A second visual stimulator allows for stimulation through the condenser lens, light from two band-pass filtered LEDs is combined by DM5 (UV: 360 BP 10; green: 510 BP 10). Figure modified from Euler et al., 2009.

4.3.2 Electrophysiological recordings

The retinal slices were placed in the microscope recording chamber and visualized with both, infrared transmission illumination and 2P fluorescence imaging. Cellular debris above a fluorescently-labeled cell was cleared using a suction pipette. Candidate cells expressing fluorescent proteins (different proteins in different mouse lines; described in section 4.1) were approached with a fresh patch pipette, after washing out extracellular SR101. Cells were recorded in tight-seal whole-cell configuration using patch pipettes (5-15 MΩ, borosilicate, O.D.: 1.0 mm, I.D.: 0.58 mm, with filament; Hilgenberg) filled with (in mM) K-aspartate 100, KCl 10, $CaCl_2$ 0.5, $(NMG)_2$-HEDTA 5, HEPES 5, ATP 1, GTP 1, K_2-phosphocreatine 10 (Sigma-Aldrich) and 200 µM SR101 (Invitrogen) while applying visual stimulation. Data were acquired using a Multiclamp amplifier (w/Digidata 1322A and pClamp8 software, Molecular Devices, Berkshire, UK), digitized (5 kHz), low-pass filtered (2 kHz) and analyzed off-line in IgorPro (Wavemetrics, Portland, OR, USA).

4.3.3 Light stimulation

Two dichromatic visual stimulators were modified and calibrated to allow defined and reproducible light stimulation: 1) A miniature display-based high resolution stimulator that projected spatio-temporal structured light onto the retina through the imaging objective of the eyecup scope. 2) A simple LED-stimulator was designed that allowed temporally modulated stimulation through the microscope condenser.

To assure constant stimulation conditions the intensities of both stimulators were frequently monitored at the level of the recording chamber using a photometer (Model 840, Newport, Darmstadt, Germany) and calibrated when necessary.

LCoS-display stimulator

The first stimulator used an 800x600 pixel miniature "liquid crystal on silicon" (LCoS) display, removed from a pair of commercial head-mounted virtual reality (VR) goggles (i-glasses, EST, Kaiserslautern, Germany), that was alternately illuminated by two band pass-filtered (green: 578 BP 10; blue: 400 BP 20, AHF/Chroma) light emitting diodes (LEDs), with an 80 Hz refresh rate (Euler et al., 2009). It used custom-written software running on a PC (with Windows XP, Microsoft). The light of the LCoS-display stimulator was coupled into the main optical path of the microscope so that the stimuli were projected onto the retinal slice through the objective lens (XLUMPlanFL 20× water-immersion, 0.95 NA, Olympus). Note that the choice of the blue band (see below) was limited by transmission properties of the microscope components and the fact that the display did not efficiently modulate wavelengths < 400 nm.

The stimulus protocol used for electrophysiological recordings was a bright spot (diameter 80 µm - 200 µm) on back-ground illumination of ≈ 20%, centered on the photoreceptors distal to the recorded bipolar cell (compare with Figure 18 A). Within the applied stimulation range, we did not observe any effect of stimulus diameter on chromatic tuning of bipolar cell responses. We

therefore decided to pool all data recorded with different spot diameters. The intensities of the respective blue and green components were stepped (flashes) or modulated sinusoidally (at 1 Hz, in-phase or phase-shifted by 180°) in sync or independently (Figure 16 B, C).

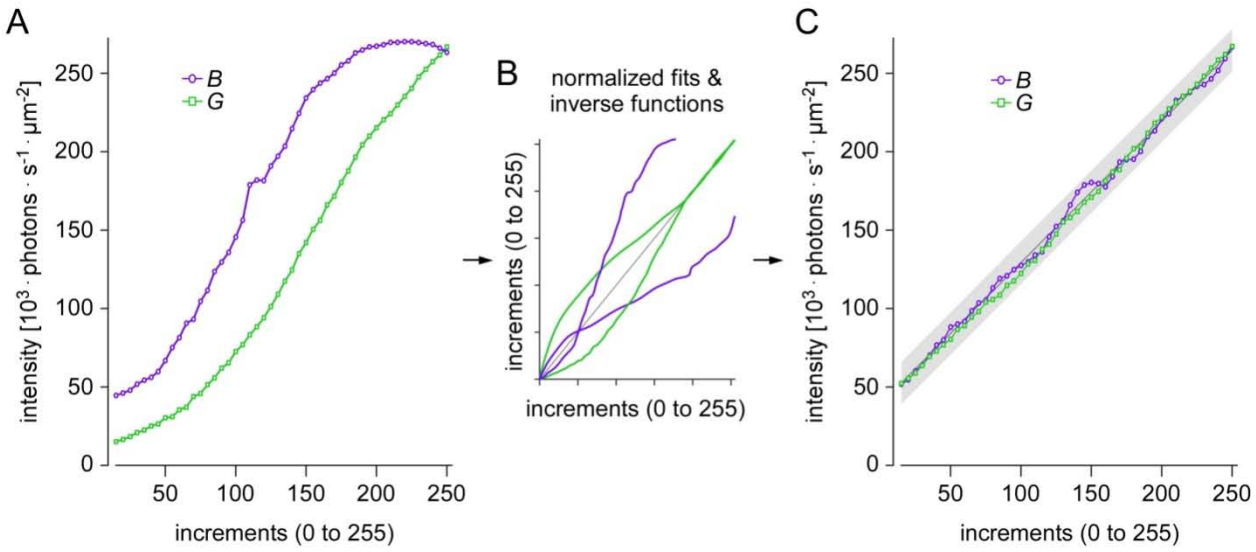

Figure 11 A: The nonlinear stimulator intensity curves (*B*, "blue" and *G*, "green") over the software output (increments from 0 - 255) were fitted with polynomial fit functions (see B). B: Inversed fit functions were used as look-up tables to correct for the nonlinearity of the stimulator. C: The measured resulting intensity functions (over software output increments) showing that the nonlinearity of the stimulator intensity was compensated over the stimulation range (from ≈10 % to ≈ 90 %) with an error < ± 5 % (dark gray, line fit; light gray: confidence interval ± 5 %).

The stimulation intensity (irradiance) ranges for both, the blue and green stimulus components were adjusted each to 50 to 270 (in 10^3 photons·s^{-1}µm^{-2}). Green evoked 1.7 to 9.0 (in 10^3 photo-isomerizations per second and M-cone; assuming exclusively M-opsin expression), and blue evoked 2.7 to 14.8 (in 10^3 photo-isomerizations per second and S-cone). The background illumination ≈ 10^5 photons·s^{-1}·µm^{-2} of the LCoS-display stimulator, which was continuously on during all electrophysiological recordings, evoked ≈ $5.1 \cdot 10^3$ rod photo-isomerizations per second; therefore, stimulation conditions were in the photonic range (compare with Field et al., 2009). This intensity is predicted to suppress ≈ 96.7 % rod responses (Nikonov et al., 2006).

Due to the stimulation bands (see next paragraph) relative to the opsin absorption curves, the "iso-intensity" definition (= same photon irradiance for green and blue stimulus component) for the LCoS-display stimulator did not produce the same number of photo-isomerizations in M- and S-cones. The probability for the green (578 nm) stimulus to induce photo-isomerizations in M-cones was lower than for the blue (400 m) stimulus in S-cones by a factor $\Phi_{M/S} = 0.6$. The data analysis of the present work (Figure 21 and Figure 22) and the statistical model (Figure 23) accounted for the differences in photo-isomerizations

The LCoS-display stimulator wavelengths (peaks: 400 nm and 578 nm) did not perfectly match the sensitivity maxima of the mouse opsins. Due to a resulting overlap of the blue stimulus

component with the absorption spectra of mouse M-opsin, even a cell that contacts exclusively M-cones with no S-opsin co-expression was expected to somewhat respond to blue. This co-excitation for the M-opsin by the blue stimulus component was calculated to be ≈ 40 % of the S-cone excitation by blue (see $\varepsilon_{blue,M}$ and $\varepsilon_{blue,M}$ in Methods and legend of Figure 23). We kept the stimuli simple by modulating both wavelengths within the same photon irradiance without attempting to correct for differences in cone sensitivities to the stimulation wavelengths. Also we kept the non-modulated stimulus component (during only green or blue stimulus condition) at constant ≈ 20 % of the maximum instead of trying to isolate one cone type by silent substitution method (Estevez and Spekreijse, 1982). Cone isolating stimuli did not seem to be useful in our experiments due to unknown co-expression levels in M-cones.

Simple LED-stimulator

The second light stimulator was a simple LED-stimulator (Figure 10) mounted below the recording chamber and consisted of two band pass-filtered (UV: 360 BP 10, green: 520 BP 10; AHF/Chroma) LEDs. Their light was combined by a beam-splitter (400 DCLP, AHF/Chroma), focused by the condenser lens (NA = 0.63 air, Zeiss) and projected through the transparent bottom of the plastic recording chamber. Due to the lack of a spatial modulator, this device was limited to a spot (250 µm to 300 µm) determined by an iris-aperture that was introduced in the condenser setup; background illumination outside the light spot was not possible. The LEDs were driven by a custom-made electronic circuit, which incorporated an open-source microprocessor board (http://arduino.cc).

The stimulus intensities (irradiance) for UV and green were adjusted each to 1.1 to 24 (in $10^3 \cdot photons \cdot s^{-1} \cdot \mu m^{-2}$), equivalent to photo-isomerization rates of 0.2 to 4.8 (in 10^3 photo-isomerizations per second and cone) in both M- and S-cones. The background illumination ($\approx 2.2 \cdot 10^3 \cdot photons \cdot s^{-1} \cdot \mu m^{-2}$) of the LED-stimulator, which was continuously on during the electrical recording, evoked ≈ $0.6 \cdot 10^3$ rod photo-isomerizations per second and therefore in the low photopic range (compare with Field et al., 2009); this intensity is predicted to suppress ≈ 77.1 % rod responses (Nikonov et al., 2006).

4.3.4 Data analysis

We performed spectral analysis (compare with Hausselt et al., 2007) to extract phase and amplitude information from the voltage traces recorded during the sinusoidal light stimulation. The first recorded second was discarded to avoid initial transients (Figure 12 A; compare with Figure 18 and Figure 19). We calculated power spectra for each stimulus condition (Figure 12 B) and determined the amplitude and phase of the fundamental component ($V_1 =$ the frequency component at $F_{Stim} = 1\ Hz$; Figure 12 C). In addition, we calculated the power spectrum of the "noise" from voltage trace sections without sinusoidal stimulation; only responses with a signal-to-noise ration ≥ 15 were considered to be significant and used for analysis.

For quantifying the chromatic tuning of a cell, we trial-wise calculated $\varphi_{BG} = tan^{-1}(R_{BG})$ with $R_{BG} = V_1(B)/V_1(G)$ and $R_{IW} = V_1(I)/V_1(W)$ $R_{IW} = V_1(I)/V_1(W)$ and took the averages. To statistically compare sets of bipolar cells we used the Wilcoxon Rank test.

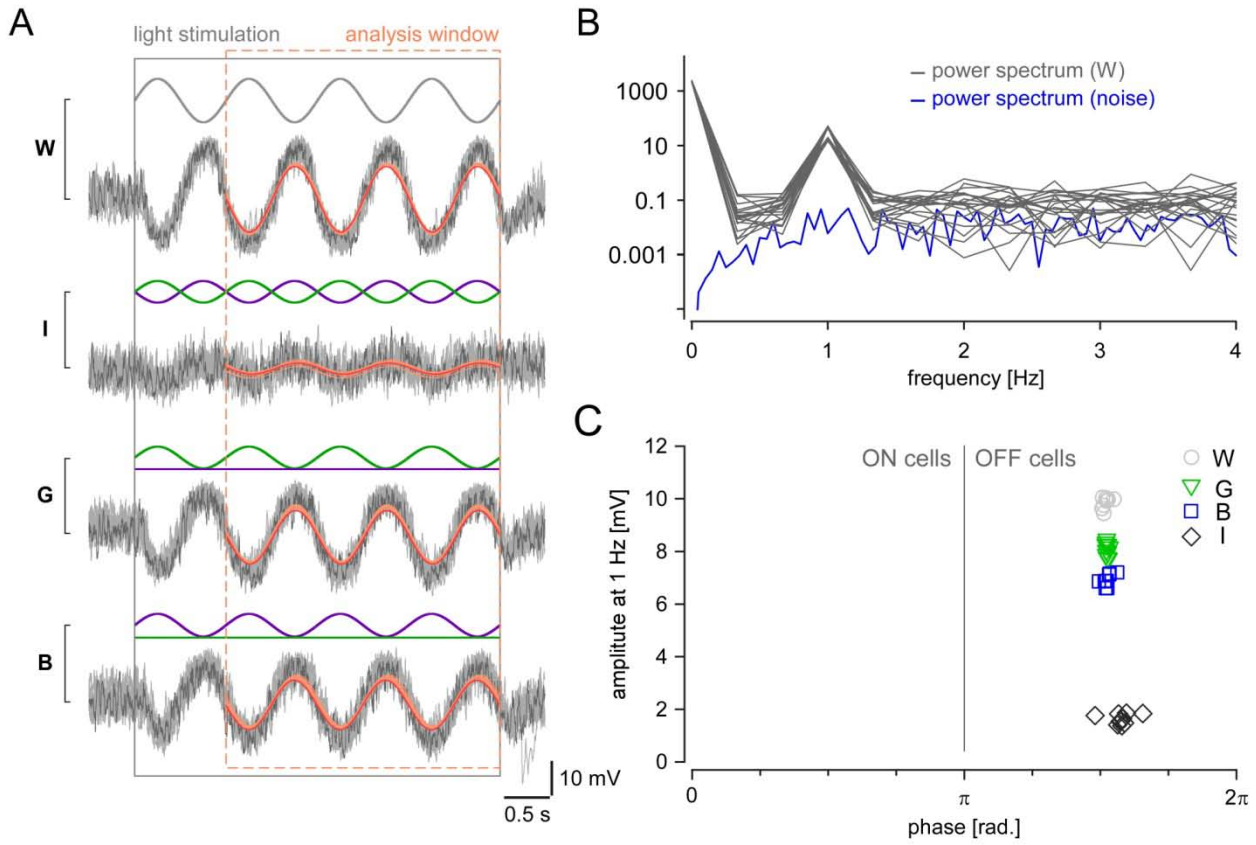

Figure 12 A: Exemplary voltage responses of a type-2 bipolar cell to a spot (130 µm in diameter) for which the green (filter: 578 nm BP 10 nm) and/or the blue (filter: 400 nm BP 20 nm) stimulus components were sinusoidally modulated in time, as indicated by stimulus traces above voltage responses: blue and green in sync (*W*, "white"), blue and green phase-shifted by 180° (*I*, "iso-intense"), green only (*G*) and blue only (*B*). (n = 10 individual trials in gray; curves reconstructed from amplitude and phase of fundamental component (see C) shown in red; single example trial indicated in darker colors; black rectangle indicates stimulus presentation.) B: Power spectra (black curves) calculated from single trial responses to "white" (from cell shown in A); only data within the analysis window (dashed orange rectangle in A) was used. The power spectrum for the noise (blue curve) was calculated from data recorded with steady illumination. C: Fundamental voltage component at the stimulus frequency (1 Hz) for the different stimulus conditions (*W*, circles; *I*, diamonds; *G*, triangles; *B*, squares) as a function of the respective phase. The present example cell showed OFF-responses to both *B* and *G*, with a slight preference for *G*.

4.3.5 Statistical model

To simulate the chromatic tuning (φ_{BG}) of bipolar cell populations (section 5.3; Figure 23) we calculated the response of single bipolar cells "connected" to a subset of cones, ($n_{cones} = n_M + n_S$, taken from Wassle et al., 2009), consisting of S- (n_S) and M-cones (n_M), using the S-cone density (4 % of all cones; taken from Haverkamp et al., 2005) as S-cone contact

probability (p_S). For each M-cone, the opsin co-expression ratio (R_{SM}) was drawn from a Gaussian, with center (x_{SM}) and standard deviation (σ_{SM}) estimated from mRNA data (Applebury et al., 2000). For S-cones, we used $R_{SM} = 1$. The photo-isomerization factor $\Phi_{M/S}$ was calculated to account for the differences in probability of M-opsin isomerizations by green (578 nm) vs. S-opsin isomerization by blue (400 nm) photons (Nikonov et al., 2006). The total cone input to a bipolar cell in response to blue was calculated using

$$V_B = \sum_{i=1}^{n_M} \{q \cdot w_{syn,M} \cdot \Phi_{M/S} \cdot [R_{SM,i} + (1 - R_{SM,i}) \cdot \varepsilon_{blue,M}]\} + \sum_{i=1}^{n_S} \{q \cdot w_{syn,S}\} \qquad \text{Equation 1}$$

with the maximal response contribution per cone ($q = 1/n\_cones$), the relative excitation of M-opsin by 400 nm ($\varepsilon_{blue,M}$) and S-opsin by 578 nm ($\varepsilon_{green,S}$), and the weight of synaptic connections from S- and M-cones to bipolar cells ($w_{syn,S}$ and $w_{syn,M}$, respectively). The respective response component to green was determined using

$$V_G = \sum_{i=1}^{n_M} \{q \cdot w_{syn,M} \cdot \Phi_{M/S} \cdot [(1 - R_{SM,i}) + R_{SM,i} \cdot \varepsilon_{green,S}]\} + \sum_{i=1}^{n_S} \{q \cdot w_{syn,S} \cdot \varepsilon_{\mathrm{green,S}}\} \qquad \text{Equation 2}$$

The actual parameter values we used are given in legend of Figure 23. From the simulated response components we determined the chromatic tuning angle $\varphi_{BG} = \tan^{-1}(V_B/V_G)$. This was repeated for $n = 2 \cdot 10^4$ cells and the results were plotted as a histogram (Figure 23 B).

5 RESULTS

5.1 Anatomical results

All immunohistochemical experiments were carried out by S. Haverkamp and C. Puller at the MPI for brain research (Frankfurt a.M., Germany). Since our close collaboration has addressed the same scientific question with complementary methods the results are presented together in this work (for contributions, see 3.6.2).

5.1.1 Identification of mouse cone types

To determine whether a specific mouse bipolar cell type contacts both M- and S-cones non-selectively or systematically avoids one cone type, M- and S-cone pedicles had to be reliably distinguished. In primate retina, S-cone pedicles are smaller in comparison to M-/L-cone pedicles and the processes of their postsynaptic partners are more densely packed than at M-/L-cones (Ahnelt et al., 1990; Haverkamp et al., 2001b). We used two different immunohistochemical markers, glycogen phosphorylase (glypho, for size of pedicle base) and peanut agglutinin (PNA, for cone invaginations) to find out if there are also differences between the synapses of S- and M-cones in mouse. While there were no obvious differences in the overall shape of glypho-labeled S- and M-cones pedicles, the quantitative analysis of the area of the cone pedicle base – represented by the glypho fluorescence – revealed a small, statistically significant difference between the two cone types; M-cone pedicles (26.5 μm^2 ± 4.9 μm^2, n = 288) were on average larger than S-cone pedicles (22.4 μm^2 ± 4.3 μm^2, n = 25; $p < 0.001$), consistent with the findings from primate retina (Haverkamp et al., 2001b; Lee et al., 2005).

These findings strengthen the view that S-cones are not merely variations of cones (as only defined by opsin expression) but a distinct photoreceptor type. Although differences were significant it was not possible to reliably assign the identity of individual cones just by glypho-or PNA-labeling. For the following experiments we decided to visualize all cone pedicles using only glypho and identify S-cones either by their contacts with type-9 bipolar cells in CLM1 mice (Haverkamp et al., 2005) or by co-staining with S-opsin antibodies. In addition, the dendrites of distinct bipolar cell types were labeled using either selective antibodies or transgenic mouse lines (for overview, see Figure 4, and Wassle et al., 2009).

5.1.2 Postsynaptic contacts of ON-bipolar cells at cone pedicles

The PNA labeling data suggest that S-cone pedicles are contacted by fewer invaginating dendritic tips of ON-bipolar cells than M-cones. To test if this hypothesis is true for a specific type of ON-bipolar cell, we performed triple labeling against GFP, S-opsin, and glypho in whole-mounted retinas of Gus-GFP mice (Figure 13, Wong et al., 1999), in which type-7 bipolar cells are GFP-positive (Huang et al., 2003; Ghosh et al., 2004). We restricted the analysis to the dorsal retinal periphery, where the mouse cone distribution resembles that of most mammalian species and where the level of S-opsin co-expression is low (Applebury et al., 2000; Szél and

Roehlich, 1992). S-opsin-labeled cones were traced down from the outer segment to identify the respective pedicle. We measured the area of Gus-GFP-immunoreactivity (Figure 13 A4) in single optical sections at M-cone pedicles (1.7 µm^2 ± 0.8 µm^2; n = 31) and S-cones (1.4 µm^2 ± 0.6 µm^2; n = 9) and found no significant differences (p = 0.295) in the connectivity with the two cone types, suggesting that type-7 ON-bipolar cells non-selectively contact both types of cones. Whether this is also the case for other types of ON-bipolar cells (type-5, -6 and -8 cells; Figure 4; for type 9, see Haverkamp et al., 2005) remains to be seen due to a lack of cell type specific markers.

5.1.3 Postsynaptic contacts of OFF-bipolar cells at cone pedicles

It has been shown for a few di- and trichromatic mammals, that the expression of post-synaptic ionotropic glutamate receptors on the tips of OFF-bipolar cells is reduced at S-cone pedicles (Haverkamp et al., 2001b; Li and DeVries, 2006; Puller et al., 2007). In monkey and ground squirrel retina, this reduction is thought to reflect that certain OFF-bipolar cell types avoid contacting S-cones (Lee et al., 2005; Li and DeVries, 2006; Puller et al., 2007). A reduction of GluR1 (data not shown) and GluR5 (Haverkamp et al., 2005) at S- compared to M-cone pedicles has also been found in the mouse retina. However, it is not yet known whether this reduced GluR-expression is due to a general reduction of OFF-bipolar cell contacts at S-cones or because one (or more) OFF-bipolar cell types avoid S-cones – as seen in ground squirrel.

To address this question, we triple-labeled horizontal cryosections of CLM1 mouse retina against GFP, glypho, and one of the following OFF-bipolar cell markers (Wassle et al., 2009): NK3R (type 1 and 2; Figure 13 B), HCN4 (type 3a; Figure 13 C), and calsenilin (type 4; Figure 13 D). S-cone pedicles were identified by their contacts with CLM-positive type-9 bipolar cell dendrites (Figure 13 B1 - D1). The quantification of the NK3R-immunoreactive area (Figure 13 B2, B3) per pedicle revealed a strong, statistically significant reduction of NK3R-staining at S-cone pedicles (1.9 µm^2 ± 1.2 µm^2; n = 36) in comparison to M-cone pedicles (5.2 µm^2 ± 1.8 µm^2; n = 134; p < 0.001, Wilcoxon Rank test; Figure 13 B4), indicating that type-1 and/or type-2 bipolar cells avoid contacting S-cones. The experiments with HCN4 (Figure 13 C2-4; M-cones, 2.0 µm^2 ± 0.6 µm^2, n = 56; S-cones, 1.7 µm^2 ± 0.6 µm^2, n = 17; p = 0.064) and calsenilin (Figure 13 D2 - D4; M-cones 2.3 µm^2 ± 1.0 µm^2, n = 70; S-cones 1.8 µm^2 ± 0.9 µm^2, n = 20; p < 0.05) showed rather uniform cone pedicle labeling, suggesting that type-3a and -4 bipolar cells non-selectively contact S- and M-cones. That the immunoreactive area for these cells tended to be smaller at S-cones is likely due to the smaller S-cone pedicle size (compare with section 5.1.1).

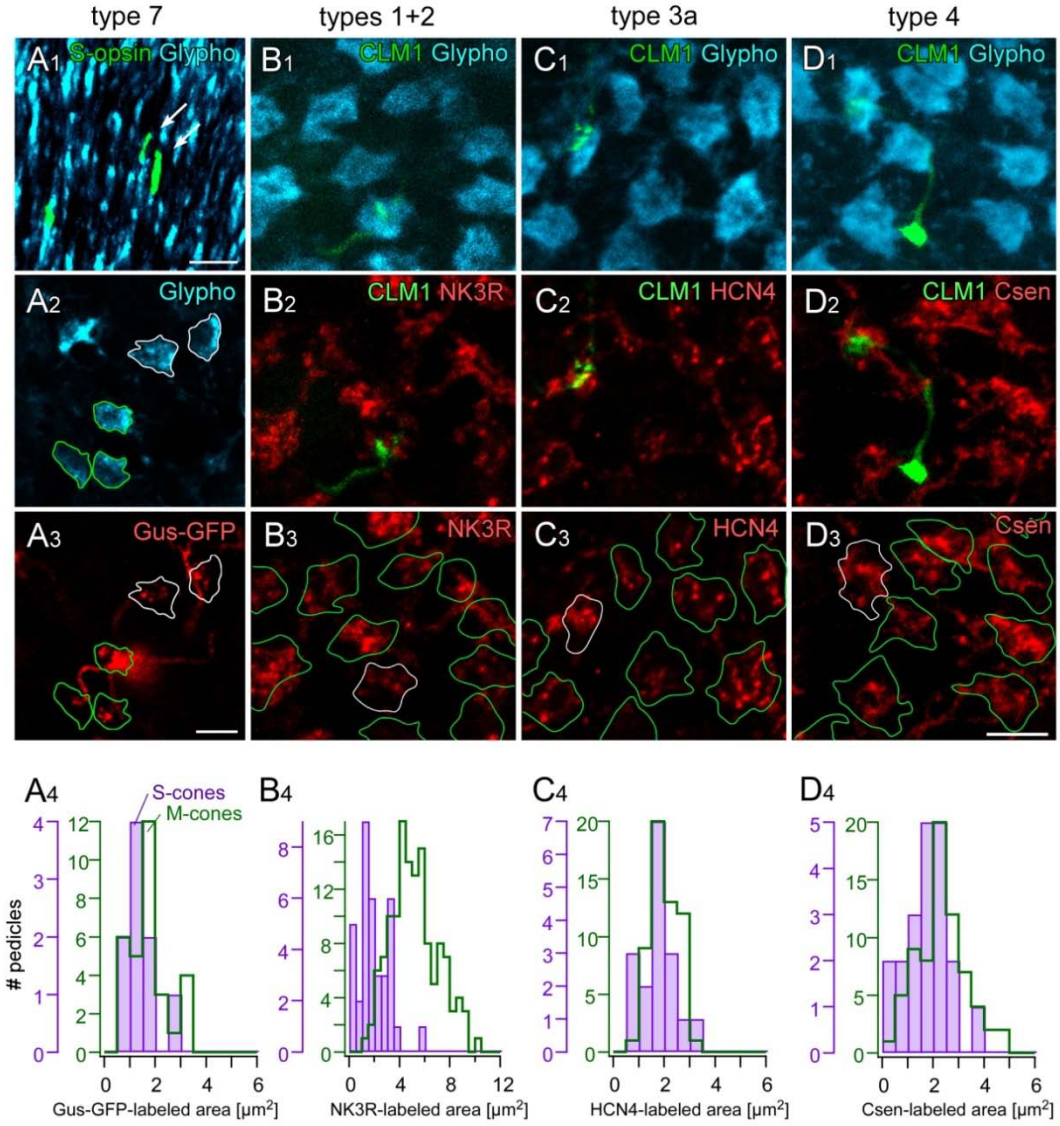

Figure 13: Dendritic contacts of bipolar cell types at M- and S-cones in the mouse retina. A1 - A3: Whole-mounted Gus-GFP mouse retina triple labeled against S-opsin, GFP, and glypho. A1: Projection of a confocal image stack showing glypho-labeled cone outer segments (cyan) in the dorsal retina. Three S-cone outer segments are labeled against S-opsin (green), two of which (arrows) were traced to their pedicles (white outlines in A2). Glypho-labeled cone pedicles in a single optical section; pedicles in contact with a type-7 bipolar cell (A3) are outlined (S-cones in white, M-cones in green). A3: Same region as in A2, with the Gus-GFP-labeled type-7 cell (red) shown. A4: Histograms of the normalized Gus-GFP area for S- (n = 9) and M-cones (n = 31). B1 - B3: Projections of an ApoTome image stack of horizontally sectioned CLM1 mouse retina triple labeled against GFP, NK3R and glypho. B1: Glypho-labeled cone pedicles (cyan), one of which is contacted by a CLM-positive type-9 bipolar cell dendrite (anti-GFP, green). B2: NK3R-labeled dendrites of type-1 and -2 OFF-bipolar cells (same field as in B1). B3: Outlines of glypho-stained pedicles (from B2) superimposed with the NK3R-positive dendrites (red, from B2). B4: Histograms of the normalized NK3R area for S- (n = 36) and M-cones (n = 134). C1 - C3, D1 - D3: Triple staining analog to B1 - B3 but with HCN4 to label type-3a OFF-bipolar cells (red, C2 - C3) and calsenilin (Csen) to label type-4 OFF-bipolar cells (red, D2 - D3), respectively. C4, D4: Histograms of the normalized immunolabeled area for S- (HCN4, n = 17; Csen, n = 20) and M-cones (HCN4, n = 56; Csen, n = 70). Scale bars: 5 µm.

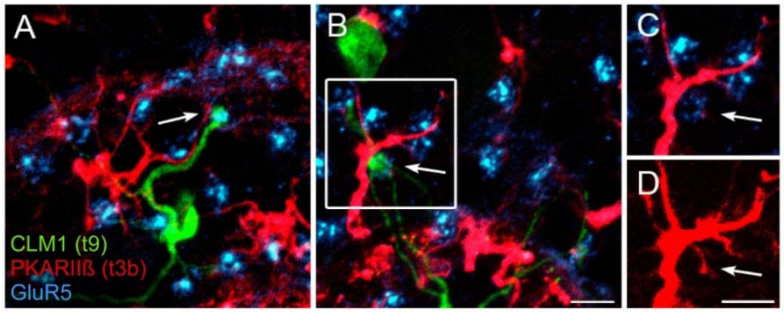

Figure 14 A, B: Projection of confocal image stacks of horizontally sectioned CLM1 mouse retina triple labeled against GFP (green, type-9 bipolar cells), PKARIIβ (red, type-3b cells), and GluR5 (cyan, cone pedicles). The dendritic tips of type-9 cells were used to identify S-cone pedicles (arrows). Some dendrites of type-3b cells are oriented towards S-cone pedicles. C, D: Magnification of the framed region in B. After increasing image brightness (D), a dendritic branchlet extending to the S-cone pedicle (arrows) becomes visible. Scale bars: 5 µm.

Stainings against GFP, GluR5 (for cone pedicles), and PKARIIβ, a specific marker for type-3b bipolar cells, in horizontally sectioned CLM1 mouse retina suggested that type-3b bipolar cell dendrites also contact S-cone pedicles (Figure 14). However, the PKARIIβ antibody labeling of the dendritic tips was too weak to allow for quantitative analysis.

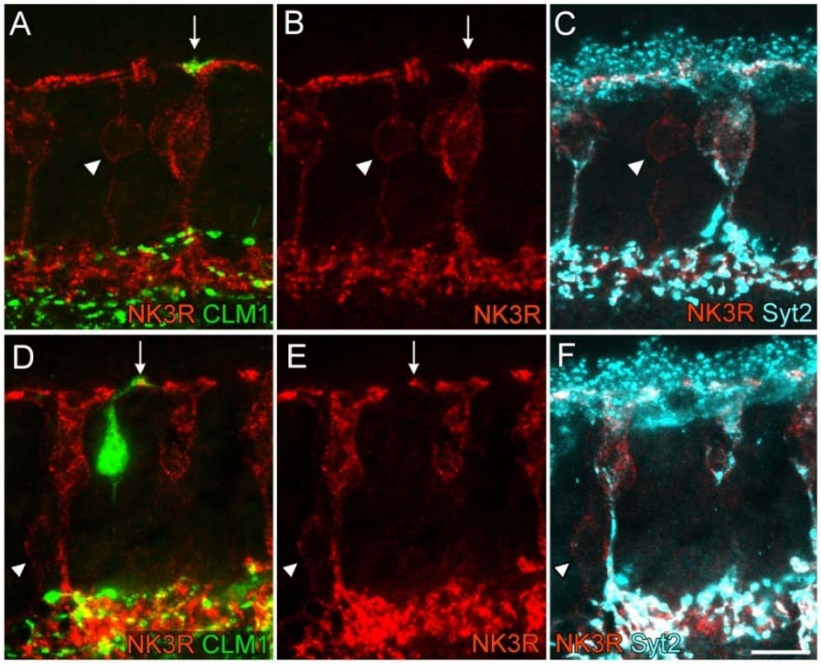

Figure 15: Dendritic contacts of type-2 OFF-bipolar cells at S-cones. A - F: Projections of confocal image stacks (A - C; D - F) of vertically sectioned CLM1 mouse retina triple labeled against GFP (green, type-9 cells), NK3R (red, type-1 and -2 cells), and synaptotagmin II (Syt2, cyan, type-2 cells). The dendritic tips of type-9 cells were used to identify S-cone pedicles (arrows), contacted by dendrites of type-2 cells. Note the Syt2-negative type-1 cells (arrow heads). In D - F the brightness of red and cyan channels were adjusted manually at the level of the INL for the better visualization of the cell bodies. Scale bar: 10 µm.

Examining separately the dendritic contacts of type-1 and type-2 OFF-bipolar cells, together with cone pedicles was difficult, because suitable markers were lacking. We therefore analyzed vertical cryosections of CLM1 mouse retinas, triple labeled against GFP, NK3R, and synaptotagmin II (Syt2). Syt2 labels cell bodies and axon terminals of type-2 bipolar cells (Fox and Sanes, 2007; Wassle et al., 2009) and was used to separate type-2 from type-1 bipolar cells in the NK3R staining (Figure 15). We identified dendritic contacts of type-2 bipolar cells at 14 (of 15) S-cones pedicles, indicating that type 2 does not avoid S-cones. However, we cannot exclude that type-1 bipolar cells contact S-cones, although we never observed such contacts in our sample.

In conclusion, type-3a and -4 OFF-bipolar cells showed no significant preference for M- or S-cone pedicles and are, therefore, presumably chromatically non-selective. The same is likely true for type-2 and -3b OFF-bipolar cells, for both of which we found contacts with S- and M-cones. This was not the case for type-1 bipolar cells, which makes this type a suitable candidate for the green^{OFF} bipolar cell of the mouse retina.

5.2 Electrophysiological results

5.2.1 Morphologies of recorded cells

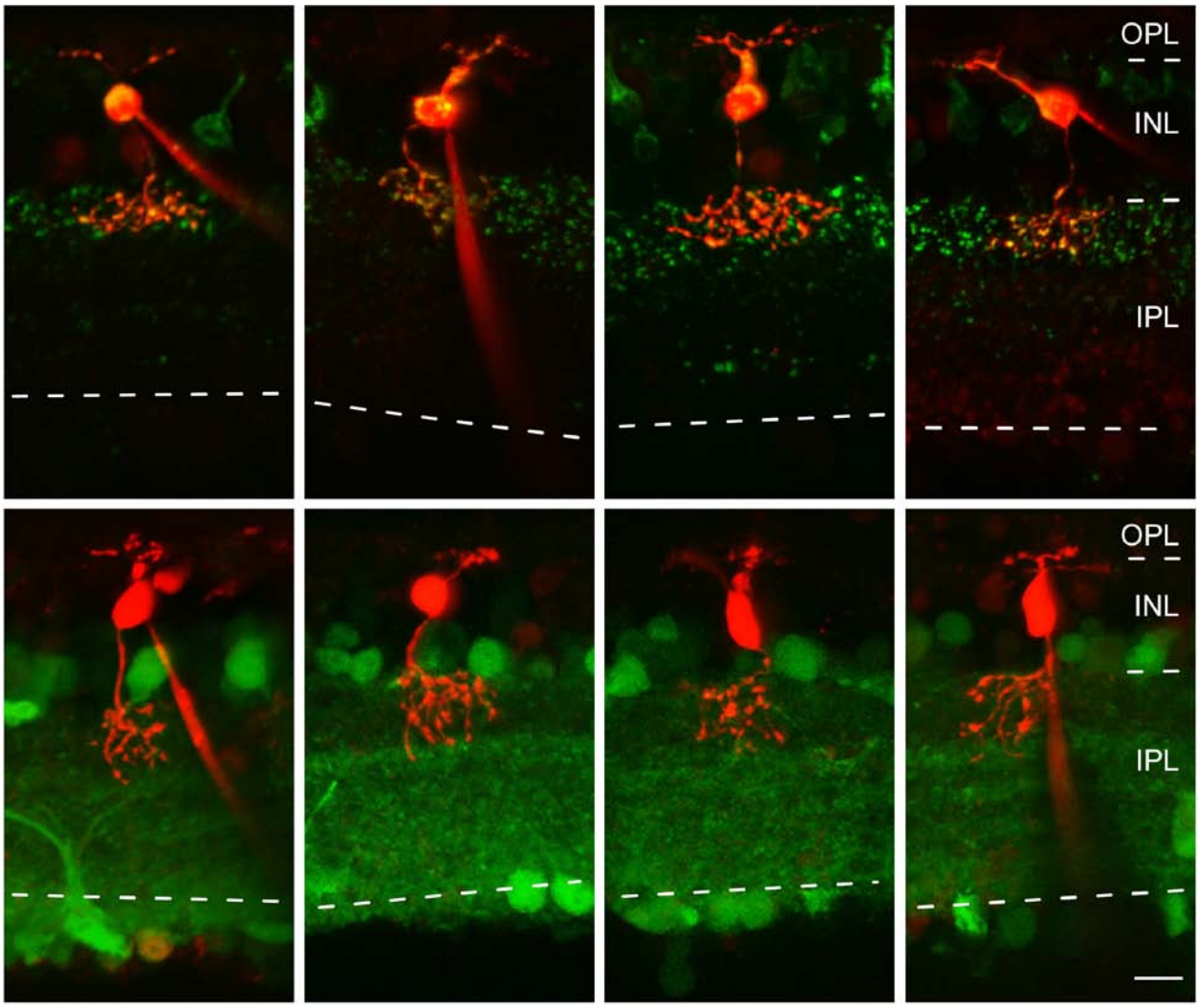

Figure 16: Maximum intensity projections (5 - 30 slices; spacing 1 µm) of type-1 (upper row) and -2 (lower row) OFF-bipolar cells. Type-1 cells were recorded in mitoP-CFP retinas. Type-2 cells were recorded in CLM12 animals; note that several amacrine and ganglion cells are fluorescent in CLM12 animals as well. All cells were filled with SR101 (red, band-pass-filter: 633 BP 36); cell expressed the fluorescent proteins CFP or clomeleon (green, band-pass filter: 535 BP 50). All cells are shown at the same scale, scale bar 10 µm. Brightness and contrast were adjusted manually using Adobe Photoshop CS v8.0.1 (San Jose, CA). Note that the patch electrode is visible in some windows as a red tail attached to the cells.

The identification of an electrically recorded bipolar cell was primarily achieved by using transgenic mouse lines expressing fluorescent proteins in defined subset of retinal neurons (section 4.1). In addition, we confirmed the cells' identities by filling them during the recordings with SR101 (concentration: 200 µM in the patch pipette) and acquiring z-stacks of the cells using

the 2P microscope (z-projections in Figure 16 and Figure 17). The morphologies of the recorded cells were largely consistent with the literature. In the mitoP-CFP mouse line (Misgeld et al., 2007) it was shown that CFP is expressed in type-1 and type-3 OFF-bipolar cells (Schubert et al., 2008). In our hands, however, almost all cells were of the type 1 and only 1 of 22 recorded and dye-filled cell was type 3 (compare Figure 17 A and Figure 16, upper row). Type-2 OFF-bipolar cells (recorded in CLM12 mice; Berglund et al., 2004) did stratify narrowly in sublamina S1 of the IPL (as reported in Ghosh et al., 2004; Wassle et al., 2009) but also ramified in S2 (Figure 16; compare with Pignatelli and Strettoi, 2004).

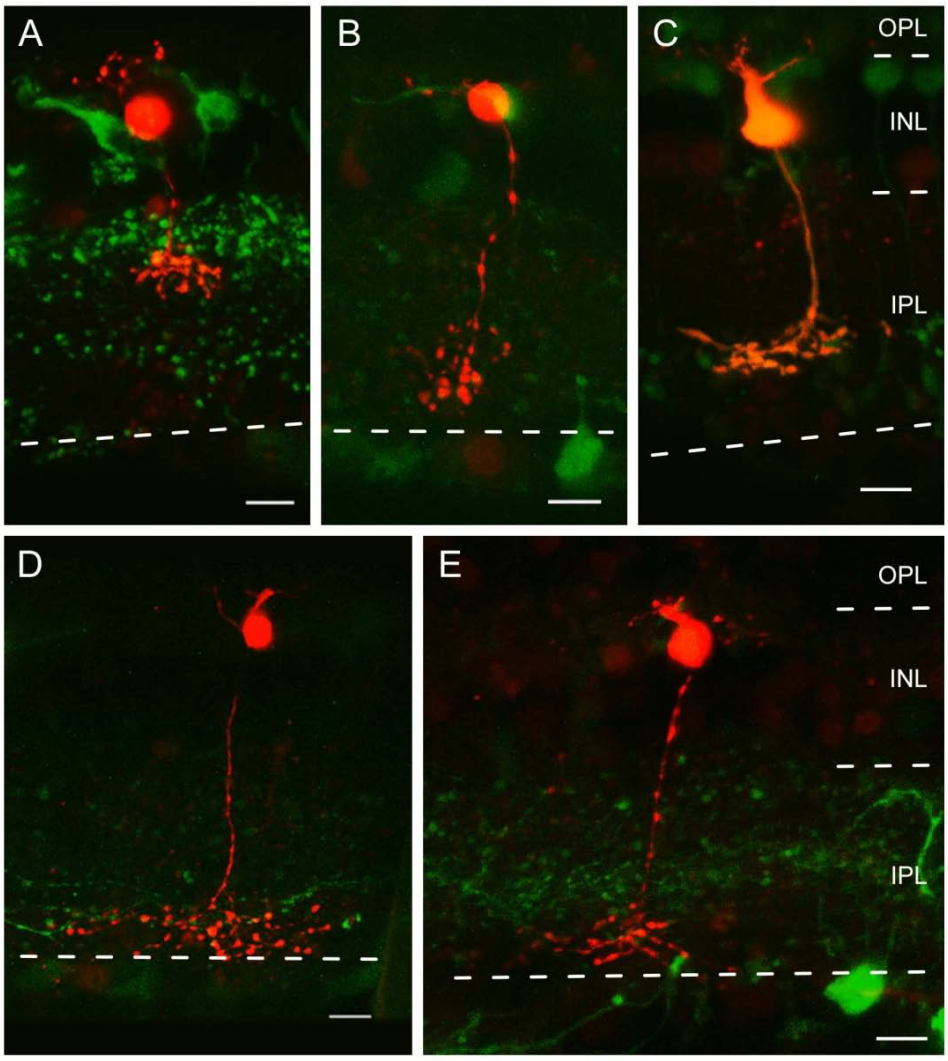

Figure 17: Maximum intensity projections (5 - 30 slices; spacing 1 µm) of five different cone bipolar cells. A: CFP positive Type-3 OFF-bipolar cell recorded in mitoP-CFP retina. B: Type-6 ON-bipolar cell, recorded in CLM1 retina; cell was clomeleon-negative; the originally targeted clomeleon-positive cell is visible next to the filled cell. C: GFP positive type-7 ON-bipolar cell recorded in Gus-GFP retina. D: Clomeleon positive type-8 ON-bipolar cell, recorded in CLM1 retina. E: Clomeleon positive type-9 ON-bipolar cell, recorded in CLM1 retina. All cells were filled with SR101 (red, band-pass-filter: 633 BP 36); the cells in panels A, C, D and E expressed the respective fluorescent proteins (green, band-pass filter: 535 BP 50). Scale bars: 10 µm. Brightness and contrast were adjusted manually using Adobe Photoshop CS v8.0.1 (San Jose, CA).

Type 7 ON-bipolar cells (Figure 17 C) were targeted in Gus-GFP mice (GUS8.4GFP: Wong et al., 1999; Huang et al., 2003), type-9 ON-bipolar cells (Figure 17 E) in CLM1 (Berglund et al., 2004). In some cases neighbors of fluorescent cells were recorded accidentally, e.g. the type-6 ON-bipolar cell next to a clomeleon positive cell (presumably type 9; see Figure 17 B). None of these (few) accidently recorded other bipolar cell types displayed a detectable chromatic preference (compare with Figure 18 and Figure 19). The type-3 (Figure 17 A) cell showed OFF-responses to both stimulus components, although slightly stronger to green than to blue – similar to type-2 cell responses (data not shown). Type-6 cells (Figure 17 B) showed ON-responses to both stimulus components (n = 2, both morphologically classified), to green slightly stronger than to blue, similar to type-7 cell responses (data not shown). Type-8 cells (Figure 17 D) displayed ON-responses to both stimulus components (n = 2, one was only morphologically classified, one was CLM-positive but morphologically identified as non type-9 cell); to green slightly stronger than to blue. Type 8 bipolar cell responses were somewhat more sustained than those of other cone bipolar cells. Because of the low cell numbers, these responses were not systematically analyzed.

5.2.2 Electrical responses of bipolar cells to dichromatic stimulation

To characterize the chromatic tuning of the different bipolar cell types, we performed whole-cell patch-clamp recordings in retinal slices (schematic experimental configuration, Figure 18 A). To relate the light responses to the local opsin expression we recorded from selected regions along the dorso-ventral axis. Unless stated, slices were taken from dorsal regions (as indicated in Figure 19). To target type-1 and type-2 OFF-bipolar cells, type-7 ON-bipolar cells and the S-cone selective type-9 ON-bipolar cell we used transgenic mouse lines (section 4.1).

A spot of light was presented to the photoreceptor array distal to the recorded bipolar cell (Figure 18 A, B). The light was composed of a green (*G*) and a blue (*B*) component generated by two bandpass-filtered and sinusoidally modulated LEDs (peaks at 400 nm and 578 nm); care was taken to keep the light intensities constant between experiments (see Methods). Four stimulus conditions were used (Figure 18 C): the two components were modulated in sync ("white", *W*), phase-shifted by 180° ("iso-intense", *I*), or separately (*G* and *B*). The idea was that the membrane voltage of a cell with a strong chromatic tuning (e.g. Figure 18 C) should be modulated by both the white and the iso-intense stimulus condition (possibly with a phase difference, depending on its chromatic preference), but show a clear difference in modulation by green and blue. The voltage of a non-selective cell (type-7 cell; Figure 18 D) should be strongly modulated by white, little to none by the iso-intense stimulus, and close to equally by green and blue. Note that although the probability for the green (578 nm) stimulus to induce photo-isomerizations in M-cones was lower than for the blue (400 nm) stimulus in S-cones (factor: $\Phi_{M/S} = 0.6$), nonselective bipolar cells displayed a balanced response behavior to both stimulus components and were little modulated by the iso-intense stimulus condition.

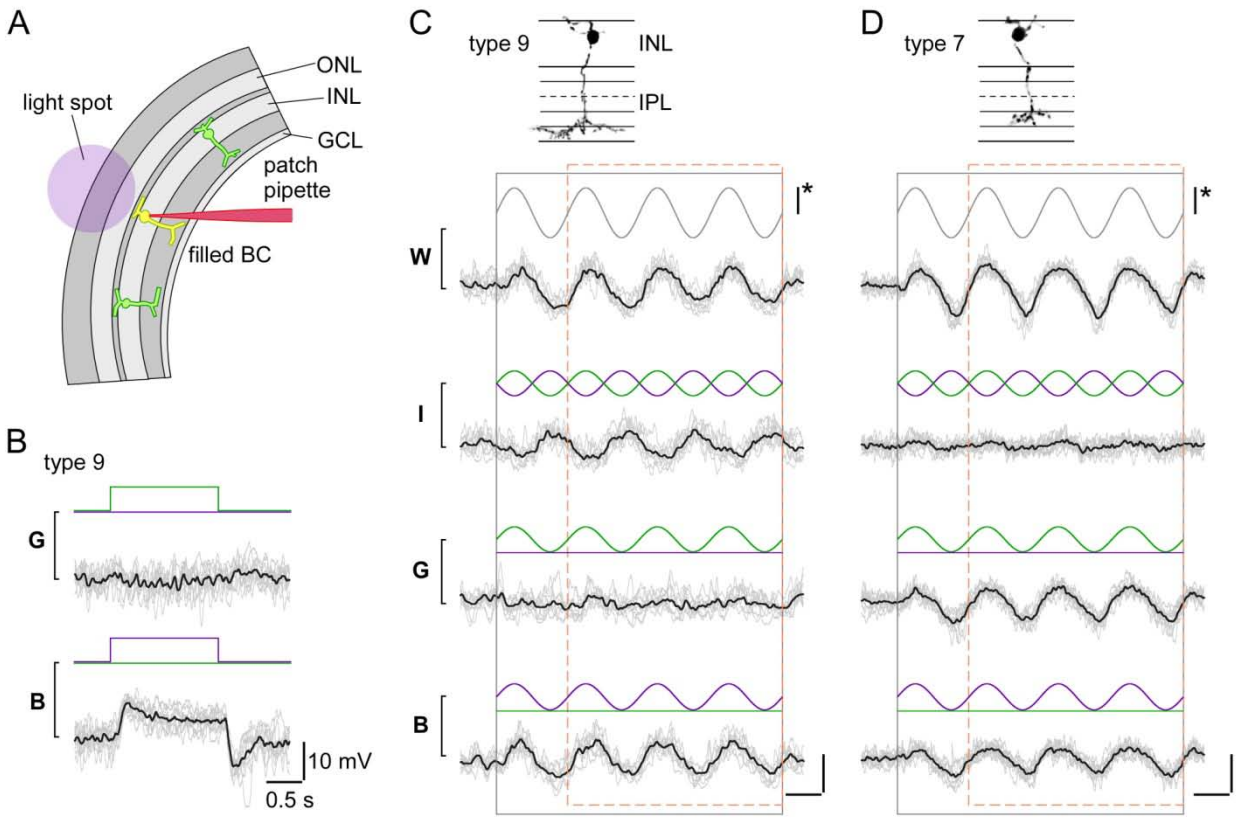

Figure 18: Voltage responses of type-9 and type-7 on-bipolar cells to chromatic stimulation. A: Schematic drawing shows experimental configuration: Fluorescent protein-labeled bipolar cells in slices from transgenic mice were electrically recorded while presenting light spots of different wavelengths to the photoreceptors (spot diameters: 80 µm – 200 µm). B: Voltage responses of a type-9 on-bipolar cell, recorded in a CLM1 mouse, to spots of green (G; filter: 578 BP 10, see Methods) and blue (B; filter: 400 BP 20) light. Average responses in black, n = 10 individual trials in gray. Intensity scale bar (*): $3 \cdot 10^5$ ph · s^{-2} · μm^{-2}. C: Voltage responses of another type-9 bipolar cell to spots for which the blue and/or the green stimulus components were sinusoidally modulated in time, as indicated by stimulus traces (B, blue; G, green) above voltage responses: blue and green in sync (W, "white"), blue and green phase-shifted by 180° (I, "iso-intense"), green only (G) and blue only (B). Black and dashed orange rectangles indicate stimulus presentation and analysis windows, respectively. See Methods for details. Morphology of the recorded cell, which was filled with SR101 during the recording, shown above the traces (from a maximum projected micrograph stack; INL, inner nuclear layer; IPL, inner plexiform layer). D: Voltage responses of a type-7 on-bipolar cell recorded in Gus-GFP transgenic mouse retina in an experiment analog to C.

5.2.3 Type-9 ("blue cone bipolar cell") ON-bipolar cell responses

As expected from its exclusive contacts with S-cones (Haverkamp et al., 2005), type-9 bipolar cells (n = 3 cells) were strongly modulated by iso-intense and blue but not by green stimuli (compare with Figure 18 C). They depolarized during the up-swing of the blue intensity (blue^{ON}). In one cell we observed a weak hyperpolarizing modulation to green (green^{OFF}), suggestive of an antagonistic blue/green signal (Figure 20 D), as predicted by S-cone recordings in primate retina

(Packer et al., 2010). However, we did not investigate this further, because only few type-9 cell recordings were successful: the weak fluorescence in our CLM1 mice together with the low density of type-9 bipolar cells (≈ 1% of all mouse bipolar cells, Haverkamp et al., 2005) rendered finding suitable cells in slices difficult.

5.2.4 Type-7 ON-bipolar cell responses

As a representative for an ON-cone bipolar cell that contact both M- and S-cones (Figure 13 A) we recorded type-7 cells. Six out of seven type-7 bipolar cells recorded in the dorsal retina showed little modulation to iso-intense stimuli, and displayed ON-responses with comparable amplitudes to green and blue (example shown in Figure 18 D). One ventrally recorded type-7 cell was strongly modulated by iso-intense ($blue^{ON}$) and blue stimuli, but showed little modulation to green (data not shown). This suggests that M-opsin levels in ventral M-cones are too low to have a substantial effect on the cones' output and is consistent with measurements of the opsin mRNA ratio along the dorso-ventral axis (Applebury et al., 2000). Note that the dorsal type-7 cells contained one outlier that displayed responses similar to the ventrally recorded cell.

5.2.5 Type-1 and -2 OFF-bipolar cell responses

Our immunohistological data (Figure 13 B and Figure 15) indicated that type-1 (and not type-2) OFF-bipolar cells may exhibit green-biased responses. However, dorsal type-1 cells (n = 12) showed little or no voltage modulation to iso-intense stimuli and depolarized with comparable amplitudes during the intensity down-swings of green and blue stimuli (OFF-responses; Figure 19 A). Most dorsal type-2 bipolar cells (n = 12 of 14) displayed weak modulation to iso-intense stimuli and tended to have somewhat larger OFF-responses to green than to blue (Figure 19 B). In two (of 14) dorsal type-2 cells we found an exceptionally strong blue preference – reminiscent of the "outlier" among type-7 ON-bipolar cells – but in none of the dorsally recorded type-1 cells. This suggests larger response variability between type-2 cells compared to type-1 cells and also was the impulse to design a simple statistical model (section 5.3). In the ventral retina, the responses of type-1 (Figure 19 C) and type-2 bipolar cells (Figure 19 D) resembled each other, looking like "OFF-versions" of ventral type-7 responses: strong voltage modulations to iso-intense and blue stimuli but almost no response to green.

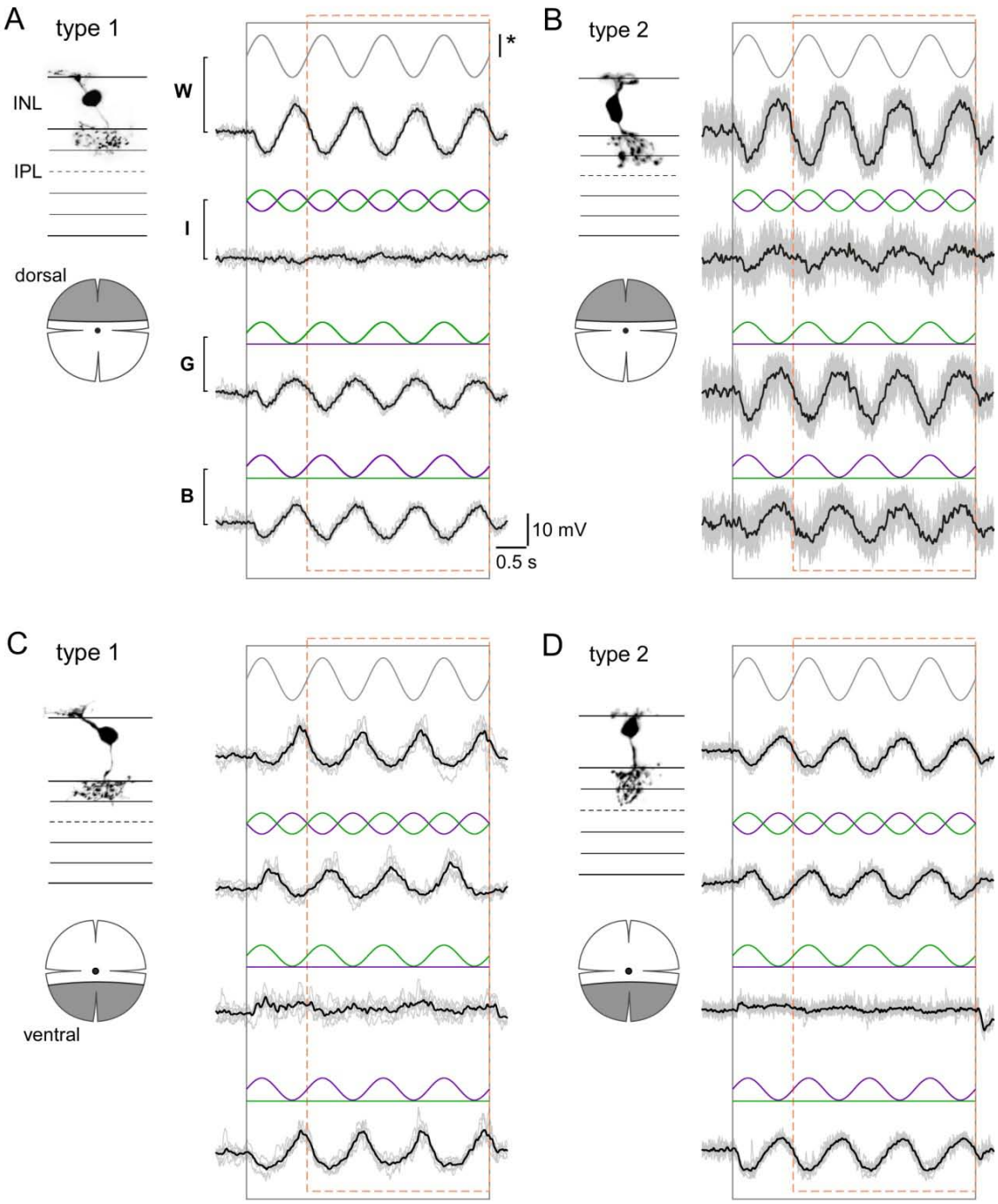

Figure 19: Voltage responses of type-1 and type-2 OFF-bipolar cells to chromatic stimulation.
A - D: Voltage responses to sinusoidally modulated spot stimuli (analog to Figure 18 C, D) recorded from type-1 OFF-bipolar cells in mitoP mice (A, C) and type-2 OFF-bipolar cells in CLM12 mice (B, D). The cells' morphologies (from maximum projected micrograph stacks) are shown next to the traces. Schematic drawing below the cell morphology indicates retinal region (shaded gray) from which the slices were cut. Average responses in black, individual trials in gray (A: n = 6, B: n = 10, C: n = 7, D: n = 10). Black and dashed orange rectangles indicate stimulus presentation and analysis windows, respectively. See Methods for details. The cells in A and B were recorded in the dorsal third; the cells in C and D were recorded in the ventral third of the retina. Intensity scale bar (*): $3 \cdot 10^5$ ph$\cdot$s$^{-1}\cdot\mu$m^{-2}.

5.2.6 Chromatic tuning of type-1, -2, -7 and -9 bipolar cells

Response behaviour, amplitude vs. phase

The relative response to blue and green varied between bipolar cells of the same type. Therefore, we quantified the responses, focusing on the modulation at the stimulus frequency $F_{Stim} = 1\ Hz$, using spectral analysis (Figure 12 in section 4.3.4; see also Hausselt et al., 2007). In brief, from the voltage responses to the four stimulus conditions we calculated power spectra to determine phase and amplitude (V_1) of the fundamental component at stimulus frequency of 1 Hz (Figure 20). The amplitude vs. phase plot reflects self-contained the response polarity of the recorded ON- and OFF-bipolar cells; each data point represents the averaged response amplitude of one cell.

As expected for OFF-cells, type-1 and type-2 bipolar cells phase-locked to the down-swings in the intensity of white, green and blue (type 1, dorsal, n = 18; ventral, n = 3; type 2, dorsal, n = 21; ventral, n = 3). For the iso-intense stimulus, type-2 cells exhibited a somewhat tighter phase-locking (lower phase variability) to down-swings of green than type-1 cells (Figure 20 A and B), consistent with a stronger green bias in the majority of type-2 bipolar cells. In contrast, ventral OFF-cells locked to blue down-swings in the iso-intense stimulus. Dorsal type-7 and type-9 ON-bipolar cells phase-locked to up-swings in intensity: Type-7 cells (n = 7) displayed a very broad phase distribution for the iso-intense stimulus, suggesting the lack of a clear chromatic preference (Figure 20 C). Dorsal type-9 ON-bipolar cells (n=3) phase-locked well to the blue up-swing of the iso-intense and only weakly to the green stimulus, as expected for S-cone selective blue^{ON} bipolar cells.

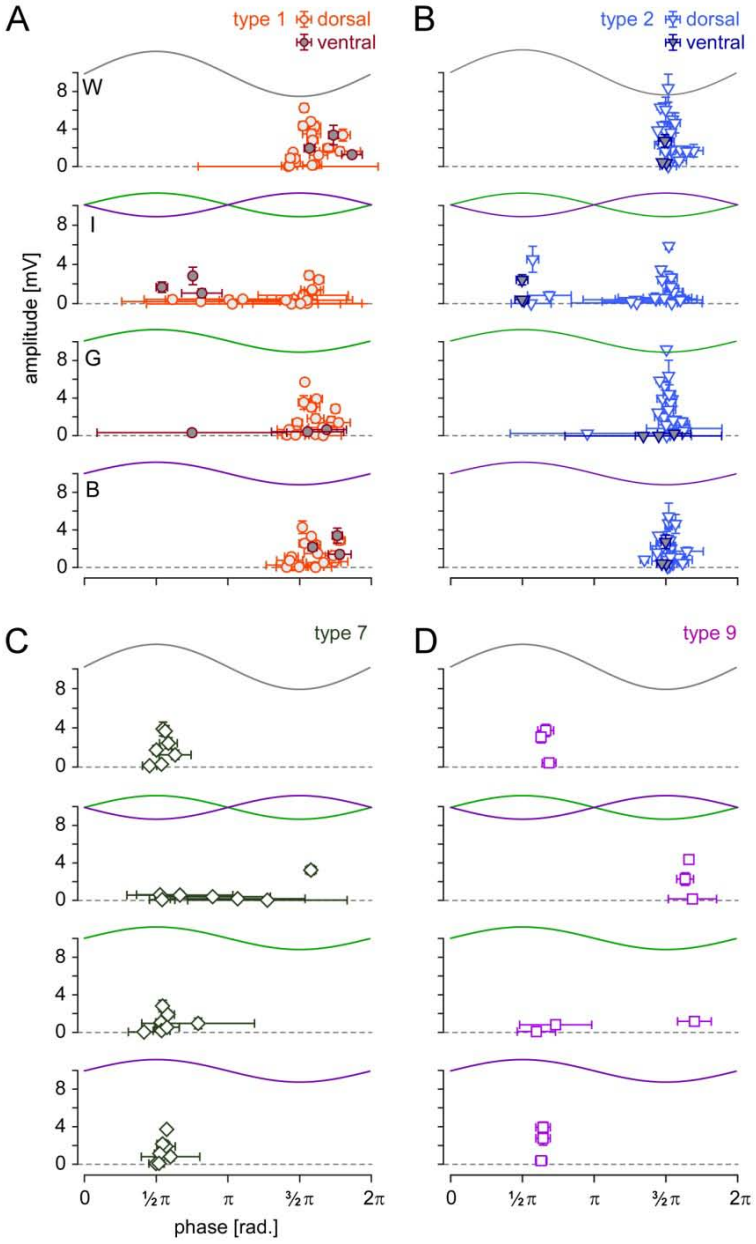

Figure 20: Scatter plots showing the fundamental component (voltage amplitude V_1 at stimulus frequency = 1 Hz) of the responses to "white" (W), iso-intensity (I), green (G) and blue (B) (compare with Figure 18 and Figure 19) indicated by the curve above data points. Amplitudes and phases were measured using spectral decomposition analysis; all cells included exhibited response amplitudes $V_1 \geq 15$ times the noise (see Methods). For every stimulus condition, each data point represents a cell (open symbols, dorsal cells; shaded symbols, ventral cells). A, B: As expected, type-1 (A, dorsal, n=18; ventral, n=3) and type-2 OFF-bipolar cells (dorsal, n=21; ventral, n=3) phase-lock to intensity down-swings of white, green and blue. Dorsal type-1 and -2 cells in more often responded stronger to the green component of the iso-intense stimulus; in contrast all ventral cells responded much stronger to the blue stimulus component. C: Dorsal type-7 on-cells (n=7) were phase-locked to intensity up-swings. The broad phase distribution of type-7 cells suggests the lack of a clear chromatic preference. D: Dorsal type-9 on-cells (n=3) phase-locked strongly to the blue up-swing of the iso-intense stimulus and only weakly to the green stimulus, as expected for S-cone selective on-cells. Note that one type-9 cell shows a green^{OFF} response component.

Chromatic tuning of type-1, -2, -7, and -9 bipolar cells

To quantify the chromatic tuning of the cells we calculated two ratios from the fundamental component amplitudes for each cell: iso-intense vs. white $R_{IW} = V_1(I)/V_1(W)$, and blue vs. green $V_1(B)/V_1(G)$. The results of both ratios (R_{IW} and R_{BG}) contain similar information. From the ratio $R_{BG} = V_1(B)/V_1(G)$ we calculated the respective chromatic tuning angle $\varphi_{BG} = \tan^{-1}(R_{BG})$ for better visualization (Figure 21; compare with Figure 22). Taking into account stimulus wavelengths and intensities as well as the mouse cone pigment absorption spectra (Jacobs et al., 2004), we expect for bipolar cells selective for S-cones or "pure" M-cones (w/o S-opsin co-expression) values around $\varphi_{BG} = 1.571$ and $\varphi_{BG} = 0.381$, respectively.

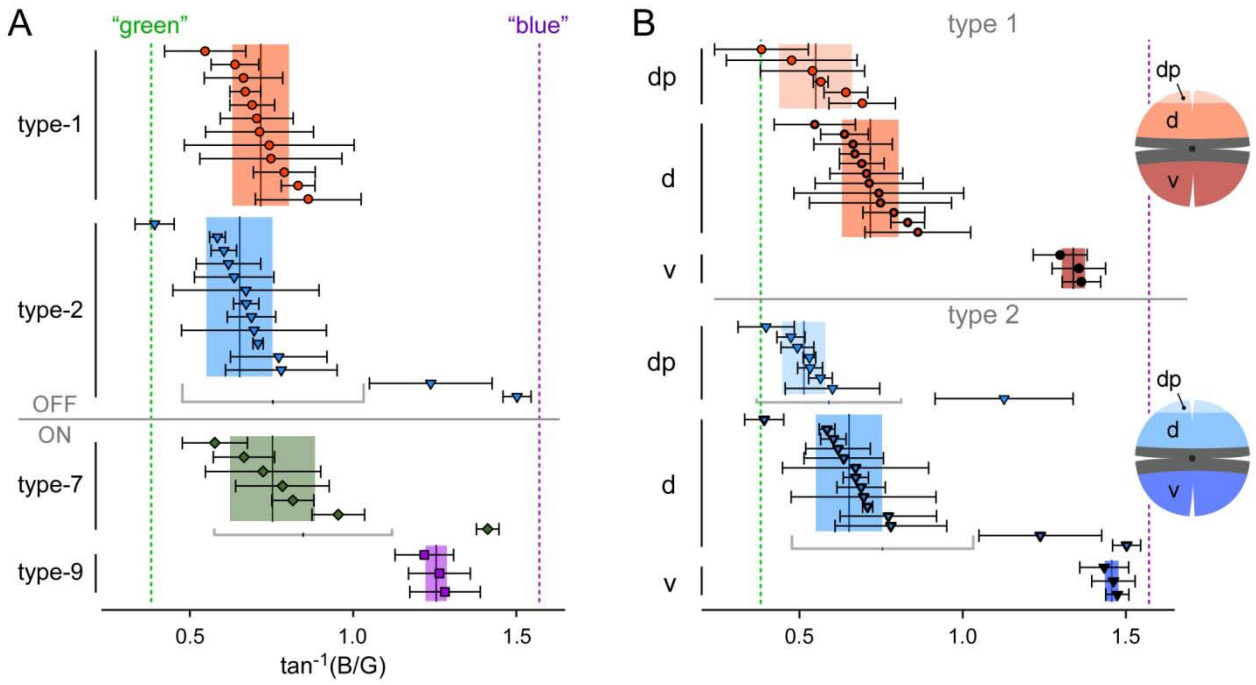

Figure 21: Chromatic tuning (blue vs. green) A: Scatter plot showing the chromatic tuning of type-1, -2, -7 and -9 bipolar cells in dorsal retina. Chromatic tuning is expressed as angle $\varphi_{BG} = tan^{-1}(V_1(B)/V_1(G))$ $\omega_{BG} = tan^{-1}[V_1(B)/V_1(G)]$(in radians $\pm$ $s.d.$) with $V_1(B)$ and $V_1(G)$ being the amplitudes of the fundamental components (= at the stimulus frequency 1 Hz) of the responses to the blue and green stimulus condition, respectively (see Methods). Small φ_{BG} indicate a preference for green, large φ_{BG} a preference for blue. Data from Figure 20 was used; each symbol represents a cell. For each bipolar cell type, vertical lines and shaded areas behind data points represent mean and S.D., respectively. Dotted lines indicate theoretically expected angles for bipolar cells with pure M-cone (no co-expression) or S-cone input (see text for details). B: Scatter plot analog to A but for type-1 and -2 cells in different retinal regions along the dorso-ventral axis (dp = dorsal periphery, d = dorsal, v = ventral).

Chromatic tuning angles for type-9 ON-cells were clearly blue-biased but did not reach those predicted for S-cone selective cells (Figure 21; all values in Table 1). The most likely reason for this is that due to noise, $V_1(G)$ is always larger than zero – even in the absence of a detectable modulation by green. Another possibility is the contribution from rods through gap junctions between AII amacrine cells and blue-cone bipolar cells (Yin et al., 2009). However,

since our stimulation intensities were in the photopic range, rods are likely saturated (but see Demontis et al., 1993; further discussed in section 6.6). For the other bipolar cell types – at least in the dorsal retina – φ_{BG} was clearly green-biased but rarely reached the value predicted for bipolar cells selectively contacting "pure" M-cones. Without the blue-biased outliers, the average φ_{BG} for type-2 bipolar cells was more biased towards green than it was for type-1 (Figure 21). With these outliers included, type-2 bipolar cells were somewhat less biased towards green and displayed a much larger variability in φ_{BG} than type-1 bipolar cells. In both cases, the difference between dorsal type-1 and type-2 cells was not statistically significant (p = 0.462, w/o outliers p = 0.128).

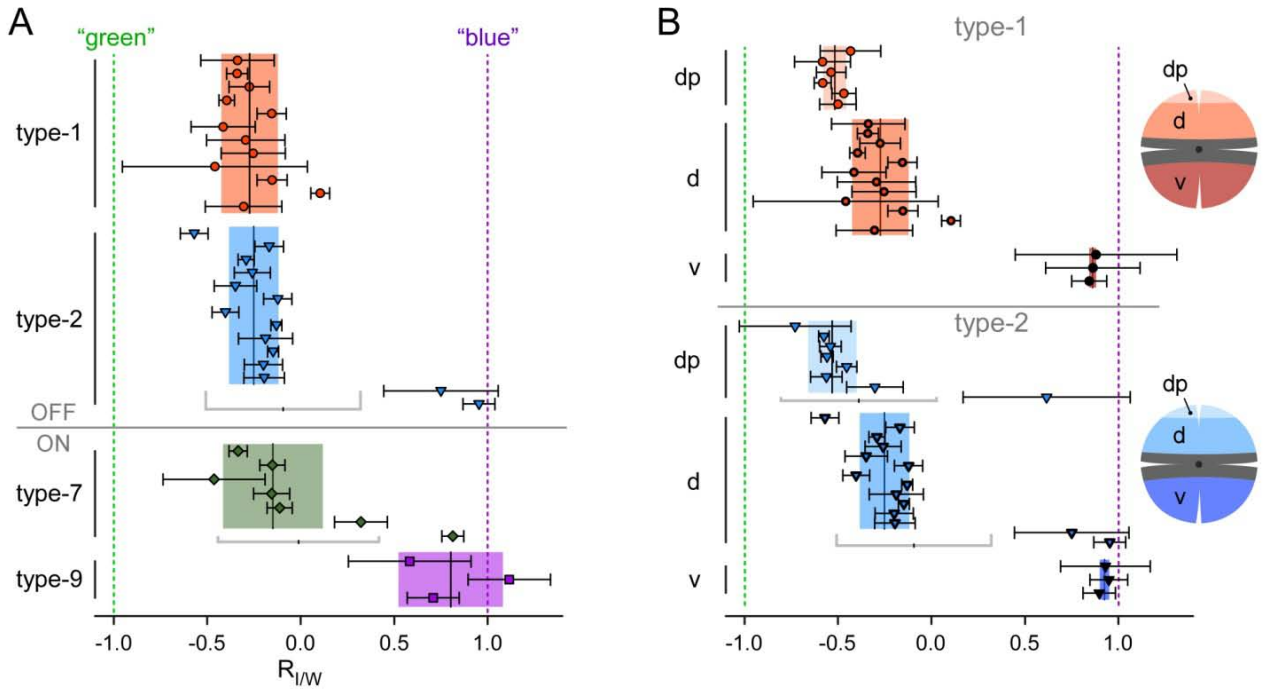

Figure 22: Chromatic tuning (iso-intense vs. white) A: Scatter plot showing the chromatic tuning of type-1, -2, -7 and -9 bipolar cells in dorsal retina. Chromatic tuning is expressed as ratio $R_{IW} = V_1(I)/V_1(W)$ $(\pm\, s.d.)$ with $a = 1$ for $V_1(B) > V_1(G)$ and $a = -1$ for $V_1(B) < V_1(G)$. $V_1(I, W, B, G)$ are the amplitudes of the fundamental components (= at the stimulus frequency, 1 Hz) of the responses to the iso-intense, white, blue or green stimulus condition. R_{IW} close to zero indicate little chromatic preference, cells with $R_{IW} < 0$ are OFF-, cells with $R_{IW} > 0$ are ON-types. Data from Figure 20 were used (cells are shown in the same order as in Figure 21); each symbol represents a cell. For each bipolar cell type, vertical lines and shaded areas behind data points represent mean and s.d., respectively. Note that one type-9 bipolar cell shows a ratio > 1, indicativefor blue^{ON}/green^{OFF} opponency. B: Scatter plot analog to A but for type-1 and -2 cells in different retinal regions along the dorso-ventral axis (dp = dorsal periphery, d = dorsal, v = ventral).

To test if the selected stimulus wavelengths prevented us from separating the chromatic tuning of the two OFF-bipolar cells, we used a second, simplified stimulator which had band pass-filtered LEDs (peaks: 360 nm and 520 nm) that closely matched the mouse cone peak sensitivities (360 nm and 511 nm, respectively, Jacobs et al., 2004). This reduced the co-excitation of the

M-opsin by blue from 40% to 11%. With this stimulator the difference in φ_{BG} between type-1 and -2 remained statistically insignificant (p = 0.836; Table 1), which suggests that the co-excitation by the stimulation wavelengths was not a critical limitation.

type of bipolar cell	**region**	**n**	**chromatic tuning angle:** φ_{BG} *(with "blue" outliers)*	**ratio (I/W):** R_{IW} *(with "blue" outliers)*
Stimulation wavelengths (peaks, in nm): 400, 578				
type 1	dp	6 *(0)*	0.550 ± 0.112	-0.517 ± 0.061
	d	12 *(0)*	0.717 ± 0.086	-0.273 ± 0.151
	v	3	1.339 ± 0.035	0.863 ± 0.019
type 2	dp	7 *(8)*	0.513 ± 0.066 *(0.590 ± 0.225)*	-0.532 ± 0.130 *(-0.388 ± 0.423)*
	d	12 *(14)*	0.652 ± 0.102 *(0.754 ± 0.282)*	-0.252 ± 0.133 *(-0.094 ± 0.421)*
	v	3	1.457 ± 0.021	0.926 ± 0.026
type 7	d	6 *(7)*	0.753 ± 0.130 *(0.847 ± 0.276)*	-0.149 ± 0.267 *(-0.012 ± 0.438)*
	v	1	1.350	0.869
type 9	d	3	1.255 ± 0.033	0.803 ± 0.279
all outliers (types 2 and 7)	*d*	*4*	*1.320 ± 0.169*	*0.784 ± 0.140*
Stimulation wavelengths (peaks, in nm): 360, 520				
type 1	dp	6	0.658 ± 0.087	-0.365 ± 0.176
type 2	dp	7	0.598 ± 0.164	-0.416 ± 0.201
IPA-S4/5	d	4	0.619 ± 0.035	-0.440 ± 0.186

Table 1: Chromatic tuning angle (φ_{BG}) and I/W ratio for the different bipolar cell types and retinal positions along the dorsal-ventral axis (dp = dorsal periphery; d = dorsal; v = ventral). See also Figure 21 and Figure 22.

Two factors – S-opsin co-expression in M-cones and contacts with S-cones – may be responsible for our finding that φ_{BG} for both type-1 and type-2 bipolar cells clearly deviated from what was theoretically expected for M-cone selective cells. To find out which of these factors

predominated we recorded an additional set of bipolar cells in the very periphery of the dorsal retina (Figure 19 B and D). If it was mainly synaptic input from S-cones that determined the bipolar cells' chromatic tuning, φ_{BG} should not differ in the dorsal periphery vs. the mid-dorsal region, because "true" S-cones are homogenously distributed along the dorso-ventral axis (Haverkamp et al., 2005). If, however, co-expression was the dominant factor, then φ_{BG} should be more green-biased in the dorsal periphery, where co-expression is at its minimum (Applebury et al., 2000). For both OFF-bipolar cell types recorded in the dorsal periphery we indeed measured a green shift that was statistically significant compared to mid-dorsal cells (type 1, $p < 0.01$; type 2, $p < 0.05$; Figure 21 B and Table 1). Note that also in the dorsal periphery we found a strongly blue-biased outlier among type-2 but not type-1 cells. Ventral type-1 and -2 cells displayed values in the range of those measured for type-9 cells. Taken together, this suggests that opsin co-expression in M-cones strongly influences the chromatic tuning of type-1 and -2 OFF-bipolar cells. Co-expression may also be the reason for the observed variability in φ_{BG} since this variability tended to be smaller in the distal periphery (minimal co-expression) and ventral regions (predominant S-opsin expression) compared to mid-dorsal retina.

In view of our histological data it is puzzling that type-7 ON-bipolar cells and type-2 OFF-bipolar cells, both of which clearly contact S-cones (Figure 13 A and Figure 15), did not substantially differ in their average chromatic tuning from type-1 OFF-bipolar cells, which appear to avoid S-cones. An intriguing possibility is that the strongly blue-biased outliers – as were observed among type-2 (3 out of 22 = 14 %) and type-7 (1 out of 7 = 14 %) but not type-1 cells (0 out of 18 = 0 %) – represent a subset of bipolar cells with S-cone input. To better understand how opsin co-expression, input from two cone types and cone-to-bipolar cell convergence affects bipolar cell chromatic tuning, we created a simple statistical model.

5.3 Statistical model of M- and S-cone input to bipolar cells

Using data on cone density (Haverkamp et al., 2005), opsin co-expression (Applebury et al., 2000) and spectral sensitivity (Jacobs et al., 2004), as well as cone-to-bipolar cell convergence (Wassle et al., 2009) and probability of photo-isomerizations at the stimulus wavelengths, we generated dorsal bipolar cell populations and estimated their chromatic tuning (Figure 23). An individual bipolar cell response consisted of the summed outputs of a given number of M-cones and, depending on the bipolar cell type, S-cones (Figure 23 A; Equation 1 and Equation 2). Each M-cone output was modulated by its individual opsin co-expression ratio – randomly drawn from a Gaussian (Figure 23 B, inset). In addition, we introduced "synaptic weight" factors ($w_{syn,M}$, $w_{syn,S}$) to be able to adjust any relative input strength of the two cone types.

The chromatic tuning angle for the simulated type-1 population (no S-cone contacts, $n_{cones} = 8 \pm 1,\ \varphi_{BG} = 0.683 \pm 0.116$, Figure 23 B) was similar to that of the cells recorded in dorsal retina (Table 1, d + dp). The simulated type-2 population (S-cone contacts permitted, $n_{cones} = 5 \pm 1$) showed a distribution with two main peaks, reminiscent of the recorded data: a larger "green" peak that consisted of bipolar cells contacting only M-cones (81.3% of the cells; $\varphi_{BG} = 0.681 \pm 148$), and a smaller "blue" peak that consisted of cells contacting one or more

S-cones. The mean φ_{BG} of the secondary ("blue") peak depended strongly on $w_{syn,M}$. To match the mean φ_{BG} of the "blue" peak in the model ($\varphi_{BG} = 1.256 \pm 0.111$) with that of the recorded "outlier cells" (Table 1) we had to assume the input from S-cones to be ≈ 4 times stronger than that from M-cones ($w_{syn,S}/w_{syn,M} = 4$; Figure 23). Nevertheless, the fraction of simulated type-2 cells with S-cone contacts (18.7 % with one or more S-cones contacts) was consistent with the fraction of blue-biased outliers in the recorded data (outliers ≈ 14%).

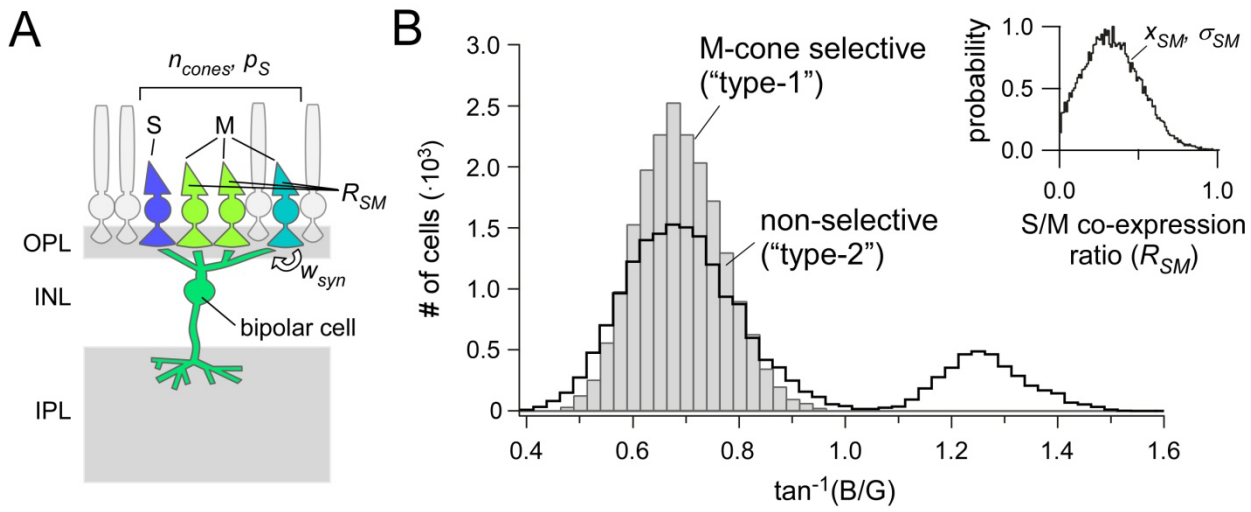

Figure 23: Statistical model of chromatic tuning in mouse bipolar cells. A: Drawing showing the concept of the statistical model with some of its parameters. B: Histogram showing the distribution of chromatic tuning in simulated populations of type-1 (gray bars) and type-2 (black curve) OFF-bipolar cells ($n = 2 \cdot 10^4$ cells simulated for each type). Parameters (see Methods for details): Number of cone contacts per bipolar cell, $n_{cones} = 8 \pm 1$ (type 1), 5 ± 1 (type 2); probability of S-cone contacts, $p_S = 0$ (type 1), 0.04 (type 2); synaptic weight, $w_{syn,S} = 4$, $w_{syn,M} = 1$; difference in photo-isomerization probability green/blue $\Phi_{M/S} = 0.6$; and M-cone opsin co-expression ratio, R_{SM} (see *inset*), drawn from a Gaussian centered at $x_{SM} = 0.3$ ($\sigma_{SM} = 0.2$). Relative cross-excitations of M-cone by blue and S-cones by green was $\varepsilon_{blue,M} = 0.4009$ and $\varepsilon_{green,S} = 6.51 \cdot 10^{-8}$, respectively.

5.4 Role of interplexiform amacrine cells

In addition to the work on bipolar cells we characterized the light responses of one type of amacrine cell, the IPA-S4/5 cell, (section 3.3.4; and Dedek et al., 2009). IPA-S4/5 cells terminate in stratum 4 and 5 of the IPL; therefore, we wanted to test whether these cells receive input from the S-cone selective type-9 bipolar cells (Figure 4; Haverkamp et al., 2005). We recorded (whole-cell patch-clamp) from GFP-positive IPA-S4/5 cells in retinal slices of $Cx45^+$ / fl:Parv-Cre mice (section 4.1). To relate the light responses to the local opsin expression we recorded only in dorsal slices (same location as in Figure 19 A and B). Morphological results are described elsewhere (Dedek et al., 2009; for typical morphology, see Figure 24 A).

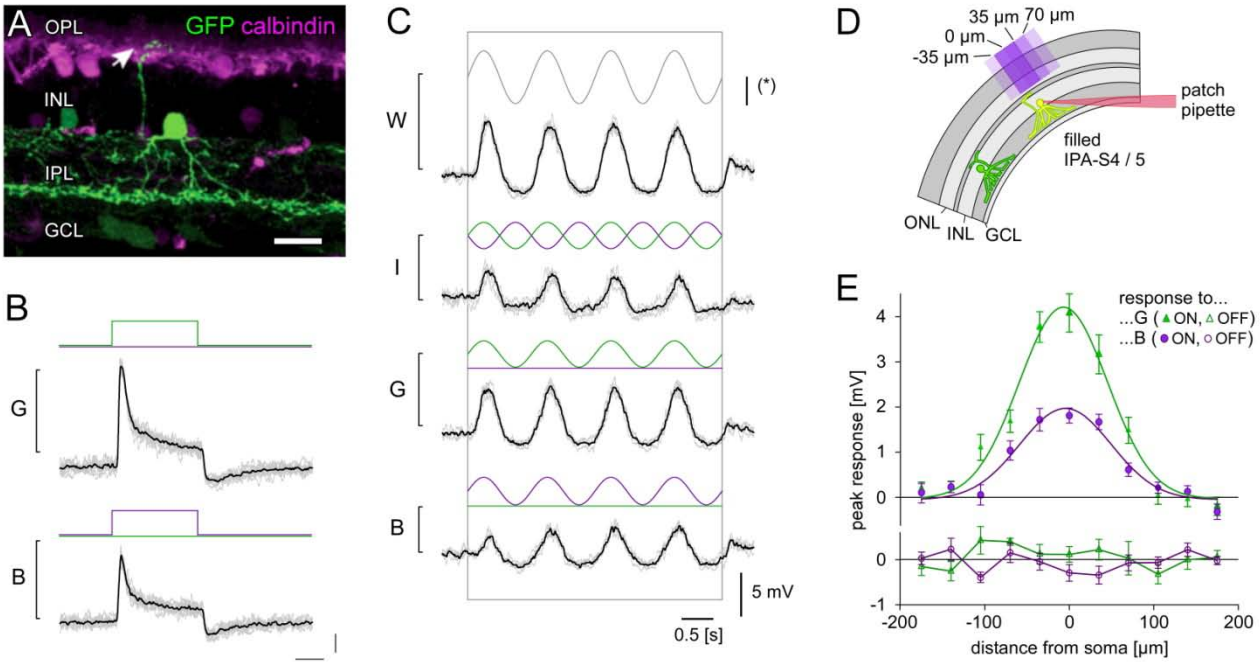

Figure 24: Morphology and physiology of GFP-positive interplexiform amacrine cells. A: Cryosection stained against GFP (green) and calbindin (magenta); the GFP positive IPA-S4/S5 cell (not calbindin-positive) stratifies in strata S4 and S5 and it sends a thin process to the OPL, where it branches. B: Voltage responses of a GFP positive IPA-S4/S5 cell. Cells were electrically recorded (slice preparation; whole-cell tight-seal) while presenting spots of dichromatic light to the photoreceptors (averaged trials in black; single trials in grey, n = 10; compare with Figure 18). C: Voltage responses of the same cell to a spot of sinusoidally modulated intensity ("white" (*W*), iso-intensity (*I*), green (*G*) and blue (*B*)), as illustrated above the traces (upper two traces averages of n = 5 trials, lower two traces averages of n = 4 trials; average in black, single trails in grey); scale bars of all voltage responses: 5 mV; time scale: 0.5 s. (C) Spatial sensitivity profile of another IPA-S4/5 cell measured with rectangular spots (70 µm x 140 µm in size; 35 µm steps) presented along the slice as illustrated (inset). Data points (symbols) are averages (± SEM; n = 6 trials; data from one cell) fit with Gaussian (curves); (spot diameters: 80 µm – 200 µm). Figure modified form Dedek et al., 2009.

In the case of significant type-9 bipolar cell input, the membrane voltage of a IPA-S4/5 cell should display strong modulation to *B* (and also to *W* and *I*) but little or no modulation to *G*; in the case of unselective input the cells should be modulated by both *B* and *G* with similar amplitude and sould show little modulation to the *I* stimulus condition. All tested IPA-S4/5 cells (n = 4) responded to both wavelength-components (*G* and *B*; Figure 24 B) with a strong depolarization to light^{ON}, which contained a pronounced transient component, and to light^{OFF} with a small transient hyperpolarization. Due to the low number of recorded cells we did not quantify the chromatic tuning analog to the recorded bipolar cells (section 5.2.6). IPA-S4/5 cells did not show a chromatic bias towards blue and, thus, it is unlikely that they receive direct input from S-cone selective type-9 bipolar cells. On the contrary, they seemed to be green biased. We did not further investigate whether the green-biased ON-responses are the consequence of input from S-cone avoiding bipolar cells or due to another mechanism.

6 DISCUSSION

6.1 Green^{OFF} pathway in mouse retina

Two lines of evidence support that type-1 bipolar cells represent a dedicated green^{OFF} pathway in mouse retina (see statistical model; Figure 26). First, our immunohistochemical data indicate that four out of five OFF-bipolar cell types described in mouse (2, 3a/b and 4; Ghosh et al., 2004; Wassle et al., 2009) non-selectively contact both cone types, whereas type-1 bipolar cells likely avoid S-cone contact (Figure 13-Figure 15). Second, the recorded population of type-2 (and -7) bipolar cells contains strongly blue-biased "outliers", which were not found among the type-1 cells (Figure 21 and Figure 22). The percentage of outliers recorded is consistent with that predicted for S-cone contacting type-2 cells by our statistical simulation (Figure 23; paragraph 5.3). Considering that type-1 bipolar cells contact on average 8 cones (vs. 5 cones for type-2 cells, taken from Wassle et al., 2009), one would expect ≈ 28 % of type-1 cells (5 out of 18) contacting one or more S-cones. Assuming blue-biased outliers represent cells with S-cone input, the lack of outliers in our recorded sample of type-1 cells is significant ($p < 0.01$, binomial test) and supports that type-1 bipolar cells avoid S-cones.

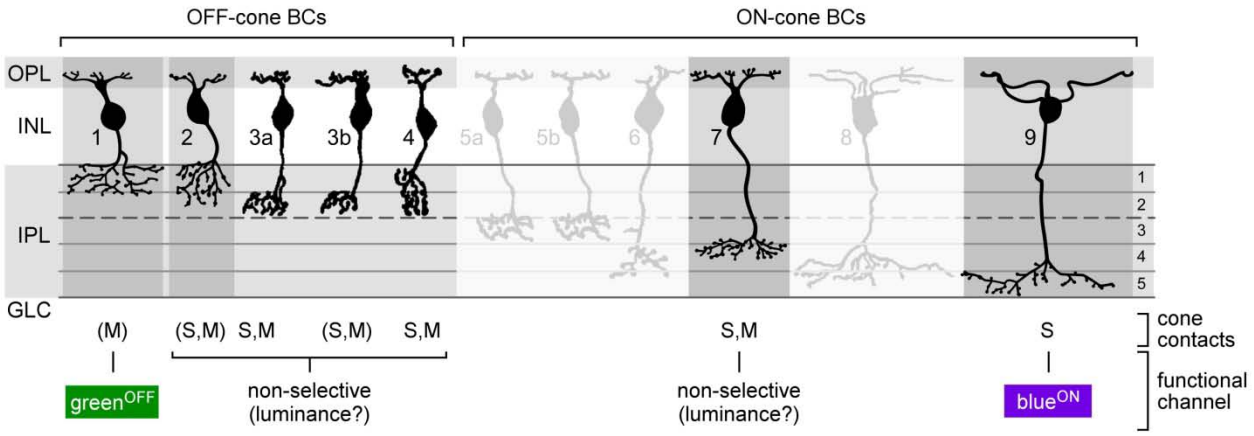

Figure 25: Bipolar cells scheme (mouse retina; compare with Figure 4). Type-2 and type-7 cells contact M- and S-cones non-selectively; they function as unselective channel. Type-9 cells selectively contact S-cones; they function as blue^{ON} channel. Type-1 cells presumably selectively contact M-cones. Type 1 is the candidate for the functional green^{OFF} channel. Anatomical results, see section 5.1; electrophysiological results, see 5.2; outlier hypothesis, see section 5.3. Cell-types in light gray panels: none or insufficient data available; cells in medium-gray panels: anatomical data supports available; brackets means data could not be statistically quantified; cells in darker-gray panels: electrophysiological and anatomical data available. Figure modified from Wassle et al., 2009.

In our study, we had to assume different synaptic weights (w_{syn}, Figure 23) for the two cone types to reconcile the statistical stimulation with the recorded bipolar cell responses: to explain the blue-biased average φ_{BG} of the outliers, S-cones would have to provide ≈ 4 times stronger input to the bipolar cells than M-cones. Such a gain difference could arise from multiple

factors, including cone type-specific differences in transduction efficiency and synaptic transmission/postsynaptic receptors. Electrical recordings from mouse cones revealed a somewhat higher gain (1.4x, see Nikonov et al., 2006) in cones that are more sensitive to stimulation at 360 nm compared to stimulation at 510 nm. However, since Nikonov et al., 2006 detected both opsins (at different ratios) in almost all cones of their sample it is likely that they mainly recorded from M-cones that co-express both opsins, and not from "true" S-cones. Anatomical data from primates suggest differences in the synaptic machinery of S- and M-cone pedicles (e.g. S-cone pedicles contain shorter, more densely packed ribbons; Haverkamp et al., 2001b; Puller et al., 2007), yet little functional data comparing the release properties of different cone types is available. Paired recordings from cones and bipolar cells in ground squirrel revealed that current injection into M-cones evoke larger bipolar cell responses than into S-cones (Zhaoping, 2006). While in ground squirrel the difference in cone input is opposite to what we would expect from our data in mouse, it demonstrates that, in principle, the strength of cone-to-bipolar cell transmission can be cone type-dependent.

The spectral sensitivity of mice measured by flicker-evoked ERGs, which mainly reflect photoreceptor and bipolar cell activity, indicates for the wavelengths we used a ≈10 fold higher sensitivity to blue than to green (Jacobs et al., 2004; Jacobs et al., 2007). This higher sensitivity to short wavelengths – so far only observed in mouse – is in contrast to the spectral sensitivity determined in behavioral experiments, where the two cone mechanisms appear to be balanced (Jacobs et al., 2004). In part, the higher blue/UV sensitivity is likely due to the increased S-opsin expression in mouse (roughly 3:1, estimated from mRNA levels, (Applebury et al., 2000); see discussion in (Jacobs et al., 2007; Jacobs et al., 2004), but it may also reflect a difference in cone output strength, at similar levels than we predicted by our statistical model. Although its specific functional role is still unclear, it is commonly agreed that UV vision is important for mice and other species with UV-shifted S-cones (for review, see Peichl, 2005). In view of the low frequency of S-cones (in mammals ≈ 3- 15 % of all cones; Szel et al., 1996), differential amplification of the S-cone signal would not be surprising. Also in mammals with peak sensitivities > 400 nm the low S-cone density should be compensated at some level. For instance, a recent study of guinea pig retina revealed that S/M opponent ganglion cell responses are well balanced (Yin et al., 2009). Taking into account presynaptic convergence and relative cone type density, the authors estimated that S-cone signals need to be amplified by a factor of ≈20 (compared to M-cone signals) to explain their measurements in ganglion cells. (Yin et al., 2009), however, assumed the same input strength for the two cone types and attributed the required gain to blue-cone bipolar cells.

6.2 Consequences of the presence of blue-biased outliers

It remains possible that the blue-biased outliers observed among type-2 and -7 cells are not representative for their types and that they may be of a different bipolar cell (sub)-type. The possibility is intriguing, because it would suggest the presence of a blue^{OFF} channel. However, since we used genetically labeled mouse lines to target bipolar cell types, this seems unlikely. Another possible explanation for the outliers may be slicing artifacts (i.e. single cone input by a

strongly S-opsin expressing cone), although then the lack of these artifacts among type-1 cells would be surprising.

If we ignored the blue-biased outliers, our data would suggest that a type-2 cell with S-cone input does not differ substantially in chromatic tuning from one connected to strongly S-opsin expressing M-cones. In other words, the presence of S-cone contacting (type-2) cells would be obscured by the wide range of co-expression ratios in M-cones. Then it would make functionally little difference, whether a potential color-opponent ganglion cell contacted type-1 or -2 bipolar cells, because opsin co-expression strongly affects bipolar cell chromatic tuning (Figure 21 B) and, thus, the presumed mouse blue/green circuit in any case compares S-cone signals with a mixture of S- and M-opsin mediated signals from M-cones. If, however, S-cone signals were more dominant as suggested by our statistical model, then color discrimination should benefit from selecting type-1 bipolar cell signals for green^{OFF}. To gauge this effect we estimated the "chromatic contrast" $C_{BG} = (\varphi_{BG,ON} - \varphi_{BG,OFF})/(\varphi_{BG,ON} + \varphi_{BG,OFF})$ of a bistratified ganglion cell (diameter: ≈ 150 µm) that contacts – in addition to type-9 – either type-1 or type-2 cells. Indeed, utilizing type-1 instead of type-2 cells increases C_{BG} mildly from 24% to 27%. Note that this estimate considers only direct synaptic signals from cones via bipolar cells to ganglion cells; it is conceivable than amacrine cells are also involved and may contribute to enhance C_{BG}.

6.3 Bipolar cell types in other mammals

Of the five OFF-bipolar cell types in mouse (Figure 4; Figure 25; Ghosh et al., 2004; Wassle et al., 2009) we found only one (type-1) that selectively contacts M-cones and could therefore serve as a reliable green^{OFF} pathway to the inner retina. In many aspects, the situation in mouse is similar to what was reported for a cone-dominated dichromatic mammal, the ground squirrel (Zhaoping, 2006), where the connectivity was investigated by recording cone bipolar cell pairs. Ground squirrel b7 OFF-bipolar cells morphologically resemble mouse type-1 cells: they stratify in IPL stratum 1 and selectively contact M-cones. Type b2 OFF-bipolar cells, which stratify in the middle of the IPL's OFF-sublamina (see Figure 2 in Zhaoping, 2006) – homologous to mouse type-3a/b cells – are non-selective. In ground squirrel no blue^{OFF} bipolar cell was found as well. In contrast to what we found in mice, ground squirrels possess a second type of OFF-bipolar cell (b3) that avoids S-cones (Zhaoping, 2006). However, the b3 in ground squirrel as well as its presumed counterpart in mouse, the type 2, have small dendritic fields. As a consequence, a substantial fraction of bipolar cells find no S-cone within their dendritic field, as reflected by the bimodal distribution of chromatic tuning we found in type-2 cells (Figure 23 B). In primate retina the diffuse OFF-bipolar cells form contacts with S-cones but their overall dendritic connections are biased against them (Lee and Grunert, 2007).

Of the cone-contacting ON-bipolar cells, we morphologically analyzed only type 7 (for type 9, see Haverkamp et al., 2005), which contacts non-selectively both cone types, consistent with ground squirrel data, where type b5 ON-bipolar cells (homologous to mouse type-7 cells) are non-selective (Li and DeVries, 2006). In primate retina the ON-bipolar cells investigated so far (DB4 and DB6) show small reduction but no complete avoidance of S-cone contacts compared to

M-/L-cones (60% and 75% S-cone contacts, respectively; Lee and Grunert, 2007). In ground squirrel "non-b5 ON-bipolar cells" (except for the blue-cone bipolar cell) also show a reduction in S-cone but no clear avoidance of S-cones (Li and DeVries, 2006).

Mouse type-9 ON-bipolar cells displayed blue^{ON} responses, as expected from their selective contacts with S-cones (Haverkamp et al., 2005). This is, to our knowledge, the first time that chromatic light responses were recorded from this cell type. Because S-cones possess an antagonistic surround due to horizontal cell feedback (Packer et al., 2010) blue-cone bipolar cells may inherit this surround and become blue^{ON}/green^{OFF} antagonistic themselves. This is also conceivable in mice, because their single type of horizontal cell contacts both cone types (Peichl and González-Soriano, 1994) and therefore relays mixed S/M signals. Furthermore, it is possible that horizontal cells also contribute to bipolar cell blue^{ON}/green^{OFF} opponency via GABAergic feed-forward connections (as discussed in Duebel et al., 2006). We observed only in one out of the three recorded type-9 cells a weak green^{OFF} response (Figure 20 D and Figure 22 A); there are several possible reasons for not observing it in the other two cells. One reason might be due to the dictation of the intracellular Cl^- concentration by the patch-pipette solution, the feedforward mechanism from horizontal cells might be altered. Other possible reasons are slicing artifacts (e.g. disturbed feedback to cones) or rod input to bipolar cells (further discussed in paragraph 6.6). Since stable recordings from this bipolar cell type were very infrequent, we did not further pursue this question.

6.4 Possibility of further cone-selective bipolar cell channels

In other mammalian species there is evidence that some ON-cone bipolar cells (not homologues of type 7) might avoid S-cone contacts (see above, section 6.3; Lee and Grunert, 2007; Li and DeVries, 2006). We cannot exclude cone-specific connectivity in the mouse ON-bipolar cell types (5a/b, 6 and 8) not studied here in detail. In non-selective cone pedicle stainings ON-bipolar cells appeared to contact all cones within their dendritic field (Wassle et al., 2009).

The light responses of the few recorded non-type-7or -9 ON-bipolar cells (type 6, n = 2; type 8, n = 2) displayed no particular chromatic bias; therefore S-cone selectivity (like in the case of type-9 cells) can be excluded. However, when considering our outlier hypothesis (section 5.3), we should not be able to distinguish between the light responses of M-cone selective and unselective cells in such a limited number of cells; therefore it remains possible that type-6 or type-8 cells are biased against S-cones. Due to a lack of data we cannot predict connectivity of type-5 ON-bipolar cells.

Interestingly, the IPA-S4/5 amacrine cells we tested with chromatic stimulation displayed green-biased ON-responses; the origin of this bias was not further investigated. One possibility might be the direct input to IPA-S4/5 cells form an S-cone avoiding ON-bipolar cell. Possible non-type-7or -9 ON-bipolar candidate cells based on co-stratification are Type-6 or -8 bipolar cells.

6.5 Chromatic circuitry in the mouse retina

The presence of green^{OFF} (type-1) and blue^{ON} (type-9) bipolar cells supports the view that a blue/green (or, due to opsin co-expression, rather S vs. S+M) chromatic circuitry exists in mouse (see hypothetical pathway; Figure 24) – homologues to the blue^{ON}/yellow^{OFF} (S vs. L+M) opponent circuitry that was described in primate retina (reviewed in Calkins, 2001; Dacey and Packer, 2003).

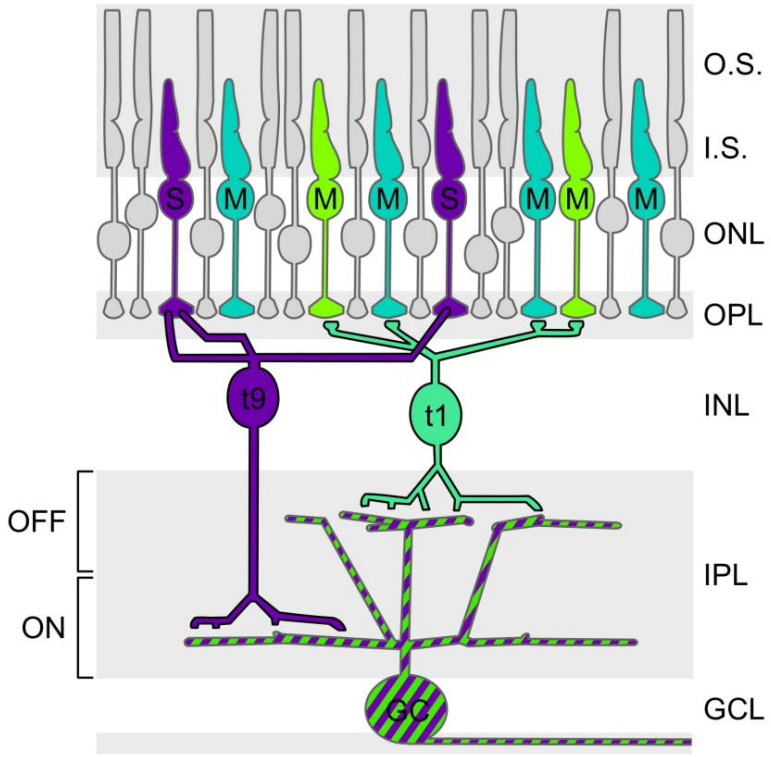

Figure 26: Hypothetical pathway for chromatic processing in the mouse retina. S-cone (S) selective type-9 ON-cone bipolar cells (t9, see (Haverkamp et al., 2005)) provide synaptic input to a certain type of ganglion cell (GC) that displays blue^{ON}/green^{OFF} responses (pathway is homolog to findings in primate retina; Dacey1994). S-cone avoiding OFF-bipolar cells (presumably type-1 bipolar cells; t1) contacting M-cones with varying amounts of S-opsin act as counterparts to create blue^{ON}/green^{OFF}-opponent signals.

That mouse retina contains color-opponent ganglion cells was shown using extracellular recordings (≈ 2% of all ganglion cells, Ekesten and Gouras, 2005). A suitable mouse ganglion cell type has been morphologically described ("type 1" in Schubert et al., 2005; G12 in Volgyi et al., 2009). It is bistratified, with dendrites ramifying in the IPL strata 1 and 5, where they could contact type-1 and -9 bipolar cells. Furthermore, color-opponent ganglion cells are not necessarily bistratified, since both macaque and guinea pig contain large monostratified ganglion cells with dendrites in the ON-sublamina of the IPL and color-opponent responses (Dacey and Packer, 2003; Yin et al., 2009). Guinea pig even appears to lack a bistratified color-opponent ganglion cell type. Therefore it is possible that also in mice monostratified ganglion cell types turn out to be color-opponent. Ganglion cells with "inverse" color opponency, as described in primate (yellow-

^{ON}/blue^{OFF}; for review, see Dacey and Packer, 2003) and guinea pig (green^{ON}/blue^{OFF}; Michael, 1968; Yin et al., 2009), have not yet been found in mouse (Ekesten and Gouras, 2005). To implement blue^{ON}/green^{OFF} (or green^{ON}/blue^{OFF}) in a monostratified ON-ganglion cell presumably requires amacrine cells to generate the necessary green^{OFF} (or blue^{OFF}) signals in the IPL's ON-sublamina (for review, see Dacey and Packer, 2003).

6.6 Rod pathway contribution under stimulation conditions

Because this work focuses on chromatic processing, the discussion about the contribution of achromatic rod pathways may seem irrelevant. Because there is only one rod type in mammalian retina, chromatic discrimination is not supported under conditions of rod-only vision. Yet, rod saturation requires relatively high light levels and suppression of rod responses at low photopic light levels is not as complete as formerly believed; therefore rods in principle can contribute somewhat to color perception even at low photopic light levels (Reitner et al., 1991; Demontis et al., 1993; Nikonov et al., 2006). For instance the small bistratified ganglion cells, which show blue^{ON}/yellow^{OFF} light responses, receive significant rod input even at mesopic to low photopic light levels (Field et al., 2009). Because this possibility may be particularly relevant to the mouse as a predominantly nocturnal species, rod pathways are discussed here with respect to our findings.

In the classical rod pathway, rod bipolar cells receive direct glutamatergic input from rod photoreceptors (reviewed in Bloomfield and Dacheux, 2001; Oesch and Diamond, 2009). Rod bipolar cells do not directly provide input to ganglion cells, but release glutamate onto AII amacrine cells. AII amacrine cells distribute the signal to ON- and OFF-bipolar cells via electrical synapses and inhibitory glycinergic synapses, respectively. Finally, the rod signal is transmitted to ganglion cells using the available cone pathways (the rod pathway "piggybacks" onto the cone pathways.). Recently it has been shown, that among the ON-bipolar cell types electrically coupled to the AII amacrine cells is also the blue-cone bipolar cell (Field et al., 2009), therefore under mesopic light levels, rod signals may contribute to chromatic processing. This is likely not the case for the two alternative rod pathways: Rod-cone coupling via gap junctions are the basis for the second rod pathway. In this pathway light responses from rods are transmitted, via the cone synapse, to ON- and OFF-bipolar cells, bypassing the classical rod pathway. The second rod pathway is functional at scotopic light conditions. It has also been shown that rods make also direct chemical synapses with specific types of OFF-bipolar cells (Hack et al., 1999; Mataruga et al., 2007; Haverkamp et al., 2008; Li et al., 2010). Note that mouse type-1 or type-2 bipolar cells do not receive direct rod input (Mataruga et al., 2007; Haverkamp et al., 2008). This third rod pathway might be functional under twilight conditions. The classical rod pathway has a higher sensitivity than second and third rod pathway, which is mainly due to nonlinear synaptic transmission between rods and rod bipolar cells. However, due to this nonlinearity, it has a narrower operational range than the second and third rod pathway (Li et al., 2010; Dunn et al., 2006).

For the LCoS-display stimulator, the stimulation intensity (irradiance) used in our electrophysiological experiments was always in the photopic range (≈ 5,100 photo-isomerizations per second and rod); this background intensity is predicted to suppress ≈ 96.7 % rod responses

(Nikonov et al., 2006). For the simple LED-stimulator, the background intensity (≈ 590 photo-isomerizations per second and rod) was in the mesopic to low photopic range (compare with (Field et al., 2009). This background intensity is predicted to suppress ≈ 77.1 % rod responses (Nikonov et al., 2006). Taken together, rod input to the S-cone selective type-9 bipolar cell is expected to be insignificant in the experiments using the LCoS-display stimulator – which was used in the great majority of experiments. With the simple LED-stimulator, there could have been some small rod contribution to the type-9 bipolar cell responses.

6.7 Influence of the opsin co-expression gradient

Our data indicate that the dorso-ventral opsin co-expression gradient in the mouse retina (Roehlich et al., 1994) has a tremendous effect on chromatic tuning of bipolar cells (Figure 21 and Figure 22), and therefore likely also on color discrimination. In the ventral retina, where S-opsin expression in M-cones is the highest (Applebury et al., 2000), bipolar cell responses are – almost irrespective of the type – strongly blue-biased. Yet, extracellular recordings suggest the presence of (a few) blue/green opponent ganglion cells in the ventral retina (Ekesten et al., 2000; but see Ekesten and Gouras, 2005), which suggest that the retina's chromatic circuitry might be able to amplify small differences in chromatic tuning.

Opsin co-expression gradients have been found in several mammalian species, including mouse, rabbit and guinea pig (Juliusson et al., 1994; Roehlich et al., 1994). The specific layout of the gradient varies between species (Roehlich et al., 1994). The effect of the gradient on horizontal cells and ganglion cell responses has been studied in guinea pig retina (Leamey et al., 2009; Yin et al., 2009), where it was demonstrated that the local degree of opsin co-expression directly relates to the chromatic tuning of the neurons – similar to what we observed in mouse bipolar cells. In guinea pig color opponent ganglion cells were also across the whole retina, however, the ganglion cells recorded ventrally showed reduced opponency, likely due to smaller M-opsin driven signals (Yin et al., 2009). Regional opsin co-expression may offer important functional advantages, e.g. to enhance contrast detection against different spectral backgrounds (i.e. blue sky vs. greenish-brownish ground, see (Leamey et al., 2009).

In summary, our combined anatomical and electrophysiological data as well as the results from simple statistical simulation suggests that mice feature at least two chromatic bipolar cell pathways – green^{OFF} via type-1, and blue^{ON} via type-9 bipolar cells. They likely represent parts of a conserved chromatic circuit that resembles the one of primates (for review, see Dacey, 2000) and ground squirrel (Zhaoping, 2006), supporting the view that blue/green (blue/yellow) opponency results from a common blueprint in mammalian retina.

7 REFERENCES

Ahnelt, P., Keri, C., and Kolb, H. (1990). Identification of pedicles of putative blue-sensitive cones in the human retina. J Comp Neurol *293*, 39-53.

Ahnelt, P., and Kolb, H. (1994). Horizontal cells and cone photoreceptors in primate retina: a Golgi-light microscopic study of spectral connectivity. J Comp Neurol *343*, 387-405.

Amthor, F.R., Takahashi, E.S., and Oyster, C.W. (1989). Morphologies of rabbit retinal ganglion cells with complex receptive fields. J Comp Neurol *280*, 97-121.

Applebury, M.L., Antoch, M.P., Baxter, L.C., Chun, L.L., Falk, J.D., Farhangfar, F., Kage, K., Krzystolik, M.G., Lyass, L.A., and Robbins, J.T. (2000). The murine cone photoreceptor: a single cone type expresses both S and M opsins with retinal spatial patterning. Neuron *27*, 513-523.

Badea, T.C., and Nathans, J. (2004). Quantitative analysis of neuronal morphologies in the mouse retina visualized by using a genetically directed reporter. J Comp Neurol *480*, 331-351.

Barlow, H.B., Hill, R.M., and Levick, W.R. (1964). Rabbit retinal ganglion cells responding selectively to direction and speed of image motion in the rabbit. JPhysiol *173*, 377-407.

Barnes, S., and Bui, Q. (1991). Modulation of calcium-activated chloride current via pH-induced changes of calcium channel properties in cone photoreceptors. J Neurosci *11*, 4015-4023.

Barnes, S., Merchant, V., and Mahmud, F. (1993). Modulation of transmission gain by protons at the photoreceptor output synapse. Proc Natl Acad Sci U S A *90*, 10081-10085.

Bennett, M.V., and Goodenough, D.A. (1978). Gap junctions, electrotonic coupling, and intercellular communication. Neurosci Res Program Bull *16*, 1-486.

Berglund, K., Dunbar, R.L., Lee, P., Feng, G., and Augustine, G.J. (2004). Imaging synaptic inhibition with Clomeleon, a genetically encoded chloride indicator. In Imaging in Neuroscience and Development: A Laboratory Manual, R. Yuste, and A. Konnerth, eds. (New York, Cold Spring Harbor Laboratory Press).

Bloomfield, S.A., and Dacheux, R.F. (2001). Rod vision: pathways and processing in the mammalian retina. Prog Retin Eye Res *20*, 351-384.

Bloomfield, S.A., and Volgyi, B. (2009). The diverse functional roles and regulation of neuronal gap junctions in the retina. Nat Rev Neurosci *10*, 495-506.

Bokil, H., Laaris, N., Blinder, K., Ennis, M., and Keller, A. (2001). Ephaptic interactions in the mammalian olfactory system. J Neurosci *21*, RC173.

Boycott, B.B. (1988). Horizontal cells of mammalian retinae. Neurosci Res Suppl *8*, S97-111.

Boycott, B.B., and Wassle, H. (1991). Morphological Classification of Bipolar Cells of the Primate Retina. Eur J Neurosci *3*, 1069-1088.

Boycott, B.B., and Wässle, H. (1991). Morphological classification of bipolar cells of the primate retina. EuropJNeurosci *3*, 1069-1088.

Brandstatter, J.H., and Hack, I. (2001). Localization of glutamate receptors at a complex synapse. The mammalian photoreceptor synapse. Cell Tissue Res *303*, 1-14.

Burkhardt, D.A. (1993). Synaptic feedback, depolarization, and color opponency in cone photoreceptors. Vis Neurosci *10*, 981-989.

Burns, M.E., and Baylor, D.A. (2001). Activation, deactivation, and adaptation in vertebrate photoreceptor cells. Annu Rev Neurosci *24*, 779-805.

Byzov, A.L., and Shura-Bura, T.M. (1986). Electrical feedback mechanism in the processing of signals in the outer plexiform layer of the retina. Vision Res *26*, 33-44.

Cadetti, L., and Thoreson, W.B. (2006). Feedback effects of horizontal cell membrane potential on cone calcium currents studied with simultaneous recordings. J Neurophysiol *95*, 1992-1995.

Caldwell, J.H., and Daw, N.W. (1978). New properties of rabbit retinal ganglion cells. J Physiol *276*, 257-276.

Calkins, D.J. (2001). Seeing with S cones. Prog Retin Eye Res *20*, 255-287.

Calkins, D.J., Schein, S.J., Tsukamoto, Y., and Sterling, P. (1994). M and L cones in macaque fovea connect to midget ganglion cells by different numbers of excitatory synapses. Nature *371*, 70-72.

Calkins, D.J., and Sterling, P. (1999). Evidence that circuits for spatial and color vision segregate at the first retinal synapse. Neuron *24*, 313-321.

Calkins, D.J., Tsukamoto, Y., and Sterling, P. (1998). Microcircuitry and mosaic of a blue-yellow ganglion cell in the primate retina. Journal of Neuroscience *18*, 3373-3385.

Chalfie, M., Tu, Y., Euskirchen, G., Ward, W.W., and Prasher, D.C. (1994). Green fluorescent protein as a marker for gene expression. Science *263*, 802-805.

Chan, T.L., and Grunert, U. (1998). Horizontal cell connections with short wavelength-sensitive cones in the retina: a comparison between New World and Old World primates. J Comp Neurol *393*, 196-209.

Cleland, B.G., and Levick, W.R. (1974). Properties of rarely encountered types of ganglion cells in the cat's retina and an overall classification. J Physiol *240*, 457-492.

Conway, B.R. (2009). Color vision, cones, and color-coding in the cortex. Neuroscientist *15*, 274-290.

Coombs, J., van der List, D., Wang, G.Y., and Chalupa, L.M. (2006). Morphological properties of mouse retinal ganglion cells. Neuroscience *140*, 123-136.

Crook, J.D., Davenport, C.M., Peterson, B.B., Packer, O.S., Detwiler, P.B., and Dacey, D.M. (2009). Parallel ON and OFF cone bipolar inputs establish spatially coextensive receptive field structure of blue-yellow ganglion cells in primate retina. J Neurosci *29*, 8372-8387.

Curcio, C.A., Sloan, K.R., Jr., Packer, O., Hendrickson, A.E., and Kalina, R.E. (1987). Distribution of cones in human and monkey retina: individual variability and radial asymmetry. Science *236*, 579-582.

Dacey, D.M. (1993). The mosaic of midget ganglion cells in the human retina. J Neurosci *13*, 5334-5355.

Dacey, D.M. (1996). Circuitry for color coding in the primate retina. ProcRSocLondB *93*, 582-588.

Dacey, D.M. (2000). Parallel pathways for spectral coding in primate retina. Annu Rev Neurosci *23*, 743-775.

Dacey, D.M., and Lee, B.B. (1994). The 'blue-on' opponent pathway in primate retina originates from a distinct bistratified ganglion cell type. Nature *367*, 731-735.

Dacey, D.M., Lee, B.B., Stafford, D.K., Pokorny, J., and Smith, V.C. (1996). Horizontal cells of the primate retina: cone specificity without spectral opponency. Science *271*, 656-659.

Dacey, D.M., and Packer, O.S. (2003). Colour coding in the primate retina: diverse cell types and cone-specific circuitry. Curr Opin Neurobiol *13*, 421-427.

Dacey, D.M., and Petersen, M.R. (1992). Dendritic field size and morphology of midget and parasol ganglion cells of the human retina. Proc Natl Acad Sci U S A *89*, 9666-9670.

Dacheux, R.F., and Raviola, E. (1982). Horizontal cells in the retina of the rabbit. Journal of Neuroscience *2*, 1486-1493.

Dartnall, H.J., Bowmaker, J.K., and Mollon, J.D. (1983). Human visual pigments: microspectrophotometric results from the eyes of seven persons. Proc R Soc Lond B Biol Sci *220*, 115-130.

Davenport, C.M., Detwiler, P.B., and Dacey, D.M. (2008). Effects of pH buffering on horizontal and ganglion cell light responses in primate retina: evidence for the proton hypothesis of surround formation. J Neurosci *28*, 456-464.

De Monasterio, F.M. (1978). Spectral interactions in horizontal and ganglion cells of the isolated and arterially-perfused rabbit retina. Brain Res *150*, 239-258.

Dedek, K., Breuninger, T., de Sevilla Muller, L.P., Maxeiner, S., Schultz, K., Janssen-Bienhold, U., Willecke, K., Euler, T., and Weiler, R. (2009). A novel type of interplexiform amacrine cell in the mouse retina. Eur J Neurosci *30*, 217-228.

Dedek, K., Pandarinath, C., Alam, N.M., Wellershaus, K., Schubert, T., Willecke, K., Prusky, G.T., Weiler, R., and Nirenberg, S. (2008). Ganglion cell adaptability: does the coupling of horizontal cells play a role? PLoS One *3*, e1714.

Demontis, G.C., Bisti, S., and Cervetto, L. (1993). Light sensitivity, adaptation and saturation in mammalian rods. Prog Brain Res *95*, 15-24.

Deng, Q., Wang, L., Dong, W., and He, S. (2006). Lateral components in the cone terminals of the rabbit retina: horizontal cell origin and glutamate receptor expression. J Comp Neurol *496*, 698-705.

Denk, W., Strickler, J.H., and Webb, W.W. (1990). Two-photon laser scanning fluorescence microscopy. Science *248*, 73-76.

DeVries, S.H. (2000). Bipolar cells use kainate and AMPA receptors to filter visual information into separate channels. Neuron *28*, 847-856.

DeVries, S.H., Qi, X., Smith, R., Makous, W., and Sterling, P. (2002). Electrical coupling between mammalian cones. Curr Biol *12*, 1900-1907.

Diller, L., Packer, O.S., Verweij, J., McMahon, M.J., Williams, D.R., and Dacey, D.M. (2004). L and M cone contributions to the midget and parasol ganglion cell receptive fields of macaque monkey retina. J Neurosci *24*, 1079-1088.

Duebel, J., Haverkamp, S., Schleich, W., Feng, G., Augustine, G.J., Kuner, T., and Euler, T. (2006). Two-Photon Imaging Reveals Somatodendritic Chloride Gradient in Retinal ON-Type Bipolar Cells Expressing the Biosensor Clomeleon. Neuron *49*, 81-94.

Dunn, F.A., Doan, T., Sampath, A.P., and Rieke, F. (2006). Controlling the gain of rod-mediated signals in the Mammalian retina. J Neurosci *26*, 3959-3970.

Ecker, J.L., Dumitrescu, O.N., Wong, K.Y., Alam, N.M., Chen, S.K., LeGates, T., Renna, J.M., Prusky, G.T., Berson, D.M., and Hattar, S. (2010). Melanopsin-expressing retinal ganglion-cell photoreceptors: cellular diversity and role in pattern vision. Neuron *67*, 49-60.

Edwards, F.A., Konnerth, A., Sakmann, B., and Takahashi, T. (1989). A thin slice preparation for patch clamp recordings from neurons of the mammalian central nervous system. Pflugers Arch *414*, 600-612.

Ekesten, B., and Gouras, P. (2005). Cone and rod inputs to murine retinal ganglion cells: evidence of cone opsin specific channels. Vis Neurosci *22*, 893-903.

Ekesten, B., and Gouras, P. (2008). Cone inputs to murine striate cortex. BMC Neurosci *9*, 113.

Ekesten, B., Gouras, P., and Yamamoto, S. (2000). Cone inputs to murine retinal ganglion cells. Vision Res *40*, 2573-2577.

Enz, R., Brandstatter, J.H., Wassle, H., and Bormann, J. (1996). Immunocytochemical localization of the GABAc receptor rho subunits in the mammalian retina. J Neurosci *16*, 4479-4490.

Estevez, O., and Spekreijse, H. (1982). The "silent substitution" method in visual research. Vision Res *22*, 681-691.

Euler, T., Hausselt, S.E., Margolis, D.J., Breuninger, T., Castell, X., Detwiler, P.B., and Denk, W. (2009). Eyecup scope--optical recordings of light stimulus-evoked fluorescence signals in the retina. Pflugers Arch *457*, 1393-1414.

Euler, T., Schneider, H., and Wässle, H. (1996). Glutamate responses of bipolar cells in a slice preparation of the rat retina. JNeurosci *16*, 2934-2944.

Euler, T., and Wässle, H. (1995). Immunocytochemical identification of cone bipolar cells in the rat retina. J Comp Neurol *361*, 461-478.

Euler, T., and Wässle, H. (1998). Different contributions of GABAA and GABAC receptors to rod and cone bipolar cells in a rat retinal slice preparation. Journal of Neurophysiology *79*, 1384-1395.

Fahrenfort, I., Klooster, J., Sjoerdsma, T., and Kamermans, M. (2005). The involvement of glutamate-gated channels in negative feedback from horizontal cells to cones. Prog Brain Res *147*, 219-229.

Famiglietti, E.V. (1992). Polyaxonal amacrine cells of rabbit retina: size and distribution of PA1 cells. J Comp Neurol *316*, 406-421.

Famiglietti, E.V., and Sharpe, S.J. (1995). Regional topography of rod and immunocytochemically characterized blue and green cone photoreceptors in rabbit retina. VisNeurosci *12*, 1151-1175.

Field, G.D., Greschner, M., Gauthier, J.L., Rangel, C., Shlens, J., Sher, A., Marshak, D.W., Litke, A.M., and Chichilnisky, E.J. (2009). High-sensitivity rod photoreceptor input to the blue-yellow color opponent pathway in macaque retina. Nat Neurosci *12*, 1159-1164.

Field, G.D., Sher, A., Gauthier, J.L., Greschner, M., Shlens, J., Litke, A.M., and Chichilnisky, E.J. (2007). Spatial properties and functional organization of small bistratified ganglion cells in primate retina. J Neurosci *27*, 13261-13272.

Fox, M.A., and Sanes, J.R. (2007). Synaptotagmin I and II are present in distinct subsets of central synapses. J Comp Neurol *503*, 280-296.

Franze, K., Grosche, J., Skatchkov, S.N., Schinkinger, S., Foja, C., Schild, D., Uckermann, O., Travis, K., Reichenbach, A., and Guck, J. (2007). Muller cells are living optical fibers in the vertebrate retina. Proc Natl Acad Sci U S A *104*, 8287-8292.

Fuchs, E.C., Zivkovic, A.R., Cunningham, M.O., Middleton, S., Lebeau, F.E., Bannerman, D.M., Rozov, A., Whittington, M.A., Traub, R.D., Rawlins, J.N.*, et al.* (2007). Recruitment of parvalbumin-positive interneurons determines hippocampal function and associated behavior. Neuron *53*, 591-604.

Furukawa, T., and Furshpan, E.J. (1963). Two inhibitory mechanisms in the Mauthner neurons of goldfish. J Neurophysiol *26*, 140-176.

Ghosh, K.K., Bujan, S., Haverkamp, S., Feigenspan, A., and Wassle, H. (2004). Types of bipolar cells in the mouse retina. J Comp Neurol *469*, 70-82.

Giguere, V., Isobe, K., and Grosveld, F. (1985). Structure of the murine Thy-1 gene. EMBO J *4*, 2017-2024.

Goodchild, A.K., Chan, T.L., and Grünert, U. (1996a). Horizontal cell connections with short-wavelength-sensitive cones in macaque monkey retina. Visual Neuroscience *13*, 833-845.

Goodchild, A.K., Ghosh, K.K., and Martin, P.R. (1996b). Comparison of photoreceptor spatial density and ganglion cell morphology in the retina of human, macaque monkey, cat, and the marmoset Callithrix jacchus. JCompNeurol *366*, 55-75.

Goodenough, D.A. (1974). Bulk isolation of mouse hepatocyte gap junctions. Characterization of the principal protein, connexin. J Cell Biol *61*, 557-563.

Greferath, U., Grunert, U., Muller, F., and Wassle, H. (1994). Localization of GABAA receptors in the rabbit retina. Cell Tissue Res *276*, 295-307.

Grunert, U., Greferath, U., Boycott, B.B., and Wassle, H. (1993). Parasol (P alpha) ganglion-cells of the primate fovea: immunocytochemical staining with antibodies against GABAA-receptors. Vision Res *33*, 1-14.

Guo, C., Hirano, A.A., Stella, S.L., Jr., Bitzer, M., and Brecha, N.C. (2010). Guinea pig horizontal cells express GABA, the GABA-synthesizing enzyme GAD 65, and the GABA vesicular transporter. J Comp Neurol *518*, 1647-1669.

Hack, I., and Peichl, L. (1999). Horizontal cells of the rabbit retina are non-selectively connected to the cones. Eur J Neurosci *11*, 2261-2274.

Hack, I., Peichl, L., and Brandstatter, J.H. (1999). An alternative pathway for rod signals in the rodent retina: rod photoreceptors, cone bipolar cells, and the localization of glutamate receptors. Proc Natl Acad Sci U S A *96*, 14130-14135.

Hare, W.A., and Owen, W.G. (1996). Receptive field of the retinal bipolar cell: a pharmacological study in the tiger salamander. J Neurophysiol *76*, 2005-2019.

Hausselt, S.E., Euler, T., Detwiler, P.B., and Denk, W. (2007). A dendrite-autonomous mechanism for direction selectivity in retinal starburst amacrine cells. PLoS Biol *5*, e185.

Haverkamp, S., Ghosh, K.K., Hirano, A.A., and Wassle, H. (2003). Immunocytochemical description of five bipolar cell types of the mouse retina. J Comp Neurol *455*, 463-476.

Haverkamp, S., Grunert, U., and Wassle, H. (2000). The cone pedicle, a complex synapse in the retina. Neuron *27*, 85-95.

Haverkamp, S., Grunert, U., and Wassle, H. (2001a). Localization of kainate receptors at the cone pedicles of the primate retina. J Comp Neurol *436*, 471-486.

Haverkamp, S., Grunert, U., and Wassle, H. (2001b). The synaptic architecture of AMPA receptors at the cone pedicle of the primate retina. J Neurosci *21*, 2488-2500.

Haverkamp, S., Specht, D., Majumdar, S., Zaidi, N.F., Brandstatter, J.H., Wasco, W., Wassle, H., and Tom Dieck, S. (2008). Type 4 OFF cone bipolar cells of the mouse retina express calsenilin and contact cones as well as rods. J Comp Neurol *507*, 1087-1101.

Haverkamp, S., Wassle, H., Duebel, J., Kuner, T., Augustine, G.J., Feng, G., and Euler, T. (2005). The primordial, blue-cone color system of the mouse retina. J Neurosci *25*, 5438-5445.

He, S., and Masland, R.H. (1997). Retinal direction selectivity after targeted laser ablation of starburst amacrine cells. Nature *389*, 378-382.

Hirasawa, H., and Kaneko, A. (2003). pH changes in the invaginating synaptic cleft mediate feedback from horizontal cells to cone photoreceptors by modulating Ca2+ channels. J Gen Physiol *122*, 657-671.

Hofer, H., Carroll, J., Neitz, J., Neitz, M., and Williams, D.R. (2005). Organization of the human trichromatic cone mosaic. J Neurosci *25*, 9669-9679.

Hornstein, E.P., Verweij, J., and Schnapf, J.L. (2004). Electrical coupling between red and green cones in primate retina. Nat Neurosci *7*, 745-750.

Huang, L., Max, M., Margolskee, R.F., Su, H., Masland, R.H., and Euler, T. (2003). G protein subunit G gamma 13 is coexpressed with G alpha o, G beta 3, and G beta 4 in retinal ON bipolar cells. J Comp Neurol *455*, 1-10.

Hurvich, L.M., and Jameson, D. (1957). An opponent-process theory of color vision. Psychol Rev *64, Part 1*, 384-404.

Jacobs, G.H., Neitz, J., and Deegan, J.F.d. (1991). Retinal receptors in rodents maximally sensitive to ultraviolet light. Nature *353*, 655-656.

Jacobs, G.H., Williams, G.A., Cahill, H., and Nathans, J. (2007). Emergence of novel color vision in mice engineered to express a human cone photopigment. Science *315*, 1723-1725.

Jacobs, G.H., Williams, G.A., and Fenwick, J.A. (2004). Influence of cone pigment coexpression on spectral sensitivity and color vision in the mouse. Vision Res *44*, 1615-1622.

Jonas, J.B., Schneider, U., and Naumann, G.O. (1992). Count and density of human retinal photoreceptors. Graefes Arch Clin Exp Ophthalmol *230*, 505-510.

Juliusson, B., Bergstrom, A., Rohlich, P., Ehinger, B., van Veen, T., and Szel, A. (1994). Complementary cone fields of the rabbit retina. Invest Ophthalmol Vis Sci *35*, 811-818.

Jusuf, P.R., Martin, P.R., and Grunert, U. (2006). Random wiring in the midget pathway of primate retina. J Neurosci *26*, 3908-3917.

Kamermans, M., and Fahrenfort, I. (2004). Ephaptic interactions within a chemical synapse: hemichannel-mediated ephaptic inhibition in the retina. Curr Opin Neurobiol *14*, 531-541.

Kamermans, M., Fahrenfort, I., Schultz, K., Janssen-Bienhold, U., Sjoerdsma, T., and Weiler, R. (2001). Hemichannel-mediated inhibition in the outer retina. Science *292*, 1178-1180.

Kamermans, M., and Spekreijse, H. (1999). The feedback pathway from horizontal cells to cones. A mini review with a look ahead. Vision Res *39*, 2449-2468.

Kaneko, A., and Tachibana, M. (1986). Effects of gamma-aminobutyric acid on isolated cone photoreceptors of the turtle retina. J Physiol *373*, 443-461.

Kikkawa, S., Nakagawa, M., Iwasa, T., Kaneko, A., and Tsuda, M. (1993). GTP-binding protein couples with metabotropic glutamate receptor in bovine retinal on-bipolar cell. Biochem Biophys Res Commun *195*, 374-379.

Kolb, H., and Dekorver, L. (1991). Midget ganglion cells of the parafovea of the human retina: a study by electron microscopy and serial section reconstructions. J Comp Neurol *303*, 617-636.

Kolb, H., Mariani, A., and Gallego, A. (1980). A second type of horizontal cell in the monkey retina. J Comp Neurol *189*, 31-44.

Kolb, H., and Marshak, D. (2003). The midget pathways of the primate retina. Doc Ophthalmol *106*, 67-81.

Kong, J.H., Fish, D.R., Rockhill, R.L., and Masland, R.H. (2005). Diversity of ganglion cells in the mouse retina: unsupervised morphological classification and its limits. J Comp Neurol *489*, 293-310.

Korn, H., and Axelrad, H. (1980). Electrical inhibition of Purkinje cells in the cerebellum of the rat. Proc Natl Acad Sci U S A *77*, 6244-6247.

Kouyama, N., and Marshak, D. (1992). Bipolar cells specific for blue cones in the macaque retina. JNeurosci *12*, 1233-1252.

Kryger, Z., Galli-Resta, L., Jacobs, G.H., and Reese, B.E. (1998). The topography of rod and cone photoreceptors in the retina of the ground squirrel. Vis Neurosci *15*, 685-691.

Leamey, C.A., Van Wart, A., and Sur, M. (2009). Intrinsic patterning and experience-dependent mechanisms that generate eye-specific projections and binocular circuits in the visual pathway. Curr Opin Neurobiol *19*, 181-187.

Lee, B.B., Kremers, J., and Yeh, T. (1998). Receptive fields of primate retinal ganglion cells studied with a novel technique. Vis Neurosci *15*, 161-175.

Lee, S.C., and Grunert, U. (2007). Connections of diffuse bipolar cells in primate retina are biased against S-cones. J Comp Neurol *502*, 126-140.

Lee, S.C., Jusuf, P.R., and Grunert, U. (2004). S-cone connections of the diffuse bipolar cell type DB6 in macaque monkey retina. J Comp Neurol *474*, 353-363.

Lee, S.C., Telkes, I., and Grunert, U. (2005). S-cones do not contribute to the OFF-midget pathway in the retina of the marmoset, Callithrix jacchus. Eur J Neurosci *22*, 437-447.

Lennie, P. (1980). Parallel visual pathways: a review. Vision Res *20*, 561-594.

Li, W., Chen, S., and DeVries, S.H. (2010). A fast rod photoreceptor signaling pathway in the mammalian retina. Nat Neurosci *13*, 414-416.

Li, W., and DeVries, S.H. (2004). Separate blue and green cone networks in the mammalian retina. Nat Neurosci *7*, 751-756.

Li, W., and DeVries, S.H. (2006). Bipolar cell pathways for color and luminance vision in a dichromatic mammalian retina. Nat Neurosci *9*, 669-675.

Linberg, K.A., Suemune, S., and Fisher, S.K. (1996). Retinal neurons of the California ground squirrel, Spermophilus beecheyi: a Golgi study. J Comp Neurol *365*, 173-216.

MacNeil, M.A., and Gaul, P.A. (2008). Biocytin wide-field bipolar cells in rabbit retina selectively contact blue cones. J Comp Neurol *506*, 6-15.

MacNeil, M.A., and Masland, R.H. (1998). Extreme diversity among amacrine cells: implications for function. Neuron *20*, 971-982.

Mariani, A.P. (1984). Bipolar cells in monkey retina selective for the cones likely to be blue-sensitive. Nature *308*, 184-186.

Martin, P.R., Lee, B.B., White, A.J., Solomon, S.G., and Ruttiger, L. (2001). Chromatic sensitivity of ganglion cells in the peripheral primate retina. Nature *410*, 933-936.

Masland, R.H. (2001). The fundamental plan of the retina. Nat Neurosci *4*, 877-886.

Masland, R.H. (2005). The many roles of starburst amacrine cells. Trends Neurosci *28*, 395-396.

Mataruga, A., Kremmer, E., and Muller, F. (2007). Type 3a and type 3b OFF cone bipolar cells provide for the alternative rod pathway in the mouse retina. J Comp Neurol *502*, 1123-1137.

Maxeiner, S., Dedek, K., Janssen-Bienhold, U., Ammermuller, J., Brune, H., Kirsch, T., Pieper, M., Degen, J., Kruger, O., Willecke, K*., et al.* (2005). Deletion of connexin45 in mouse retinal neurons disrupts the rod/cone signaling pathway between AII amacrine and ON cone bipolar cells and leads to impaired visual transmission. J Neurosci *25*, 566-576.

Michael, C.R. (1968). Receptive fields of single optic nerve fibers in a mammal with an all-cone retina. 3. Opponent color units. J Neurophysiol *31*, 268-282.

Misgeld, T., Kerschensteiner, M., Bareyre, F.M., Burgess, R.W., and Lichtman, J.W. (2007). Imaging axonal transport of mitochondria in vivo. Nat Methods *4*, 559-561.

Nakajima, Y., Iwakabe, H., Akazawa, C., Nawa, H., Shigemoto, R., Mizuno, N., and Nakanishi, S. (1993). Molecular characterization of a novel retinal metabotropic glutamate receptor mGluR6 with a high agonist selectivity for L-2- amino-4-phosphonobutyrate. J Bio Chem *268*, 11868-11873.

Nakanishi, S., Masu, M., Bessho, Y., Nakajima, Y., Hayashi, Y., and Shigemoto, R. (1994). Molecular diversity of glutamate receptors and their physiological functions. [Review]. EXS *71*, 71-80.

Nelson, R. (1985). Spectral properties of cat horizontal cells. Neurosci Res Suppl *2*, S167-183.

Nelson, R., Famiglietti, E.V., and Kolb, H. (1978). Intracellular staining reveals different levels of stratification for ON- and OFF-center ganglion cells in cat retina. JNeurophysiol *41*, 472-483.

Newman, E., and Reichenbach, A. (1996). The muller cell - A functional element of the retina. Trends in Neurosciences *19*, 307-312.

Nikonov, S.S., Kholodenko, R., Lem, J., and Pugh, E.N., Jr. (2006). Physiological features of the S- and M-cone photoreceptors of wild-type mice from single-cell recordings. J Gen Physiol *127*, 359-374.

Oesch, N., and Diamond, J. (2009). A night vision neuron gets a day job. Nat Neurosci *12*, 1209-1211.

Olveczky, B.P., Baccus, S.A., and Meister, M. (2003). Segregation of object and background motion in the retina. Nature *423*, 401-408.

Oyster, C.W. (1968). The analysis of image motion by the rabbit retina. J Physiol *199*, 613-635.

Packer, O.S., Verweij, J., Li, P.H., Schnapf, J.L., and Dacey, D.M. (2010). Blue-yellow opponency in primate S cone photoreceptors. J Neurosci *30*, 568-572.

Pan, F., and Massey, S.C. (2007). Rod and cone input to horizontal cells in the rabbit retina. J Comp Neurol *500*, 815-831.

Paulus, W., and Kroger-Paulus, A. (1983). A new concept of retinal colour coding. Vision Res *23*, 529-540.

Peichl, L. (2005). Diversity of mammalian photoreceptor properties: Adaptations to habitat and lifestyle? Anat Rec A Discov Mol Cell Evol Biol *287*, 1001-1012.

Peichl, L., and Gonzalez-Soriano, J. (1994). Morphological types of horizontal cell in rodent retinae: a comparison of rat, mouse, gerbil, and guinea pig. Vis Neurosci *11*, 501-517.

Peichl, L., and González-Soriano, J. (1994). Morphological types of horizontal cell in rodent retinae: a comparison of rat, mouse, gerbil and guinea pig. VisNeurosci *11*, 501-517.

Pfeiffer-Guglielmi, B., Fleckenstein, B., Jung, G., and Hamprecht, B. (2003). Immunocytochemical localization of glycogen phosphorylase isozymes in rat nervous tissues by using isozyme-specific antibodies. J Neurochem *85*, 73-81.

Piantanida, T. (1988). The molecular genetics of color vision and color blindness. Trends Genet *4*, 319-323.

Piccolino, M., Neyton, J., and Gerschenfeld, H.M. (1984). Decrease of gap junction permeability induced by dopamine and cyclic adenosine 3':5'-monophosphate in horizontal cells of turtle retina. J Neurosci *4*, 2477-2488.

Pignatelli, V., and Strettoi, E. (2004). Bipolar cells of the mouse retina: a gene gun, morphological study. J Comp Neurol *476*, 254-266.

Polyak, S.L. (1941). The retina. Chicago: University of Chicago Press.

Provencio, I., Jiang, G., De Grip, W.J., Hayes, W.P., and Rollag, M.D. (1998). Melanopsin: An opsin in melanophores, brain, and eye. Proc Natl Acad Sci U S A *95*, 340-345.

Provencio, I., Rodriguez, I.R., Jiang, G., Hayes, W.P., Moreira, E.F., and Rollag, M.D. (2000). A novel human opsin in the inner retina. J Neurosci *20*, 600-605.

Puller, C., de Sevilla Muller, L.P., Janssen-Bienhold, U., and Haverkamp, S. (2009). ZO-1 and the spatial organization of gap junctions and glutamate receptors in the outer plexiform layer of the mammalian retina. J Neurosci *29*, 6266-6275.

Puller, C., Haverkamp, S., and Grunert, U. (2007). OFF midget bipolar cells in the retina of the marmoset, Callithrix jacchus, express AMPA receptors. J Comp Neurol *502*, 442-454.

Reid, R.C., and Shapley, R.M. (1992). Spatial structure of cone inputs to receptive fields in primate lateral geniculate nucleus. Nature *356*, 716-718.

Reitner, A., Sharpe, L.T., and Zrenner, E. (1991). Is colour vision possible with only rods and blue-sensitive cones? Nature *352*, 798-800.

Riggs, L.A. (1967). Electrical evidence on the trichromatic theory. The Jonas S. Friedenwald Memorial Lecture. Invest Ophthalmol *6*, 6-17.

Rodieck, R.W., Binmoeller, K.F., and Dineen, J. (1985). Parasol and midget ganglion cells of the human retina. J Comp Neurol *233*, 115-132.

Roehlich, P., Van Veen, T., and Szél, A. (1994). Two different visual pigments in one retinal cone cell. Neuron *13*, 1159-1166.

Satoh, H., Kaneda, M., and Kaneko, A. (2001). Intracellular chloride concentration is higher in rod bipolar cells than in cone bipolar cells of the mouse retina. Neurosci Lett *310*, 161-164.

Schubert, T., and Euler, T. (2010). Retinal processing: global players like it local. Curr Biol *20*, R486-488.

Schubert, T., Huckfeldt, R.M., Parker, E., Campbell, J.E., and Wong, R.O. (2010). Assembly of the outer retina in the absence of GABA synthesis in horizontal cells. Neural Dev *5*, 15.

Schubert, T., Kerschensteiner, D., Eggers, E.D., Misgeld, T., Kerschensteiner, M., Lichtman, J.W., Lukasiewicz, P.D., and Wong, R.O. (2008). Development of presynaptic inhibition onto retinal bipolar cell axon terminals is subclass-specific. J Neurophysiol *100*, 304-316.

Schubert, T., Maxeiner, S., Kruger, O., Willecke, K., and Weiler, R. (2005). Connexin45 mediates gap junctional coupling of bistratified ganglion cells in the mouse retina. J Comp Neurol *490*, 29-39.

Schwartz, E.A. (2002). Transport-mediated synapses in the retina. Physiol Rev *82*, 875-891.

Shimomura, O. (2005). The discovery of aequorin and green fluorescent protein. J Microsc *217*, 1-15.

Skrzypek, J., and Werblin, F. (1983). Lateral interactions in absence of feedback to cones. J Neurophysiol *49*, 1007-1016.

Soni, B.G., and Foster, R.G. (1997). A novel and ancient vertebrate opsin. FEBS Lett *406*, 279-283.

Stockman, A., and Sharpe, L.T. (2000). The spectral sensitivities of the middle- and long-wavelength-sensitive cones derived from measurements in observers of known genotype. Vision Res *40*, 1711-1737.

Stockman, A., and Sharpe, L.T. (2006). Into the twilight zone: the complexities of mesopic vision and luminous efficiency. Ophthalmic Physiol Opt *26*, 225-239.

Studholme, K.M., and Yazulla, S. (1988). Localization of GABA and glycine in goldfish retina by electron microscopic postembedding immunocytochemistry: improved visualization of synaptic structures with LR white resin. J Neurocytol *17*, 859-870.

Sun, W., Li, N., and He, S. (2002). Large-scale morphological survey of mouse retinal ganglion cells. J Comp Neurol *451*, 115-126.

Suzuki, H., and Pinto, L.H. (1986). Response properties of horizontal cells in the isolated retina of wild-type and pearl mutant mice. J Neurosci *6*, 1122-1128.

Svaetichin, G., and Macnichol, E.F., Jr. (1959). Retinal mechanisms for chromatic and achromatic vision. Ann N Y Acad Sci *74*, 385-404.

Szél, A., and Roehlich, P. (1992). Two cone types of rat retina detected by anti-visual pigment antibodies. ExpEye Res *55*, 47-52.

Szel, A., Rohlich, P., Caffe, A.R., Juliusson, B., Aguirre, G., and Van Veen, T. (1992). Unique topographic separation of two spectral classes of cones in the mouse retina. J Comp Neurol *325*, 327-342.

Szel, A., Rohlich, P., Caffe, A.R., and van Veen, T. (1996). Distribution of cone photoreceptors in the mammalian retina. Microsc Res Tech *35*, 445-462.

Tatsukawa, T., Hirasawa, H., Kaneko, A., and Kaneda, M. (2005). GABA-mediated component in the feedback response of turtle retinal cones. Vis Neurosci *22*, 317-324.

Telkes, I., Lee, S.C., Jusuf, P.R., and Grunert, U. (2008). The midget-parvocellular pathway of marmoset retina: a quantitative light microscopic study. J Comp Neurol *510*, 539-549.

Toyoda, J., and Kujiraoka, T. (1982). Analyses of bipolar cell responses elicited by polarization of horizontal cells. J Gen Physiol *79*, 131-145.

Trumpler, J., Dedek, K., Schubert, T., de Sevilla Muller, L.P., Seeliger, M., Humphries, P., Biel, M., and Weiler, R. (2008). Rod and cone contributions to horizontal cell light responses in the mouse retina. J Neurosci *28*, 6818-6825.

Vaney, D.I. (1991). Many diverse types of retinal neurons show tracer coupling when injected with biocytin or neurobiotin. NeurosciLett *125*, 187-190.

Vardi, N., and Sterling, P. (1994). Subcellular localization of GABAA receptor on bipolar cells in macaque and human retina. Vision Res *34*, 1235-1246.

Varela, C., Blanco, R., and De la Villa, P. (2005). Depolarizing effect of GABA in rod bipolar cells of the mouse retina. Vision Res *45*, 2659-2667.

Verweij, J., Kamermans, M., Negishi, K., and Spekreijse, H. (1998). GABA sensitivity of spectrally classified horizontal cells in goldfish retina. Vis Neurosci *15*, 77-86.

Verweij, J., Kamermans, M., and Spekreijse, H. (1996). HORIZONTAL CELLS FEED BACK TO CONES BY SHIFTING THE CONE CALCIUM- CURRENT ACTIVATION RANGE. Vision Research *36*, 3943-3953.

Volgyi, B., Chheda, S., and Bloomfield, S.A. (2009). Tracer coupling patterns of the ganglion cell subtypes in the mouse retina. J Comp Neurol *512*, 664-687.

Volgyi, B., Xin, D., Amarillo, Y., and Bloomfield, S.A. (2001). Morphology and physiology of the polyaxonal amacrine cells in the rabbit retina. J Comp Neurol *440*, 109-125.

Vollrath, L., and Spiwoksbecker, I. (1996). PLASTICITY OF RETINAL RIBBON SYNAPSES [Review]. Microscopy Research & Technique *35*, 472-487.

Wassle, H. (2004). Parallel processing in the mammalian retina. Nat Rev Neurosci *5*, 747-757.

Wässle, H., and Boycott, B.B. (1991). Functional architecture of the mammalian retina. PhysRev *71*, 447-480.

Wassle, H., Puller, C., Muller, F., and Haverkamp, S. (2009). Cone contacts, mosaics, and territories of bipolar cells in the mouse retina. J Neurosci *29*, 106-117.

Weng, S., Sun, W., and He, S. (2005). Identification of ON-OFF direction-selective ganglion cells in the mouse retina. J Physiol *562*, 915-923.

West, R.W. (1978). Bipolar and horizontal cells of the gray squirrel retina: Golgi morphology and receptor connections. Vision Res *18*, 129-136.

Wietsma, J.J., Kamermans, M., and Spekreijse, H. (1995). Horizontal cells function normally in ethambutol-treated goldfish. Vision Res *35*, 1667-1674.

Winslow, R.L., and Knapp, A.G. (1991). Dynamic models of the retinal horizontal cell network. Prog Biophys Mol Biol *56*, 107-133.

Wong, G.T., Ruiz-Avila, L., and Margolskee, R.F. (1999). Directing gene expression to gustducin-positive taste receptor cells. J Neurosci *19*, 5802-5809.

Wu, S.M. (1991). Input-output relations of the feedback synapse between horizontal cells and cones in the tiger salamander retina. J Neurophysiol *65*, 1197-1206.

Wu, S.M. (1992). Feedback connections and operation of the outer plexiform layer of the retina. Curr Opin Neurobiol *2*, 462-468.

Yamada, E., and Ishikawa, T. (1965). The fine structure of the horizontal cells in some vertebrate retinae. Cold Spring Harb Symp Quant Biol *30*, 383-392.

Yang, X.L., and Wu, S.M. (1991). Feedforward lateral inhibition in retinal bipolar cells: input-output relation of the horizontal cell-depolarizing bipolar cell synapse. Proc Natl Acad Sci U S A *88*, 3310-3313.

Yang, X.L., and Wu, S.M. (1993). Effects of GABA on horizontal cells in the tiger salamander retina. Vision Res *33*, 1339-1344.

Yin, L., Smith, R.G., Sterling, P., and Brainard, D.H. (2009). Physiology and morphology of color-opponent ganglion cells in a retina expressing a dual gradient of S and M opsins. J Neurosci *29*, 2706-2724.

Yoshida, K., Watanabe, D., Ishikane, H., Tachibana, M., Pastan, I., and Nakanishi, S. (2001). A key role of starburst amacrine cells in originating retinal directional selectivity and optokinetic eye movement. Neuron *30*, 771-780.

Zanazzi, G., and Matthews, G. (2009). The molecular architecture of ribbon presynaptic terminals. Mol Neurobiol *39*, 130-148.

Zhaoping, L. (2006). Theoretical understanding of the early visual processes by data compression and data selection. Network *17*, 301-334.

Zheng, J.J., Lee, S., and Zhou, Z.J. (2004). A developmental switch in the excitability and function of the starburst network in the mammalian retina. Neuron *44*, 851-864.

Zhou, Z.J., and Lee, S. (2008). Synaptic physiology of direction selectivity in the retina. J Physiol *586*, 4371-4376.